MSc in Water Management

The Heat Square: visualising urban microclimate phenomena in a small scale controlled urban environment

Tristan Cheaz - August 2024

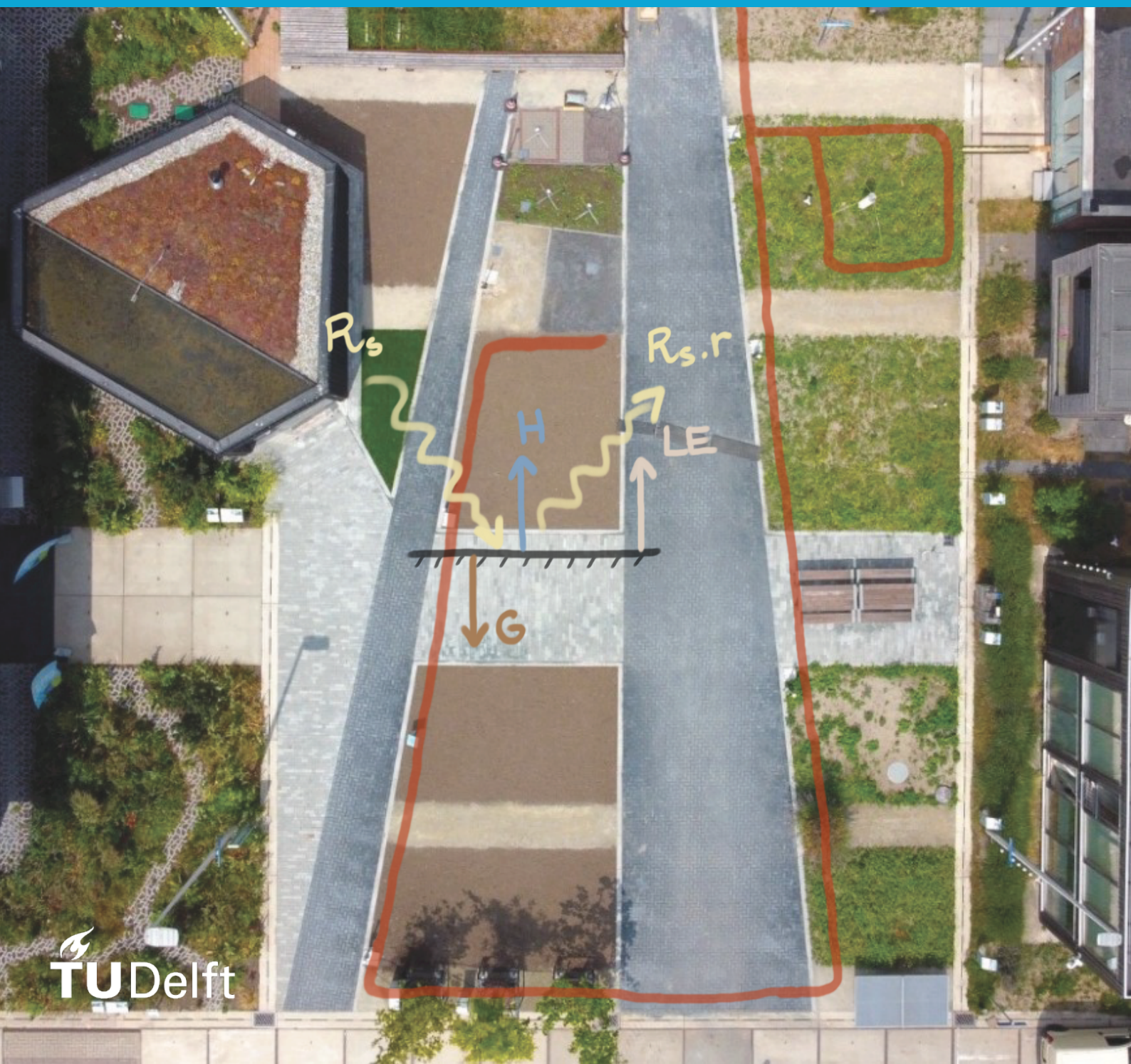

TU Delft

MSc thesis in Water Management

The Heat Square: visualising urban microclimate phenomena in a small scale controlled urban environment

Tristan Cheaz
4565762

August 2024

A thesis submitted to the Delft University of Technology in partial fulfillment of the requirements for the degree of Master of Science in Water Management

Tristan Cheaz: *The Heat Square: visualising urban microclimate phenomena in a small scale controlled urban environment* (2024)

The work in this thesis was carried out in collaboration with:

Delft University of Technology
The Green Village

Supervisors: Dr.ir. A.M. (Arjan) Droste
Dr.ir. M.M.E. (Marjolein) van Esch
ir. G.A. (Gijs) Vis

Abstract

Urban microclimates have a great impact on the thermal comfort of city inhabitants, with the Urban Heat Island (UHI) and the Subsurface Urban Heat Island (SUHI) effects posing a growing challenge under the accelerating impacts of climate change. This thesis focuses on investigating the UHI and SUHI effects and exploring potential mitigation strategies within a controlled urban environment, specifically the "Heat Square" at The Green Village in the Delft University of Technology. The Heat Square serves as an experimental urban environment designed to analyse various urban cooling measures.

To capture the spatial and temporal variations in soil temperature within the Heat Square, Distributed Temperature Sensing (DTS) technology was deployed. DTS measures high-resolution temperature data, which allows for detailed analysis of the soil temperature response to different cooling scenarios, including the implementation of green infrastructure, shading, and reflective surfaces. These in-situ measurements were then compared with urban microclimate modeling results using ENVI-met, a Computational Fluid Dynamics (CFD) tool for modeling urban microclimatic conditions. ENVI-met, along with other urban microclimate models, can predict the impact of urban design on local temperature and thermal comfort indices.

The findings of this research highlight the significant potential of green infrastructure and shading as effective strategies to mitigate the UHI effect. Specifically, the introduction of vegetation and shading elements resulted in noticeable reductions in both surface and air temperatures as well as Mean Radiant Temperature T_{mrt} within the urban environment. These findings were supported by performing simulations of different urban scenarios of the Heat Square. However, the study also highlighted challenges in accurately modeling urban microclimates, as shown by discrepancies between the DTS measurements and ENVI-met simulations. These differences suggest the need for further refinement of model parameters to better approximate the complexities of real-world urban environments.

Overall, this thesis contributes to the broader understanding of urban cooling measures and their role in enhancing the resilience of cities to climate change. The insights gained from this research are intended to inform urban planning and design practices, promoting the development of more sustainable and climate-resilient urban spaces as well as the applicability of urban microclimate monitoring tools.

Future research should focus on refining the ENVI-met model of the Heat Square to enhance its accuracy in properly simulation real-life responses of the urban environment to climatic variations. Additionally, exploring a broader range of urban cooling strategies, including water-based solutions and varying surface materials, could broaden knowledge on heat mitigation strategies. Studying soil thermal responses in other urban environments with DTS would also be valuable for studying indirect effects of the SUHI effect. Collaborations between researchers, urban planners, and policymakers are important to ensure that scientific findings are translated into practical applications that increase climate adaptability of urban environments.

Acknowledgements

This graduation project marks the culmination of my eight-year journey as a student, fulfilling the requirements for an MSc in Civil Engineering with a specialisation in Water Resources Engineering. The final phase of my education, my thesis, has proven to be the most challenging academic endeavor I have undertaken. Reflecting on my first day as a university student, I could never have imagined that I would end up here, and I am grateful for the way it all turned out. I would like to dedicate this chapter to those who helped me achieve this milestone.

First and foremost, I want to thank my graduation committee: Arjan Droste, Marjolein van Esch, and Gijs Vis. Arjan, thank you for stepping in as my main supervisor so quickly when my previous one was no longer available. I felt very comfortable during our sessions due to your relaxed yet professional demeanor, and your constructive feedback was invaluable in guiding me toward the completion of my work. Marjolein, although you joined the project later, I truly appreciate your willingness to collaborate with our group, even though you didn't witness the early stages. Your background in Architecture brought a fresh perspective that enriched the overall scope of the project. Finally, Gijs, I am immensely grateful for your support in the early stages of the project. Your instruction on DTS and hands-on assistance with the installation were invaluable, and your passion for DTS inspired me to push through this project. Lastly, I would like to thank Martine Rutten, my former main supervisor, for entrusting me with this project and allowing me to formulate my own research objectives and approach. I hope you have found fulfillment in your new pursuits after your well-deserved break from academia.

Throughout the process of my thesis, several people within the university have contributed to my work. Lisanne, thank you for working on your thesis alongside me—it often felt like we were tackling the same project. Aytac, your guidance in performing ENVI-met simulations remotely was essential; without your help, this thesis would not have been possible. Y finalmente, Diana, valoro mucho que hayas estado conmigo durante la última fase de mi tesis. Realmente necesitaba a alguien con quien charlar de vez en cuando, que estuviera en la misma situación que yo. Me alegra que ambos tengamos nuestra presentación final el mismo día.

Finally, I want to express my gratitude to those in my personal life who have motivated me and provided advice whenever I needed it. Thank you, Tim D., Tim H., Hidde, Djemie, Leon, Karim, Jay, my fellow DROP board members, and my colleagues at the Shore. Mami y Papi, gracias por creer en mí y quererme sea lo que sea. La razón principal por la que logré esto es porque ustedes dos me han enseñado el valor de una buena educación. Markus, eres el mejor hermano que podría tener. Tú y yo somos literalmente lo mismo. Cuando te graduaste, me sentí como si yo también lo hubiera hecho, y espero que sientas lo mismo ahora que me gradúo. And lastly, Emma, my wonderful girlfriend, you are simply the greatest source of inspiration I have ever known. Your passion and outlook on life are indescribable. You are so kind yet so clear-headed when it comes to what matters most. Thank you so much for pushing me through this last phase and making sure I was okay during long periods of isolation from the outside world.

Tristan Cheaz

The Hague, August 21, 2024

Contents

List of Figures

List of Tables

Acronyms

1. Introduction

1.1. The urban environment in a changing climate

It is widely accepted and recognised that extreme weather events are increasing in frequency globally due to climate change. Higher temperatures pose significant risks, including the deterioration of safe work conditions, reduced worker productivity, diminished habitability of urban areas, and compromised thermal comfort, which can lead to heat-related illnesses (Jankovic and Schultz, 2017). Additionally, there are numerous indirect consequences, such as degraded air quality, malnutrition, and the spread of vector-borne diseases (Ebi et al., 2018). Furthermore, many large cities worldwide contribute to local temperature increases by trapping solar radiation and reflecting it on heat-absorbing surfaces, a phenomenon known as the Urban Heat Island (UHI) effect (Yang et al., 2016).

Given the undeniable negative impact of global warming on human and ecological health, various international organisations and national governments have committed themselves to reduce the anthropogenic forcing on the climate by setting limits on the extent of global temperature rise (Boehm et al., 2022). However, even if further global temperature increases are prevented, urban areas may still face higher heat-related consequences due to ever increasing size of cities and the accumulation of heat-absorbing surfaces. Cities must adapt their design and construction to the changing climate while also working to mitigate global temperature increases (Matthews et al., 2017).

The UHI effect is not only experienced and measured above the surface but also in the underlying soil. A study by Edmonson et al. (2016) recorded an average increase of 0.6°C along a 5 km stretch from the city outskirts to the city centre. Shi et al. (2012) further reinforced this phenomenon by measuring an average yearly increase of 2.02°C alongside an average decrease in soil moisture in urban areas. Higher soil temperatures lead to an increase in solar radiation absorbed in the subsurface, increasing water evaporation from the soil and releasing heat into the surrounding atmosphere, thereby amplifying the temperature rise. The heating of the soil in the urban context is predominantly caused by incoming solar radiation, which can be either direct from the sun or reflected from other surfaces, as well as the absorption of solar radiation by the ground cover above the soil (Previati et al., 2022). This phenomenon is known as the Subsurface Urban Heat Island (SUHI) effect. The SUHI poses risks to the biological, chemical, and physical aspects of the soil, in addition to contributing to the general capture of urban heat. The soil temperature responses in the urban environment form the main focus of this study.

1.2. Assessing the urban microclimate

To perform soil temperature measurements, DTS is a technique that has significantly improved in recent years for monitoring the sub-surface (Dong et al., 2016). Originating from the oil and gas industry, applications of DTS can vary from transformer monitoring to hydrological studies. Implementation of DTS for urban heat monitoring is scarce in the literature. An example of DTS implementation by Solcerova et al. (2018), explores the application of an old Japanese cooling tradition to decrease air temperature in its surroundings. The study used a cage construction suspending fibre-optic cables for DTS above the surface up to a height of 1 metre as a measurement setup (Solcerova et al., 2018). DTS implementation for hydrometeorological applications is on the rise, examples of such being field campaigns for Bowen ratio measurements in the Netherlands, and turbulence analysis in Spain (Schilperoort (2018), Vis (2022)). Both of these studies were conducted to inform on future application in agriculture.

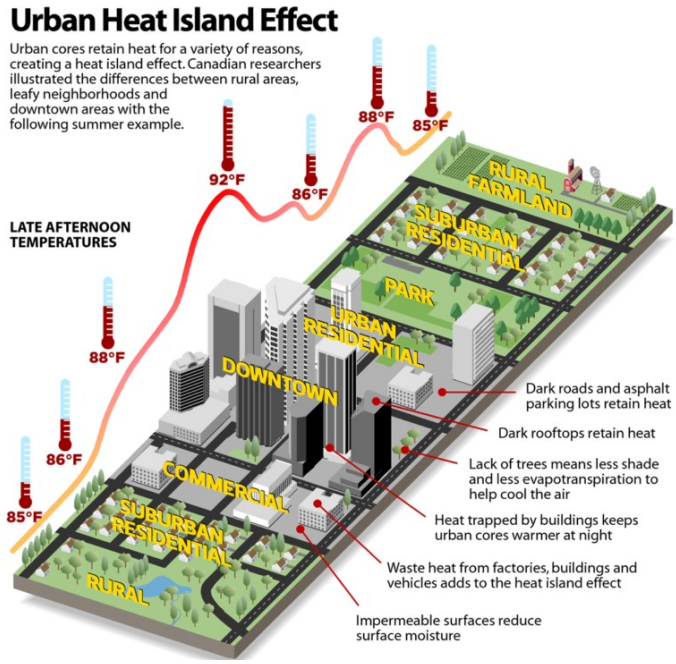

Figure 1.1.: Illustration of the UHI effect on the air temperature, along with root causes for the phenomenom (Lemmen and Warren, 2004)

Considering the main focus of this study, DTS applications have been used to measure different terms of the soil energy balance, both above and below the surface. As studies by Atefe and Reinhardt (2020) and Mathew et al. (2018) suggest, the ground heat flux greatly affects the urban microclimate and should be considered in urban design for the improvement of thermal comfort. In these studies, the soil temperature is measured with either data loggers buried at different locations or satellite imagery. Duus and Schmitz (2021) inserted a fibre optic cable through a borehole deep into the ground for DTS measurements, to study the geothermal field of an office building and its impact on its surrounding heat balance, showing the added benefit of using DTS for soil temperature measurements. A similar technique was implemented in Nanjing, China, at multiple locations to conduct city-scale monitoring of the shallow subsurface temperature variability (Zhang, 2022), for opportunities to produce geothermal energy. DTS implementation to visualise the ground heat flux in the urban microclimate remains unexplored, which is evident from the lack of research utilising DTS techniques to address the phenomenon. This provides an opportunity for research regarding the urban microclimate.

Since the installation of DTS methods at the city scale comes with logistical, technical, and financial challenges, small-scale implementation in a controlled environment could provide valuable insights. Complementary to performing measurements through DTS to understand the UHI and SUHI effects is the use of microclimate models. Depending on the study's goals, microclimate modeling can be applied at different scales in the urban environment, ranging from building-scale to city-scale (Mirzaei, 2015). With the development of computational resources and numerical simulation approaches, Computational Fluid Dynamics (CFD) models are commonly used to evaluate and visualise the urban microclimate (Toparlar et al., 2017). A challenge these models face is the significant computational power required to generate city-scale models. Using smaller-scale models to gain insights into the physical processes in the urban environment could help expand our knowledge to the city scale. Validation of CFD models through DTS can provide new insights into understanding heat stress in urban environments.

1.3. Mitigating urban heat

Understanding the processes behind the UHI and SUHI effects can help identify solutions to the risks associated with increasing urban heat. One of the most commonly adopted strategies to

reduce urban heat phenomena is to increase the number of green spaces and green surface cover in urban areas (Lee and Mayer (2018), Koch et al. (2020), Hiemstra et al. (2017)). Lafortezza et al. (2009) observes that green spaces provide benefits to human health and well-being in addition to their impact on urban hydrometeorology. The combination of mitigating human and environmental risks posed by climate change makes the implementation of vegetation an ideal standard to adopt in future urban development (Osmond and Sharifi, 2017). Significant efforts are being made by researchers, governments, climate activists, engineers, and architects to advocate for nature-inclusive design in climate-resilient cities through research, public speaking, policy-making, and education (Stache, 2021).

Another widely discussed heat mitigation strategy is increasing surface albedo in urban environments. Enhancing the albedo of certain surfaces can decrease the surrounding air temperature (Akbari et al., 2012). Surface albedo determines the amount of incoming shortwave radiation that is reflected from a surface; thus, a higher albedo results in lower heat absorption from the sun (Bonafoni et al., 2017). However, urban planners must be careful when implementing these techniques, as the reflected solar radiation can increase thermal discomfort for pedestrians, despite reducing air temperatures in the area (Taleghani, 2018b). Taleghani (2018b) also suggests that few studies in the field of heat mitigation consider thermal comfort indices, such as Mean Radiant Temperature (T_{mrt}) or Physiologal Equivalent Temperature (PET), adding another dimension to urban planning considerations for heat mitigation.

1.4. Research objectives

Due to the global importance of improving urban environments and the limited exploration of DTS in analyzing these areas, this research focuses on conducting a small-scale analysis of an urban area, with an emphasis on soil conditions. The results from this study could potentially influence decisions made by other researchers regarding urban design and approaches related to urban microclimate research. Additionally, this study aims to identify the strengths and weaknesses of the tools used in the analysis of the study area.

Two primary tools are employed for visualising the urban microclimate: a Distributed Temperature Sensing (DTS) system and a microclimate model based on Computational Fluid Dynamics (CFD). The CFD simulations of the study area were conducted using ENVI-met, a microclimate model developed by Bruse (2004). This software has been in development for over two decades and is frequently employed in microclimate analyses, as demonstrated by Taleghani (2018b), who used it to simulate part of the TU Delft University campus. The version used in this study is 'V5.5.1 Summer23'. Other measurement devices and tools are also available to support the DTS system and the CFD model.

The objective of this research is to compare the results obtained from the DTS system with those predicted by the ENVI-met model of the study area, specifically the 'Heat Square' at the Green Village within the TU Delft University campus. This comparison aims to assess the effectiveness of CFD models in computing heat distribution in urban environments, for both sub-surface and above-surface conditions. Furthermore, the study aims to simulate various urban, geographical, and meteorological scenarios of the Heat Square to provide insights into its response under different conditions. The urban climate knowledge gathered from this study can subsequently be applied to engineering and design practices in other areas of interest beyond the Heat Square, with different geographical and meteorological characteristics. To achieve these objectives, the following research questions have been formulated:

1. *'What is the soil temperature measured by the DTS system at different depths under different types of ground cover?'*
2. *'What is the soil temperature modelled by the CFD model ENVI-met at different depths under different types of ground cover?'*
3. *'How do the results from the CFD model ENVI-met compare to the measured soil temperatures by the DTS system, and how can it be further improved upon for other applications and contexts?'*

4. *'What insights does the ENVI-met model provide about the sensitivity of Heat Square responses to different urban, geographical, and meteorological model parametrisations?'*

1.5. Outline of the report

This report begins with background information on the urban heat balance and the distribution of incoming solar radiation into various heat components, along with a description of thermal comfort indices that indicate the UHI effect. Following this, the microclimate model ENVI-met is introduced, including an explanation of its structure. The cooling strategies implemented in the Heat Square are then detailed.

The report proceeds to describe how DTS and ENVI-met were utilised to meet the research objectives, followed by the presentation of results from each approach. An attempt to validate both methods is then performed, along with results from various scenarios simulated using ENVI-met.

The discussion section evaluates the results and the applicability of both DTS and ENVI-met, highlighting areas for improvement and offering recommendations for future research. The report concludes with remarks on the research objectives.

2. Background

This chapter provides background knowledge on topics relevant to this study, aiming to ensure a comprehensive understanding of the methodology used and to facilitate the interpretation of the results. It discusses the theory behind the Urban Heat Balance, the working principles of Distributed Temperature Sensing (DTS), and the structure of the CFD model used. The chapter concludes by focusing on the specific context of the study, illustrating how the previously discussed theory is applied within the area of interest.

2.1. Urban Heat Balance

The interaction between the urban environment and incoming solar (shortwave) radiation can be described using a simple energy balance. This balance relates the net shortwave radiation to the resulting heat fluxes on the surface where the radiation is incident:

$$Q_* = (1 - r)R_s \tag{2.1}$$

$$Q_* = H + LE + G \tag{2.2}$$

Where: Q_*: net shortwave radiation [W/m^2]; R_s: incoming shortwave radiation [W/m^2]; r: surface albedo [-]; H: sensible heat flux [W/m^2]; LE: latent heat flux [W/m^2]; G: ground heat flux [W/m^2].

If we assume that all net shortwave radiation is converted into either sensible heat flux, latent heat flux, or ground heat flux, then Equation 2.2 holds true. Without this assumption, the change in energy storage in a surface layer can be expressed as follows (University of Reading, 2023):

$$\frac{dQ}{dt} = Q_* - H - LE - G \tag{2.3}$$

Most models assume an infinitely thin surface layer, which implies that Equation 2.3 equals zero. In this case, the remaining energy is stored in the ground heat flux. Given a known incoming shortwave radiation and a computed latent heat flux through Equation 2.8, the remaining terms can be determined using the Bowen ratio B_0[-], which describes the ratio of sensible to latent heat flux and is surface dependent (University of Reading, 2023):

$$B_0 = \frac{H}{LE} \tag{2.4}$$

Which can be rewritten using Equation 2.2 as:

$$Q_* = (B_0 * LE) + LE + G \tag{2.5}$$

$$Q_* = LE(1 + B_0) + G \tag{2.6}$$

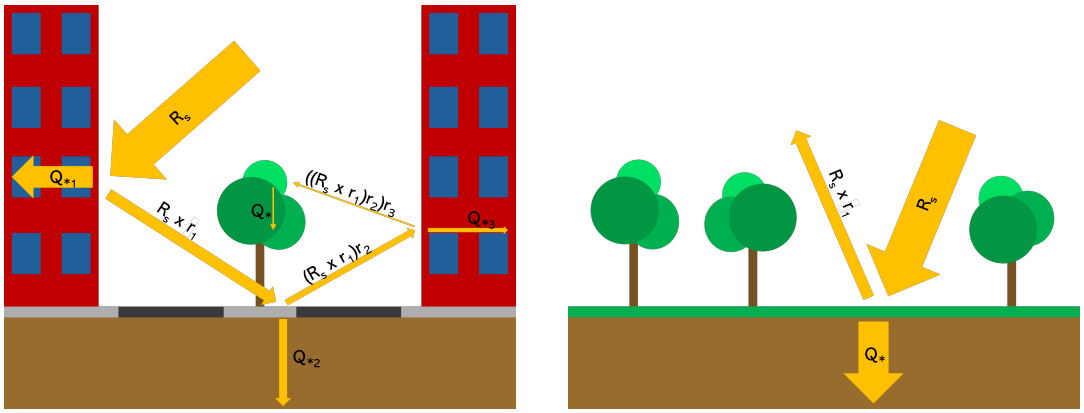

(a) (b)

Figure 2.1.: Partitioning of incoming (solar) radiation in (a) an urban environment vs. (b) a rural environment. The net radiation absorbed by the surfaces Q_* is determined by the surface albedo r and is further partitioned into sensible heat flux H, latent heat flux LE and ground heat flux G.

The value of the Bowen ratio depends on the water availability at the surface, where heat transfer can occur through sensible heat, driven by changes in temperature, or latent heat, which requires energy to evaporate water (Bowen, 1926). Arid areas, such as deserts, have a high Bowen ratio, indicating little to no water availability for conversion into water vapour ($B_0 \approx 10$), leading to high sensible heat fluxes. Conversely, areas with high surface water availability, like oceans or tropical rainforests, show a low Bowen ratio, resulting in significant water evaporation from the surface ($B_0 \approx 0.1$ - 0.3)(Lewis, 1995). In vegetated areas of the Netherlands, the Bowen ratio typically ranges between 0.4 and 0.8 but can vary significantly in diurnal periods and throughout the year (Schilperoort, 2022). In contrast, for artificial surfaces in urban areas, this ratio can spike considerably, ranging from 2 up to 6 (Pohankova and Pechanec, 2024).

By determining the ground heat flux, the soil temperature T_s at depth z can be calculated. This soil temperature is what the DTS system ultimately measures. Understanding the interaction between soil temperature and incoming shortwave radiation at their interface is crucial for comprehending the soil's response to various climatic conditions. The relationship between ground heat flux and soil temperature is described as follows (Wang and Bras, 1999):

$$G = -\rho_s c_s \kappa_s \frac{\delta T_s}{\delta z} \tag{2.7}$$

Where: ρ_s: soil density $[kg/m^3]$; c_s: heat capacity $[J/(kgK]$; κ_s: thermal diffusivity $[m^2/s]$.

2.2. UHI effect

The urban environment plays a crucial role in the lives of the global population. As of 2013, 52% of the world's population resided in urban areas, with projections indicating that this figure will rise to 67% by 2050 (Population Reference Bureau, 2013; United Nations, 2012). Understanding the dynamics and complex interrelationships between the urban environment, climate, and human health is therefore essential, especially considering the challenges posed by increased anthropogenic heat emissions (Debbage and Shepherd, 2015). The primary driving forces behind these future challenges are urbanisation and climate change, which contribute significantly to the UHI effect (Chapman et al., 2017).

To understand the emergence of the UHI effect, close attention must be paid to several characteristics of the urban environment. Urban materials, often comprising concrete, asphalt, and buildings, retain more heat compared to natural vegetation. This is due to the different material

properties, which lead to a different partitioning of incoming solar energy(shortwave radiation) (Stache et al., 2022). A fraction of the incoming energy is reflected by the surface's albedo r[-], as previously detailed in Section 2.1. The absorbed energy is then converted into convective heat ($Q_H[W/m^2]$), longwave emitted heat ($Q_R[W/m^2]$), and latent heat ($Q_E[W/m^2]$). Lower albedo values indicate more energy absorption by the material, resulting in greater heating of the environment (Stache et al., 2022). Urban environments predominantly consist of building materials such as brick, concrete, and asphalt (bitumen). A study by Stache et al. (2022) determined the albedo values of various building materials and vegetation surfaces. The albedo values for brick, concrete, and bitumen were found to be 0.26, 0.13, and 0.02, respectively, indicating a large energy absorption by these materials. Soil surfaces with vegetation have albedo values ranging from 0.05 to 0.4, depending on the soil type and vegetation coverage. Despite these low albedo values, vegetated surfaces utilise the absorbed energy for evapotranspiration, thus heating up and radiating less than building materials (Stache et al., 2022). Examples of surfaces with relatively higher albedos are wood, white plastic, or concrete, with albedo values around 0.3.

A significant difference between urban and rural areas is the reduced amount of vegetation in urban environments. Tree canopies provide shade, reducing the amount of solar energy absorbed by surfaces. This intercepted energy can be used for evapotranspiration, which cools the air (Dimoudi and Nikolopoulou, 2003). The energy available for evapotranspiration from incoming solar radiation varies by vegetation type and can be computed using different methods. One of the most common methods is the Penman-Monteith equation, which depends on the net incoming solar radiation not reflected by the vegetation's albedo (Monteith, 1965):

$$ET = \frac{\Delta(R_n - G) + \rho_a c_p (e_s - e_a)/r_a}{\Delta + \gamma(1 + \frac{r_s}{r_a})\lambda\rho_w} \tag{2.8}$$

Where: Δ: slope of the saturation vapour pressure vs. temperature curve $[mb/^\circ C]$; R_n: net incoming solar radiation $[cal/(cm^2 - s]$; G: ground heat flux $[cal/(cm^2 - s]$; ρ_a: air density $[gr/cm^3]$; c_p: specific heat of dry air $[cal/gr -^\circ C]$; e_a: actual air vapour pressure; r_a: aerodynamic resistance to turbulent heat $[s/cm]$; γ: psychrometric constant $[mb/^\circ C]$; r_s: resistance to water vapour flow from inside the leaf $[s/cm]$; λ: heat of vaporisation $[cal/gr]$; ρ_w: water density $[gr/cm^3]$.

As shown in Equation 2.8, computing the evapotranspiration of a specific vegetation type requires extensive calculations. This equation is presented to illustrate the parameters that influence the evapotranspiration of plants, though it is not further examined in this study. In summary, the reduced amount of vegetation (including trees, grass, bushes, and small plants) in urban areas leads to less shading of paved surfaces and less energy absorption for evapotranspiration. These factors together intensify the UHI effect.

In addition to increased heat retention, expanding urban areas generate more heat. The urban population is projected to grow by 2.5 billion in the next 30 years, leading to increased heat generated by vehicles, factories, and other machinery (Mahtta et al., 2022). This urban growth also results in taller buildings, which can trap heat by reflecting solar radiation between surfaces, causing more heat absorption each time the radiation contacts a surface (Mansouri and Zarghami, 2023). Taller buildings can also impede air flow, reducing heat dispersion and creating 'hotspots' in the city (Figure 1.1).

2.3. Mean Radiant Temperature

The extent to which the urban environment contributes to extreme thermal anomalies can be determined through various methods. The thermal comfort of humans in an urban environment is often determined by so-called "thermal comfort indices". In an extensive study of the UHI effect in Noida, India, researchers utilised indices such as the Urban Thermal Field Variance Index (UTFVI), Land Surface Temperature (LST), Normalized Difference Vegetation Index (NDVI), and Index-based Built-up Index (IBI) (Sharma et al., 2021). A study by Thorsson et al. (2023)

highlights the importance of thermal comfort indices for evaluating the impact of the urban microclimate on people's health. It concludes that indices such as the T_{mrt} provide a more accurate approximation of heat-related mortality rates than merely considering the air temperature in urban environments. This approach benefits the planning of heat mitigation strategies and the development of heat-warning systems (Thorsson et al., 2023).

The Mean Radiant Temperature (T_{mrt}) is a biometeorological parameter that can be best described as the homogeneous temperature distribution around a human being within an imaginary enclosed space, where the radiant heat transfer from the human body equals the radiant heat transfer within that space (ASHRAE, 2011). The T_{mrt} depends on the proximity and orientation of a point in space relative to surrounding surfaces and radiative sources. It serves as a correction for an individual's thermal comfort based on the radiant heat exchange (both short- and longwave) between the person and their environment (Thorsson et al., 2023). To calculate T_{mrt}, one must know the radiation flux densities of short- and longwave radiation and the proportion of these densities received from each direction at a given point in space. The directions refer to the six orientations relative to the point: north, south, east, west, upward, and downward. The T_{mrt} [°C] can then be computed using the Stefan-Boltzmann law (Ali-Toudert and Mayer, 2004):

$$T_{mrt} = \sqrt[4]{(S_{str}/(\varepsilon_p \sigma)} - 273.15 \tag{2.9}$$

With:

$$S_{str} = \alpha_k \sum_{i=1}^{6} K_i F_i + \alpha_l \sum_{i=1}^{6} L_i F_i \tag{2.10}$$

Where: S_{str}: total radiant flux density absorbed [W/m^2]; K_i: shortwave radiation flux density from all six directions i [W/m^2]; L_i: longwave radiation flux density from all six directions i [W/m^2]; F_i: angular factor from all six directions i[-]; α_k: shortwave radiation absorption coefficient [-]; α_l: longwave radiation absorption coefficient [-]; ε_p: emissivity of human body [-]; σ: Stefan-Boltzmann constant [$5.67 * 10^{-8} W/m^2K^4$].

Determining the angular factor for each surface can be challenging, especially in complex urban environments with numerous structural objects relative to the point of observation (Ali-Toudert and Mayer, 2004). An alternative method for determining T_{mrt} involves using globe thermometers, supported by air temperature and wind speed measurements (Holmer et al., 2007). Although this method is simpler, it has been shown to be less accurate in outdoor, complex urban settings (Ali-Toudert and Mayer, 2004). To address these limitations, T_{mrt} is often calculated using urban microclimate models instead. Additionally, many other thermal comfort indices are computed in popular microclimate models, such as the Predicted Mean Vote (PMV), PET, and Universal Thermal Climate Index (UTCI) (ENVI-met, 2024).

2.4. Distributed Temperature Sensing

This study uses Distributed Temperature Sensing (DTS) to measure the soil temperature of the Heat Square and validate the CFD model. DTS offers the advantage of obtaining high-resolution, spatially distributed soil temperature measurements without the need to install numerous individual sensors across the area. Achieving a similar spatial resolution with traditional temperature sensors would require a large number of sensors, leading to higher cost installation costs. DTS is widely used for temperature measurements along long stretches of pipelines, power cables, and storage tanks (YOKOGAWA, 2023). Recently, it has also been used in hydrology for stream temperature measurements and atmospheric air temperature measurements (Vis, 2022; Schilperoort, 2022). A recent study by Schilperoort et al. (2023) has also implemented DTS to measure the vertical soil temperature profile.

The working principle of DTS begins with a machine that emits light pulses into fiber-optic cables connected to it. These optical fibers transmit the light pulses along the entire length of the cable. As the light travels through the cable, it interacts with molecules within the fiber (primarily silica and germanium oxide), causing scattering in various directions (Schilperoort, 2022). Typically, most scattered light retains the same wavelength. However, some photons interact with molecules through the Raman effect, where the photon either gains or loses energy. This interaction results in scattering with a decrease in wavelength (Stokes Raman scattering) or an increase in wavelength (Anti-Stokes Raman scattering) (Raman, 1928).

The change in wavelength depends on the temperature of the molecule with which the photon interacts, allowing for temperature determination by measuring the ratio of Stokes to Anti-Stokes scattering of the returned light. The DTS device that emits the light also measures the intensities of the returned Stokes and Anti-Stokes backscattering. It computes the location of the backscattering by multiplying the time it took to receive the light after emission by the speed of light and dividing by two, as the distance is traveled twice (to and from the scattering point). With the known distance and the ratio of Stokes to Anti-Stokes power, the temperature T[°K] at a specific distance from the device x can be computed using the following formula (Hartog, 2017):

$$T(x,t) = \frac{\gamma}{I(x,t) + C(t) + \int_0^x \Delta\alpha(x')dx'} \tag{2.11}$$

$$I(x,t) = \ln \frac{P_+(x,t)}{P_-(x,t)} \tag{2.12}$$

Where: γ: sensitivity of Stokes and Anti-Stokes scattering to temperature; $I(x,t)$: power ratio between Stokes P_+ and Anti-StokesP_- backscattering; $C(t)$: device dependent coefficient; $\Delta\alpha$: differential attenuation.

For the machine to be able to transform the measured backscattering into temperature, several variables must be considered. The sensitivity (γ) depends on the material of the fiber, the attenuation ($\Delta\alpha$) varies along the cable and requires correction, and the device-dependent constant (C) is needed to account for signal losses from connectors or the detector of the machine (Schilperoort, 2022). These values are determined by calibrating the temperature to sections of the cable where the temperature is constant and known. Typically, sections of the cable are submerged in calibration basins with different, but constant water temperatures (Vis, 2022).

The fiber-optic cables can be connected in various configurations, either single-ended or double-ended, meaning a single connection to the machine or two connections where there are two receivers and two pulse emitters. The most advantageous setup is the double-ended configuration. With connections on both sides, attenuation is more easily accounted for because the light travels in both directions, allowing for differentiation of temperature along the cable and attenuation (Schilperoort, 2022). This assumes that the attenuation along the cable is symmetrical in both directions.

2.5. Computational Fluid Dynamics

To evaluate the performance of cooling measures without installing sensors or physical equipment on-site, models can be developed to predict and compare the effectiveness of these measures in various settings before their implementation and construction (Sinsel, 2021). A reliable model can be a highly useful tool for conducting relatively quick and low-cost assessments of different scenarios. Computational Fluid Dynamics (CFD) models are based on the conservation laws (mass, momentum, and energy) to compute predictions of fluid flow phenomena. Originally prevalent in the field of Fluid Mechanics, CFD models are among the commonly used model types for climatological analysis (Howard, 2012). One of which is ENVI-met, which is the CFD model used in this study.

In climatological analysis, CFD models describe the interactions within a specified model domain between grid cells. These interactions are influenced by factors such as radiation, wind, air temperature, air humidity, air pressure, and precipitation (Howard, 2012). Models can vary in domain size and grid cell size, allowing for simulations on any scale—from microscale models that describe the interaction between urban morphology and climate conditions, to macroscale models that describe the continental impacts of climate change (Howard, 2012). Microscale models can have resolutions ranging from 1 to 20 meters, while macroscale models can have resolutions from hundreds of meters to kilometers per grid cell.

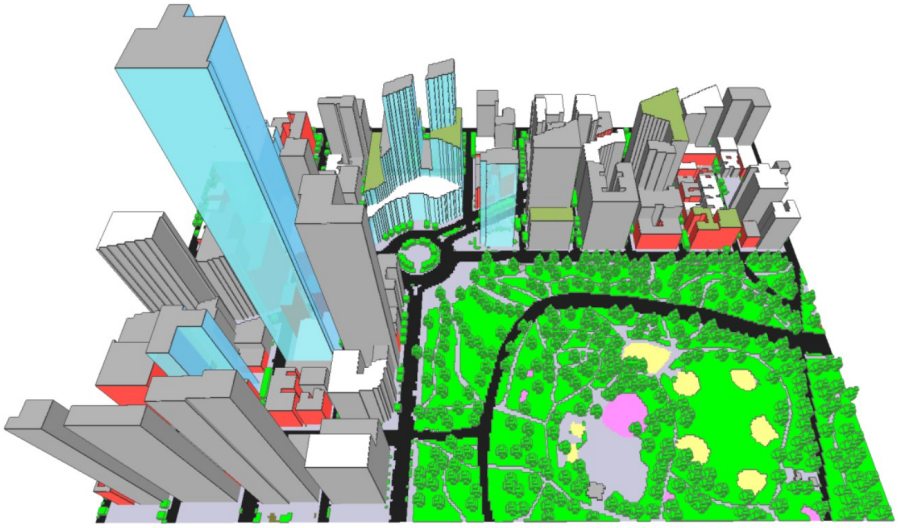

Figure 2.2.: Example of model schematisation of Central park in New York, United States for simulation of different climate scenarios. The colors indicate different material properties and are pre-defined within the ENVI-met software infrastructure (Acero and Arizzabalaga, 2018).

ENVI-met is one of the most commonly used CFD models for urban microclimate analysis, utilised for both scientific research and commercial purposes by architects and urban planners (Crank et al., 2020; Janicker et al., 2021). Developed by Michael Bruse in 1998 as part of his PhD dissertation, the model has undergone continuous development, reaching its current version 5 (Bruse and Fleer, 1998). These updates were made possible by advancements in computational power, allowing the initially formulated model to be computed more efficiently. Updates to ENVI-met have come from cross-validation through extensive research over the years. For example, Acero and Herranz-Pascual (2015) identified errors in computing thermal comfort indicators such as the Mean Radiant Temperature T_{mrt}. Other studies (Tsoka et al., 2018; Liu et al., 2021) have addressed shortcomings in the software's parameterisations. Peer review remains a crucial aspect of ENVI-met's development. All of the previously addressed issues with the model and how they have been improved are carefully laid out by Sinsel (2021).

Section 3.6 presents the structure of the ENVI-met model, while Appendix E details the process of starting a model simulation with all the required data files. Although this study primarily focuses on soil temperatures, air temperatures, radiative fluxes, and thermal comfort indices, an ENVI-met simulation computes all relevant forces for each specified timestep. These include air velocity and direction, air humidity, air pressure, turbulence, and gas and particle dispersion (Acero and Arizzabalaga, 2018). The model can be initialised with various soil and air temperature profiles to reduce the computation required at the start of the simulation. The grid cell states are computed from the beginning of the simulation with the specified forcing input, using the Reynolds-averaged Navier-Stokes equations for flow simulation. However, studies indicate that this approach can overestimate the turbulent flow around buildings (Acero and Arizzabalaga, 2018). In terms of radiation fluxes, the model accounts for all types of relevant radiation for microclimate modelling (Ali-Toudert and Mayer, 2006).

Most importantly for this study, since the approach is to validate the ENVI-met model by comparing it to soil temperatures acquired through DTS, the method of computing soil temperature is of particular interest. In ENVI-met, the soil temperature is computed in a one-dimensional

column, except for the top layer, where heat transfer is calculated in three dimensions (Bruse, 2004). The vertical resolution of the soil ranges from 0.01 m in the top layer to 0.5 m in the deepest layer. The soil temperature T and soil volumetric moisture content η are computed using the one-dimensional prognostic equations (Bruse, 2004):

$$\frac{\delta T}{\delta t} = \kappa_s \frac{\delta^2 T}{\delta z^2} \tag{2.13}$$

$$\frac{\delta \eta}{\delta t} = D_\eta \frac{\delta^2 \eta}{\delta z^2} + \frac{\delta K_\eta}{\delta z} - S_\eta(z) \tag{2.14}$$

Where: κ_s: thermal diffusivity, dependent on the available soil moisture η Tjernstrom (1989); η: volumetric water content; η_s: saturation value of soil; K_η: hydraulic conductivity; D_η: hydraulic diffusivity. These coefficients are determined through (Clapp and Hornberger, 1978).

The temperature of the surface above the soil is computed through the surface energy balance similar to Equation 2.2, except the net radiation consists of a shortwave radiation term and a longwave radiation term:

$$R_{sw,net} + R_{lw,net} = H + LE + G \tag{2.15}$$

The term G is replaced by the heat transmission (Q_w) through a wall or roof when the surface energy balance equation is applied to a building surface. The net shortwave and longwave radiation at the surface ($z = 0$)are calculated respectively as follows (Bruse, 2004):

$$R_{sw,net} = (R_{sw,dir}(z = 0) \cos \beta + R_{sw,dif}(z = 0))(1 - r) \tag{2.16}$$

Where: $R_{sw,dir}$: direct shortwave radiation flux; $R_{sw,dif}$: diffuse shortwave radiation flux; β: angle of incidence; r: surface albedo.

$$R_{lw,net}(T_0) = \sigma_{svf} R^{us}_{lw,net}(T_0) + (1 - \sigma_{svf}) R^{s}_{lw,net} \tag{2.17}$$

Where: σ_{svf}: sky-view factor, used to weigh the ratio of shielded and unshielded fraction of the net longwave radiation at the surface, which is computed after Deardorff (1978).

The ground heat flux depends on the surface temperature and the temperature of the grid cell below it (Bruse, 2004):

$$G = \lambda_s(k = -1) \frac{T_0 - T(k = -1)}{0.5 \Delta z(k = -1)} \tag{2.18}$$

Just like the soil and surface equations, ENVI-met utilises various approaches to compute air flow, air temperature and humidity, turbulence, radiative fluxes, evapotranspiration by vegetation, and gas and particle dispersion. The methodology for solving these differential equations is described in Bruse (2004).

2.6. The Heat Square

As introduced in Chapter 1, the Heat Square at the Green Village serves as the case study for this research. To examine the UHI effect at its peak, the field site was prepared for the hottest period of the year. This time frame ranged from the beginning of April 2023 until the end of September 2023, when temperatures are typically at their highest. The climate in the area is classified as a 'temperate maritime climate,' with a measured mean minimum temperature of 13.5°C and a mean maximum temperature of 21.5°C from 1991 to 2020 during July and August (KNMI, 2024). The Green Village is located within the campus grounds of Delft University of Technology, at the coordinates 51°59'48.3"N, 4°22'39.2"E. It houses various research projects, with the Heat Square being a collection of several initiatives focused on understanding and dealing with heat stress in urban environments.

The Heat Square is located near the main entrance of the Green Village. Previously an open square with concrete slabs and no vegetation, it has been renovated to research urban heat stress. This small-scale urban environment serves as a framework for future urban planning, where climate-adaptive innovations and technologies are tested before implementation in real cities (The Green Village, 2024). Figure 2.3 shows the Heat Square (a) before and (b) after renovation in June 2023.

As shown in Figure 2.3b, the new Heat Square consists of two columns of vegetated plots. The bottom three plots in the left column contain a roofing vegetation substrate up to a depth of 40 centimeters, with the underlying soil being the local sandy soil. The four plots in the right column consist entirely of the local sandy soil. This setup was designed to compare the differences in vegetation growth and heat absorption. All of the plots are sown with a mix of plant seeds. Each row undergoes a different frequency of mowing to evaluate the optimal mowing and watering frequency for the vegetation. On the left side of the square, a small plot with artificial grass was installed to compare the differences in surface and soil heating of surface covers with a similar albedo, but without the effect of evapotranspiration. At the bottom, three modules of the 'Urban Jungle Project' are situated. These modules consist of trees suspended on a steel frame, with their root systems not integrated into the soil. Designed as modular units, these trees can be placed anywhere without the need for planting them in the ground.

(a) (b)

Figure 2.3.: Layout of the Heat Square (a) before (Google, 2024) and (b) after (Middelbeek, 2024) renovation.

Various sets of sensors, as well as DTS system, are placed throughout the Heat Square. This was done to provide measurement data for current and future research. The locations of these sensors, as well as the path of the fibre-optic cable for DTS, are shown in Figure 3.1. The fibre-optic cable for DTS is connected to the DTS system in the control room, which is located in the

northeastern part of the Heat Square. Sensors have been installed to measure not only soil and air temperatures, but also air and soil moisture, incoming heat flux into the soil, wind direction and velocity, and heat dispersion and turbulence.

In addition to the different soil profiles, the Heat Square features various types of ground cover. These include dark pavement, light pavement, and sand pavements, each with distinct surface albedos, which results in varying proportions of shortwave radiation absorbed into the soil and consequently different levels of soil heating. The dark pavement is designed to accommodate heavy traffic but has an unusual shape; it starts wide at the bottom and narrows towards the end. Architect Stache (2021) hypothesises that this gradual change in width creates a heat gradient, with more heat in the wider sections and less heat in the narrower sections. This gradient should generate a light breeze, contributing to the cooling of the area (Stache, 2021).

The Heat Square houses several projects conducted by independent researchers and innovators, aimed at evaluating their effectiveness in mitigating heat stress in urban environments. A list of the currently implemented projects is shown in Appendix A.

3. Methods & Materials

3.1. Research set-up: DTS system

The renovation of the Heat Square was primarily driven by its previous condition. The Heat Square was originally surfaced with bare concrete, as shown in Figure 2.3a. Measurements were conducted by Mao (2022) to better understand the UHI effect in The Green Village (TGV). These measurements included air temperature, long and shortwave radiation, and albedo. Mao (2022) suggested conducting temperature measurements at various depths below the surface to assess how ground heat flux contributes to the urban heat balance. Consequently, the Heat Square was redesigned to include fibre-optic cables for DTS beneath its surface, alongside transforming it into a climate-adaptive square (the Green Village, 2023). Another goal of this redevelopment is to study and analyse the urban microclimate under controlled conditions while testing various climate-adaptive solutions to heat stress.

The construction of the new Heat Square, led by construction company Bam, began with foundational work, facilitating the installation of infrastructure, such as a trench at a depth of 60 centimetres for the fibre-optic cable. To ensure an uninterrupted loop without splicing, a large coil of fibreglass cable was strategically placed where the cable transitions from a depth of 60 to 30 centimetres. The cable could be rolled out from the coil at this location. The cable's end was placed near the control room, with additional loops for connections to the DTS system computer and calibration basins. The remaining cable was meticulously laid at the 60-centimetre depth, while marking the distances between every corner the cable traversed through.

After laying the cable at a depth of 60 centimetres, soil was poured and compacted to either 30 or 10 centimetres. The reason for the variance in depth is to leave room for accommodating additional infrastructure like drainage pipes and electricity wiring. The cable follows the same path as that at 60 centimetres, starting near the coil of fibreglass cable. To ensure this, wooden stakes were driven at turning points, allowing identification after soil placement. Some cable sections were encased in ribbed pipes to protect the cable from heavy traffic above. However, this introduces a potential risk of air pockets surrounding the cable, measuring air temperature instead of soil temperature, which may differ (Figure 3.1).

The shallower path (30 or 10 centimetres) received its final layer of soil, making space for pavement construction and vegetation planting. The loose cable ends were directed into the control room through air vents, located in the northeasternmost building along the boundaries of the Heat Square. Both ends of the cable are spliced and connected to the DTS computer (SiliXa Ultima M). Inside the control room, two basins are used for calibration of the DTS measurements. One end of the cable loops through these two basins before connecting to the DTS computer. To ensure proper calibration, the basins maintain constant but different water temperatures. This is achieved by installing a heating element in one of the basins, with a pump to regulate the distribution of heated water, preventing temperature gradients.

Both cable ends are connected to the DTS computer via a E2000/APC connector, enabling the computer to conduct measurements in both directions (Shallow to Deep and Deep to Shallow). This dual-direction capability contributes to error reduction by averaging measurement results. Laser pulses are emitted into each connection every 15.4 seconds. Subsequently, the sensor in the computer measures the Stokes and anti-Stokes backscattering of the emitted light to determine the temperature profile along the cable. The translation from Raman backscattering into temperature measurements and the working principle of DTS has been previously elaborated in Section 2.4. The determination of the temperature along the cable is achieved through an algorithm translating the time and phase change (Raman backscattering) of received pulses into

temperature and location. The calibration and processing of this data are further detailed in Section 3.4. The configuration and installation of the DTS system is demonstrated in Appendix B.

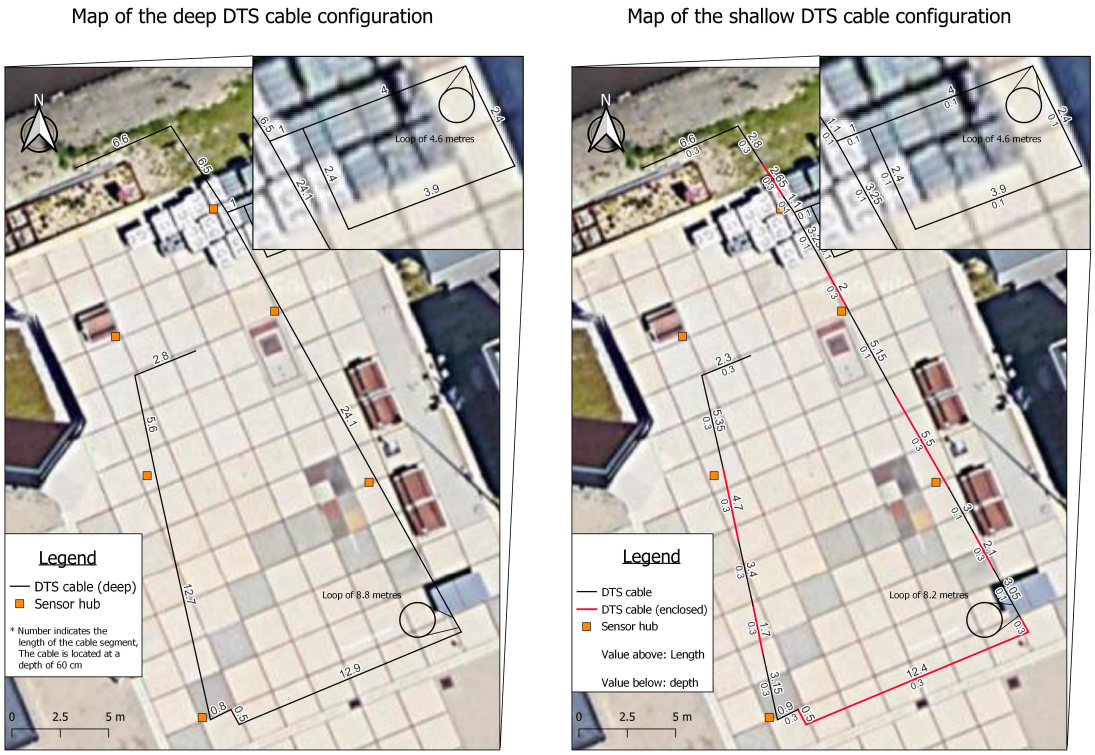

(a) (b)

Figure 3.1.: Fibre-optic cable configuration beneath the Heat Square at the Green Village. (a) "Deep" cable path at 60 centimetres depth. (b) "Shallow" cable path at either 10 or 30 centimetres depth. There are extra loops of cable laid out within the square, to leave room for supplementary DTS measurements in a vertical direction.

3.2. Transformation of DTS data into physical coordinates

To precisely assign a temperature measurement to its specific location within the Heat Square, it is necessary to establish a coordinate system. This system allows for the plotting of the cable path and facilitates the linking of temperature measurements to their corresponding locations. The wooden stakes within Heat Square were left driven into the ground to visually trace the cable path beneath the constructed square. To precisely locate these points, land surveyors were contracted to determine the coordinates of the stakes in the Dutch 'Rijksdriehoekstelsel' coordinate system, to which their land surveying gear is linked.

The data resolution of the DTS system is 25.4 centimetres. To map the outputted data into physical coordinates, it is necessary to know the coordinates at the same resolution. Each plotted point's coordinates were determined by specifying the number of equally spaced points needed between two measured coordinate points (wooden stakes) and obtaining the corresponding coordinates for these points. This process was repeated for every cable section between two wooden stakes, as illustrated in Appendix C. Once all coordinates between the points are known at a 25-centimetre resolution, a continuous list of coordinates can be generated with the correct sequence, spanning from the "shallow" cable to the "deep" cable. To facilitate working with the data, the coordinates were established at a 25-centimtetre resolution. The outputted data from the DTS system can then be resampled to this resolution using Python packages such as xarray or netcdf4.

3.3. Identification of cooling measures

The next step in unravelling the observed temperature profile involves identifying the cooling measures and ground covers in the Heat Square, along with their specific locations. Figure 3.2a delineates the various cooling measures and ground covers implemented during the DTS measurement period of this research. The cable beneath the surface traverses under various types of ground cover and cooling measures, although not all. As previously mentioned, the cable's placement was done carefully to allow space for additional sub-surface infrastructure. Other than the DTS system, other measurement devices were installed underground for supplementary research as well as to verify DTS and CFD measurements. These devices are clustered in different hubs, each logging data from connected measurement devices (Figure 3.1, Figure 3.2a). Figure 3.2a further illustrates the configuration of each data logger in the Heat Square. For a more comprehensive description of each cooling measure and ground cover, please refer to the information provided in Section 2.6.

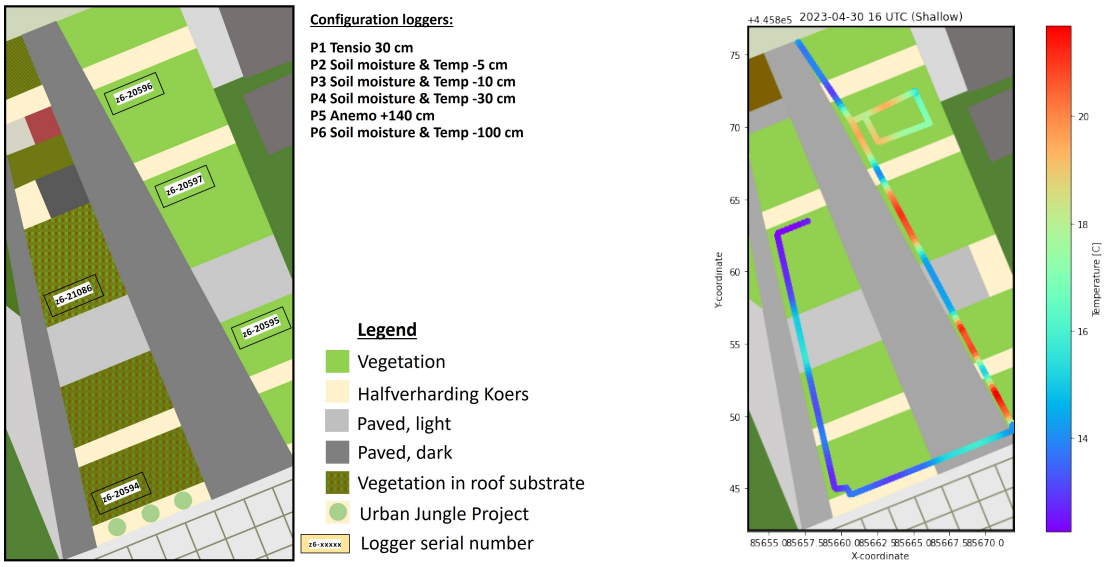

(a) Identification of cooling measures within the Heat Square as well as the data loggers. *Performed by Cheaz, T. and Middelbeek, L. (2023)*

(b) Plot of the shallow cable temperature underneath the Heat Square on April the 30th of 2023 at 16:00 UTC.

Figure 3.2.

3.4. Data workflow

The data output from the DTS system requires preprocessing before it becomes readily usable. The raw data is presented in a series of .xml files per recorded timestep, the frequency of which can be adjusted. This is interesting depending on the scope of the research and its objectives. Each .xml file contains temperature data per Length Along Fibre (LAF) point for a specific timestep. The .xml files are obtained by calling the Python package dtscalibration, developed by B. Schilperoort. These files are consolidated into a single NetCDF (.nc) file for each day of recorded data. The script that accomplishes this conversion is 'DTS_HeatSquare_processing.py,' written by Gijs Vis, one of the supporting researchers for the Heat Square with expertise in DTS. This file not only combines the daily data but also incorporates the calibration of measured temperature using the temperature data from the two calibration basins. The resulting .nc files facilitate the selection of temperature profiles along the cable for specific timesteps or the plotting of temperature variances for individual cable points. This flexibility allows for various approaches to interpret the results.

The .nc data undergoes further analysis using Python programming. Utilising xarray and the coordinates obtained in step 1, one can resample the DTS data to the resolution of the acquired

coordinates and link them together. This allows for a transformation of the data representation from Temperature vs. LAF to Temperature vs. Coordinates. Subsequently, this transformed data can be visualised by plotting the temperature profile within the Heat Square. By overlaying the temperature data on an image with the same coordinate scale as the DTS data, a visual interpretation can be made of the soil temperature beneath the Heat Square along the fibre-optic cable. An illustrative example of such an image is shown in Figure 3.2b.

3.5. Correlation and visualising data

To validate the reliability of the DTS system in measuring soil temperature, tensiometers were placed at depths of 10, 30, and 60 centimeters at different locations near the cable in different plots within the Heat Square. The locations of the tensiometers along with their corresponding plots, are illustrated in Figure 3.3. Notice that there were only tensiometers on five of the eight vegetated plots, this was due to the number of tensiometers available at the time of the study. During the installation of these tensiometers it was ensured that the tensiometers were positioned adjacent to the fibre-optic cable, allowing for direct comparison of soil temperature measurements. If the readings from both the tensiometers and the fibre-optic cable align closely, it would indicate that the DTS system is indeed reliable for validating the results obtained from the ENVI-met model.

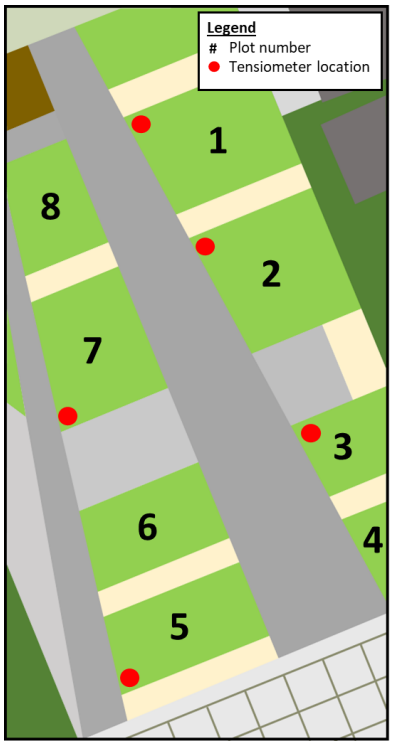

Figure 3.3.: Tensiometer location within the Heat Square, the vegetated pots are given a numbering system for reference.

Temperature data collected from both the tensiometers and the DTS system for the observation dates of September was compared. The location of the fibre-optic cable was cross-checked with the locations of the tensiometers to ensure the same soil was being measured. The temperature at these locations was extracted from both measurement methods for comparison. Given that the DTS system recorded measurements approximately every two minutes, while the tensiometers measured soil temperature every 15 minutes, the DTS data was resampled to match the frequency of the tensiometers. This was done for a direct comparison of temperature data between the two measurement devices at the same time intervals.

The validated data can subsequently be presented in various ways, varying in time and scale. Initially, the temperature profile along the cable fibre offers an indication of temperature variances throughout the Heat Square (see Appendix D). However, it may not clearly indicate the location of a specific temperature value within the Heat Square. An effective alternative is to plot temperature values on their corresponding coordinates. Overlaying this data onto a map of the Heat Square, adjusted to the right scale, provides an immediate comparative result of temperature differences caused by ground cover. Since the cable traverses through different depths under the same ground cover, it may be useful to decide whether to show the shallow or deep path. If displaying the entire cable path is necessary, a third coordinate can be added to the corresponding temperature values (the depth), as illustrated in Appendix D.

Another example of data visualisation, serving a different purpose than visualising the temperature profile, is a point measurement time-series. This displays the diurnal pattern of specific points along the cable, allowing for comparisons of subsurface temperature interactions with atmospheric temperature across different plots or ground covers (see Appendix D). Moreover, it aids in validating DTS measurements against point measurements from the sensors previously

installed beneath the Heat Square (Figure 3.1, Figure 3.2a). Studying subsurface temperature phenomena during diurnal periods can provide insights into which ground covers are most effective in mitigating extreme urban heat.

3.6. Parametrisation of model schematisation

Once the measurements and performance of the DTS system are satisfactory, the next step is to formulate the ENVI-met model for comparing DTS measurements to actual model results. After surveying and determining the parameters of the Heat Square, they can be modelled and input into ENVI-met to simulate the urban microclimate at a desired moment in time. The grid-based model consists of four modules integrated into one aggregated whole.

The ENVI-met model consists of four main components: an atmospheric model, a soil model, a vegetation model, and a built environment & building system model. The selection of ENVI-met is motivated by its capability to generate output parameters on soil data (Gal and Kantor, 2020). Given that this study relies on observations from fibre-optic cables installed in the subsurface, the ability to compare measurements with results from a microclimate model is the main benefit of utilising ENVI-met. Although ENVI-met is commonly used for determining the T_{mrt} (Geletic et al., 2021), other reputable models such as RayMan Pro and SOLWEIG serve the same purpose. Additionally, ENVI-met has been thoroughly validated by various studies, including (Tsoka et al., 2018), who concluded that the model is a valuable tool for urban climate analysis, while acknowledging its limitations in result interpretation.

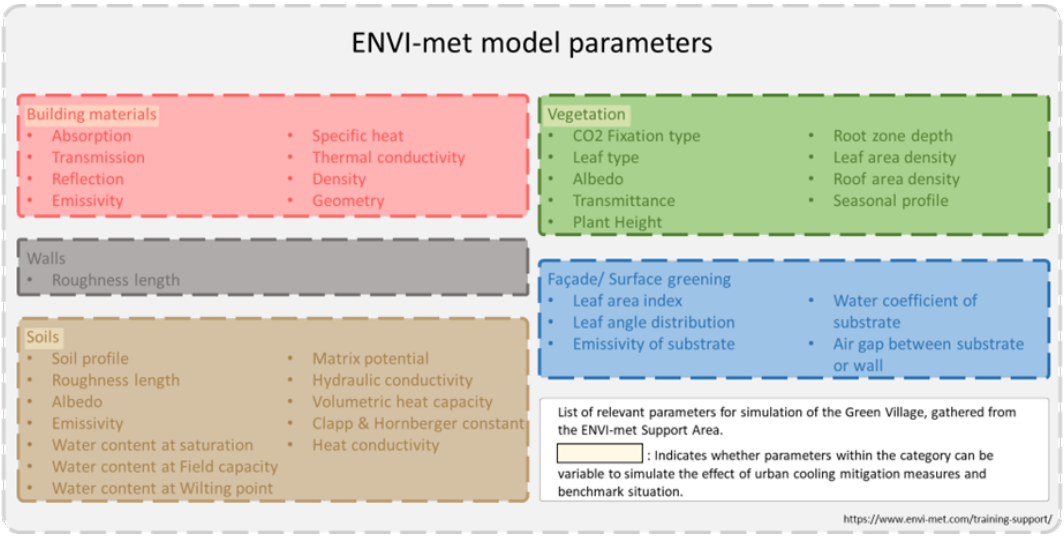

Figure 3.4.: Relevant ENVI-met parameters to be utilised in the schematisation of the Green Village for simulations of base, current, and alternative situations.

The atmospheric model within ENVI-met includes a CFD model to compute the wind field. For a predetermined grid space, the Reynolds averaged non-hydrostatic Navier-Stokes equations are solved for each time step. Drag forces from various surfaces, such as vegetation and facades, are factored into these calculations. The air temperature and air humidity are determined by various modelled sources and sinks of sensible heat and vapour, such as heat and vapour exchange from plants. Furthermore, ENVI-met is capable of modelling the radiative fluxes and the effect of shading and reflections by complex geometries and different materials, as well as turbulence using 2-equation Turbulent Kinetic Energy (TKE) model (ENVI-met, 2023a).

Most relevant to the research study, is the soil model. Within the ENVI-met modelling environment, the soil profile of the case area can be adjusted. The distribution of the soil temperature along the profile is calculated up to a depth of 4 metres, including the interphase interaction at the surface between the soil and the atmosphere. The diffusivity and heat capacity of the soil is formulated as a function of the available water content in the soil (Bruse, 2004). The vertical

resolution varies from 0.01 metres in the uppermost layers to 0.5 in the lowest layers. A water balance is integrated within the soil model to account for the cooling effect of humid soils. The soil hydrology within this model is dependent on the soil water content, the vegetation and its root systems, and water bodies located in the study area.

3D plant and root geometry, vegetation exchange processes, vegetation growth profile, and foliage temperature can be adjusted within the vegetation model of ENVI-met. As expressed in Section 1.3, vegetation has a great effect on decreasing the UHI effect and as such, it is important to properly input the vegetation in an area. Heat and vapour exchange in vegetation is dependent on the atmosphere and soil conditions in the model, and shading from vegetation has an effect on the total heat balance.

Lastly, ENVI-met incorporates a built environment & building system model. While the analysis of building energy performance and indoor climate is possible within this module, it will not be the primary focus of the study. However, the effects of building materials and their geometry on the outdoor heat balance remain of great importance in this study. For each building material it is possible to configure physical properties such as heat conductivity, radiation transmission and heat capacity. Additionally, building geometry can be adjusted to account for shading effects.

With a complete model schematisation, simulations can be run for the desired time period. The resulting output provides a series of data for each of the four modules within the model. Examples of model outputs from a simulation include façade and surface temperature from the built environment & building system model, shortwave/longwave radiation fluxes, soil moisture and temperature, and leaf temperature and transpiration fluxes.

Parametrisation of a large number of variables is essential for a complete model schematisation, hence it is crucial to determine them properly. To achieve this, a comprehensive survey of TGV with a focus on the Heat Square was carried out to determine the geometry and material properties. Figure 3.4 presents a complete list of the parameters required to run a simulation on ENVI-met (ENVI-met, 2023b), Appendix E shows the full list of parameters used in the model schematisation.

3.7. Modelling of the Heat Square

The data collected from surveying and literature was inputted into one base model of TGV. Parametrisation within the Heat Square was conducted with greater detail compared to the rest of TGV. The final iteration of the base model is constructed with a grid size of 0.5 metres in the x, y, and z directions, comprising 190, 320, and 32 cells respectively. After realising that the original model size was too large, it was reduced to 157 by 141 by 32 cells. This downsizing focused the analysis on the area surrounding the Heat Square while also reducing the computation time needed to complete a simulation.

Beneath the surface, the cells were further divided into smaller units, starting at 0.1 meters, to model soil temperature in greater detail. Once the parametrisation is deemed satisfactory, the simulation can be initiated. A satisfactory result is achieved when the simulated results closely approximate the temperature profile provided by the DTS system, allowing for some margin of error, provided that the time allocated for this study permits improving on parametrisation. Preferred boundary conditions for the simulations include no precipitation, low cloud coverage, relatively high atmospheric temperatures, and low wind speeds. This combination of conditions often contributes to high urban air temperatures, particularly in terms of weather forcing.

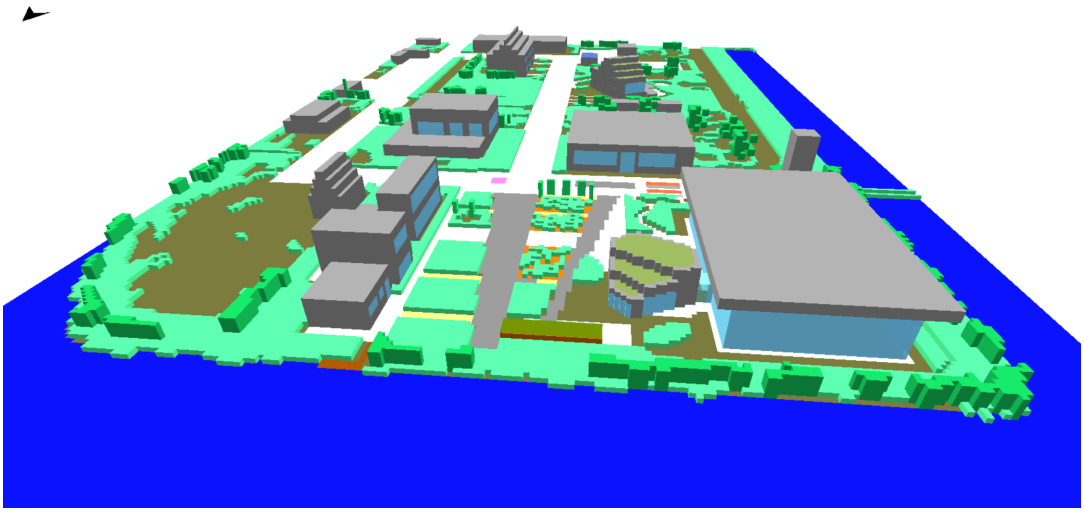

Figure 3.5.: Base model schematisation of the Green Village for ENVI-met simulations.

Based on weather data obtained from TGV and The Royal Netherlands Meteorological Institute (KNMI), simulations were conducted with weather forcing for two specific dates: the 17th of June 2023 and three consecutive days from the 7th to the 9th of September 2023. These dates were selected based on the aforementioned weather forcing criteria. The conditions of the Heat Square were surveyed on these dates to provide the correct input for the simulations.

Due to the substantial computational resources required for these simulations, they were computed using the Renderfarm service of the Faculty of Architecture at TU Delft. The Renderfarm allows the computation of simulations through a virtual computer, which can facilitate simultaneous computations of multiple simulations. The time needed to complete a model simulation of the Heat Square can vary significantly, ranging from 24 hours to 5-6 days, depending on the desired simulation duration, grid resolution, and model size.

3.8. Correlation measurements and model

The ENVI-met simulations yield various results, with soil temperature being of primary interest. From the soil parameters output, the temperature along the same trajectory as the cable of the DTS system is extracted. The ENVI-met results are selected from the corresponding depth of the fibre-optic cable and organised in the correct sequence to replicate the DTS system. By aligning the temperature profile obtained from the DTS system with an 'imaginary' cable temperature profile derived from the ENVI-met results, a direct comparison can be made between the two.

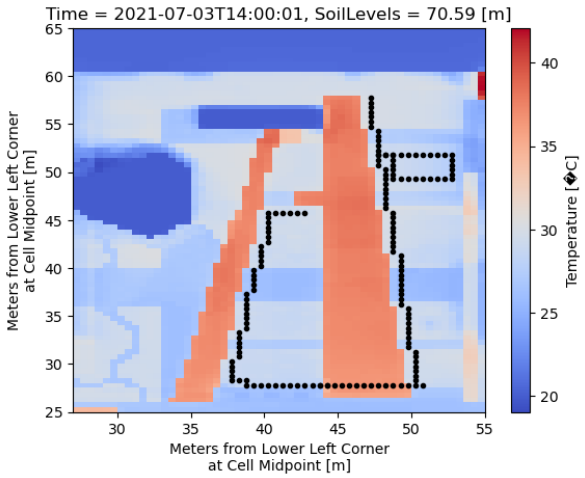

Figure 3.6.: Path the 'virtual' fibre-optic cable takes from the ENVI-met results

If the correlation between the DTS system and ENVI-met soil temperature results is not satisfactory, an alternative approach is to compare the ENVI-met model results to air temperature measurements within the Heat Square. The air temperature measurements from various anemometers placed within the Heat Square are plotted against

the air temperatures at the same locations in the ENVI-met model. The locations of these anemometers correspond to the sensor hubs shown in Figure 3.3. The anemometers used for these measurements are the ATMOS 22 ultrasonic anemometers provided by METER Group, installed at a height of 1.5 meters. Initially, these anemometers were installed to measure wind speed and direction for a different project, but since they also provide air temperature data, there was no need to install additional air temperature sensors.Given that ENVI-met is primarily used for air and surface temperature simulations, confirming that the air temperature matches the actual conditions as much as possible is of great importance.

3.8.1. ENVI-met model iterations

Given that the initial parametrisation of a model rarely results in a perfect approximation, the ENVI-met model of the Heat Square underwent several iterations. The final model reached a total of seven iterations, with successful simulation runs that did not result in crashes. Most modifications involved adjustments to parameters or materials, as well as changes to weather forcing conditions.

Out of the seven iterations, iterations 3, 5, and 7 showed improvement in the approximation of the results. On the other hand, iterations 2 and 4 did not result in any improvement or led to a worse approximation. The results from the final iteration (iteration seven) are used as the benchmark for comparison with the DTS system results and the outcomes from various modelled scenarios, as further detailed in Section 3.9.

The following sections describe the key modifications made in each of the important iterations to provide insight into the process leading to the final iteration. A visual representation of each iteration can be seen in Appendix F

First iteration

The initial iteration consisted of the entire Green Village, using light pavement, dark pavement, local soil, and grass for the ground surfaces. Buildings featured roof greening, windows, and standard insulated walls. The Green Village's geometry was mapped using a bitmap from Google satellite maps to ensure accurate building proportions, and the height of each building was surveyed and incorporated into the model. This initial model used only materials available in the program library and served as a test to verify that the simulation would run smoothly without errors, given the current resolution, geometry, and forcing settings.

For the simulation forcing of this first iteration, the 6th June was selected, and the weather forcing was used to run a 24-hour simulation. After computing for the first three hours, the model crashed due to a floating point error. This error was likely caused by wind forcing being too high for the model resolution, the upper model boundary being too close to the tallest building, or the boundaries of the model being too close to building geometry. To solve these issues, several adjustments were attempted:

1. Reducing the wind forcing to lower the flow.
2. Increasing the number of cells in the vertical direction (z-axis).
3. Creating an invisible grid boundary that extends beyond the model grid to prevent turbulent wind errors near the computed edge of the model.

After multiple attempts, it was found that the most effective solution, which minimally impacted computational time, was to decrease the wind forcing slightly while increasing the vertical grid size. Additionally, other dates with minimal wind were identified, and the selected day was changed to June 17th.

Third iteration

Changes implemented in the model simulation include extending the simulation period from 24 hours to 3 days and focusing on a smaller model area centered on the Heat Square. This adjustment was made because soil temperatures are heavily influenced by localised conditions, and simulating areas outside the Heat Square, such as the southern section of the Green Village, was deemed unnecessary. The chosen simulation period spans from September 7th to 9th, 2023,

characterised by generally clear skies, minimal wind, and relatively high temperatures for the season. If the 3-day duration proves adequate for model spin-up, future simulations will adopt these same weather conditions.

Fifth iteration

In earlier model schematisations, the ENVI-met software library's existing tools were used to input soil profiles, material properties, and vegetation characteristics. For this model iteration, albedo values were measured on-site and applied to the various surfaces within the Heat Square. Additionally, soil properties were updated based on the specifications from BAM, the construction company responsible for the site's soil distribution. Different soil types were placed in specific areas to investigate their effects on vegetation growth and cooling performance.

In summary, this updated model incorporates user-defined soil profiles and material properties to achieve a closer match with soil temperatures measured by the DTS system's fibre-optic cable. Albedo values of the various surface covers were measured as one of the properties to be input in the model (Table 3.1). Given the already substantial computation time required for a three-day simulation, the decision was made to maintain the same simulation settings as in the third iteration. Consistent weather forcing was used to facilitate a direct comparison of simulation results. This approach led to the successful completion of the fifth simulation, which produced results in ENVI-met without any crashes or errors.

Table 3.1.: Measured albedo values for different ground covers within the Heat Square

Date [dd-mm-yyyy]	Time [hh:mm]	Ground cover	Albedo [-]
30-06-2023	12:50-13:08	Semi-pavement	0.23
30-06-2023	13:14-14:24	Vegetation in sandy soil (z6-20597)	0.19
30-06-2023	13:29-14:50	Pavement, light	0.21
30-06-2023	15:55-15:15	Pavement, dark	0.13
30-06-2023	15:20-15:30	Roof substrate, no vegetation (z6-21086)	0.12
30-06-2023	15:32-15:44	Artificial grass	0.09
30-06-2023	16:15-16:30	Concrete tile(Hydrogen Square)	0.14

Seventh iteration

The seventh iteration of the Heat Square was the final attempt to approximate the soil temperature from the ENVI-met model to the temperature results of the DTS system. These results from this final iteration also provide the benchmark results to compare different scenarios and model schematisations. Due to previous improper measurement of the surface cover parameters, it was decided to use the material properties already provided in the software, selecting those that best represent the composition of the Heat Square. A benefit of this approach is the reproducibility of using the same model schematisation to perform simulations of the Heat Square for future research. Apart from this change, the geometry, weather forcing, and simulation settings were kept the same to facilitate easier analysis between the current and previous iterations.

3.9. Modelling and simulating scenarios

The results from ENVI-met initially provide qualitative insights into the heating/cooling effects of different types of ground covers and heat mitigation measures. To compare the performance of each ground cover or heat mitigation measure in cooling the urban environment, different model schematisations will be simulated. These simulations will enhance the presence of specific ground covers or heat mitigation measures solely within the Heat Square (within model constraints). The ground covers and mitigation measures can be found in Section 2.6. Additionally, a simulation will be conducted to assess the performance of the Heat Square before the new and improved design was constructed. This allows for an evaluation of how much the new design reduces urban heat compared to the previous situation.

The final simulation performed will serve as the benchmark case for the results. From this benchmark case, comparisons can be made to extreme weather scenarios, including one with

extremely hot weather based on one of the Representative Concentration Pathways (RCP) scenarios, and one without water around TGV (as it is hypothesised to provide a substantial cooling effect on the Heat Square). Given the high resolution of the current schematisation, it is also interesting to compare the results of the benchmark case to a lower resolution model of the Heat Square. If the results are similar, conclusions can be drawn regarding the feasibility of applying ENVI-met on a larger scale to map the urban heat island effect. A model with lower resolution requires less computation time, and if the quality of the results does not deteriorate significantly, it would allow for simulations to be run over longer forcing periods or across larger model grids. Running longer simulations times allows for an improved model initialisation to better approximate the real-life conditions. Additionally, mapping the urban heat island effect in larger areas can significantly contribute to a better understanding of the widespread impact of heat mitigation measures or ground covers.

Table 3.2 provides a summary of the different scenarios, including a description of the modifications made to the model in comparison to the benchmark model.

Table 3.2.: Modelled scenarios in ENVI-met and changes done with respect to the benchmark model.

Model scenario	**Model changes**
Concrete square	Heat Square is replaced by situation prior to construction of the current design, consists predominantly of bare, light coloured concrete.
Cooling measures	Enhanced heat stress mitigation: dark concrete pavement is replaced by light concrete pavement, and an increased amount of tall vegetation.
Low-resolution	Model grid size is increased to 1 x 1 x 1 metres. Model was simulated with similar weather forcing for 144 hours instead of 72 hours.
RCP2.6	Weather forcing is increased according to RCP2.6 scenario, with an overall air temperature increase of 1.7°C.
No-water	Water body surrounding the Heat Square is removed and replaced by low vegetation (i.e. grass, shrubs, and hedges).

4. Results

The results section of this study follows the methodology structure outlined previously, with the primary objective of addressing the research questions. The analysis begins by examining and describing the results obtained from the DTS system. Subsequently, these findings are compared to the results derived from the ENVI-met simulations which are supposed to reproduce the DTS measurements. The final simulation results from ENVI-met show the resulting urban microclimate phenomena of various model scenarios in the simulated environment.

4.1. DTS measurements

The DTS system became fully functional following its installation by the end of March 2023. The optimal timeframe for analysis was determined based on the local climatic conditions. The UHI effect exerts the most significant impact during dry and hot weather conditions, characterized by minimal wind and cloud cover, allowing maximum shortwave radiation to penetrate to the urban environment. With that in mind, three consecutive days from the 7th of September 2023 to the 10th of September 2023 were chosen to analyse soil temperature within the Heat Square. During this period, air temperatures ranged from a maximum of 31°C to a minimum of 19°C. The wind speed peaked at 4 m/s, with an average speed of 2 m/s. These are favorable wind conditions for the ENVI-met model, as excessively high wind speeds can lead to floating point errors in the simulation. Cloud cover, denoted as the ratio of sky cover in eighths, was observed to be 2/8. These measurements were collected from both the weather station installed at TGV and the KNMI weather station located in Rotterdam. The local timezone for TGV is UTC+2, which will be referred to as Local Time (LT) for better readability.

4.1.1. Fibre-optic cable

The temperature profile of the fibre-optic cable on the 9th of September at various times is depicted in Figure 4.1. The data is plotted as Temperature per LAF. The measurement starts at the northern point of the Heat Square near the control room, originating from the shallow cable section. The cable traverses through the Heat Square and transitions into the deep section at an estimated LAF of 211 metres. It is noticeable that the measurements commence at an LAF of 114 metres and conclude at an LAF of 308 metres. This is attributed to the 114-metre length required for the cable to reach the Heat Square from one of the connectors attached to the DTS system in the control room. Beyond 308 metres, additional cable extends back into the control room, back into the DTS computer. While the system performs measurements of these other sections as well, the focus is primarily on the cable situated beneath the Heat Square. Hence the data is displayed to the LAF corresponding to the Heat Square.

Figure 4.1 demonstrates a significant difference in the temporal variation of soil temperature between the shallow and deep cable paths. The temperature variance in the deeper soil does not exceed a temperature difference of 0.4°C throughout the day, whereas in the shallower soil, the temperature can fluctuate by up to 6°C on the 9th of September 2023. This suggests that changes in soil temperature in deeper subsurfaces require longer timescales to manifest; diurnal climatic variances are too brief to induce substantial changes. Seasonal variances are an example of timescales where notable changes in the soil temperature of deeper layers occur. The sharp fluctuations in temperature throughout the temperature profile further illustrate that heat in the soil primarily propagates in a vertical direction, with horizontal temperature variations influenced mainly by the surface above.

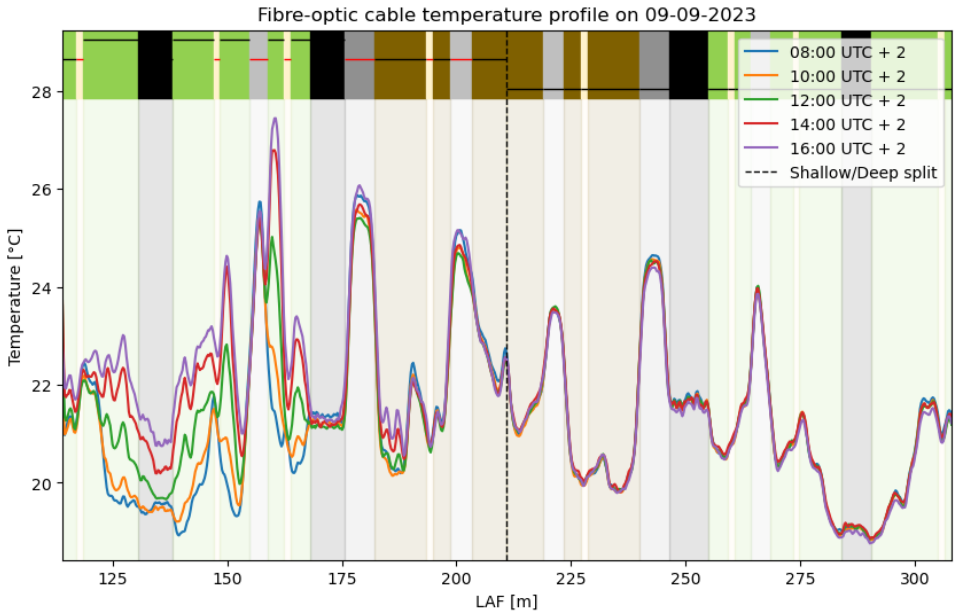

Figure 4.1.: DTS measurements on the 9th of September, displaying the temperature profile from the shallow (starting from the left) to the deep sections of the fibre-optic cable. The coloured band indicates the surface above the location of the fibre-optic cable; green = vegetation on local soil substrate, beige = sandy pavement, black = cable loops, light grey = light concrete pavement, dark grey = dark concrete pavement, brown = vegetation on roofing substrate (see Figure 3.2a). The lines on these coloured bands indicate the depth of the cable (10cm, 30cm, or 60cm) as well whether or not the cable is encased by a ribbed pipe (red).

To illustrate the temperature variation on a seasonal timescale, the temperature profile through the fibre-optic cable is depicted in Figure 4.2. At this timescale, it becomes evident that the deeper section of the cable is also influenced by climatic conditions above the surface. The temperature profile shows a similar trend, with soil underneath paved or unvegetated surfaces showing high peaks in temperature (with the exception of the sandy pavements). Conversely, on the 27th of March, a relatively cold day, the soil underneath paved and unvegetated surfaces experienced extremely low temperatures compared to the rest of the cable, particularly in the shallow sections. This suggests that increasing vegetated surfaces in the urban environment may lead to more moderated temperatures and mitigate extreme temperature fluctuations.

The DTS system conducts and processes a full measurement approximately every 125 seconds. To visualize the vast amount of available data, a contour plot can be generated, as shown in Figure 4.3. Similar to previous plots, the division between the shallow and deep cable sections is indicated by a dashed line at an LAF of around 211 metres.Individual plots of the shallow and deep sections of the fibre-optic cable are shown in Figure 4.4. As previously mentioned, the temperature in the deep sections of the cable exhibits minimal fluctuations. When observing the aggregated contour plot of both the shallow and deep sections, it appears as though the temperature remains constant. In the shallow section of the cable, the highest temperatures are observed around 17:00 LT. This is logical since heat requires time to penetrate to deeper layers, resulting in a lag in time between the warmest surface temperatures and the warmest soil temperatures. This lag is evident within the contour plot of the shallow section itself; for instance, the cable reaches its highest temperature at an LAF of 160 metres around 17:00 LT, while at an LAF of 180, it peaks around 21:00 LT. Notably, the cable is situated at depths of 10 centimetres and 30 centimetres at LAFs of 160 metres and 180 metres, respectively. Similar observations can be made when identifying the coldest point of the day, such as examining the temperature variation at an LAF of 140.

Although the contour plot provides an initial understanding of the thermal behavior of the soil beneath the Heat Square, plotting the measured soil temperature in the Heat Square can provide a further understanding of its thermal behavior and the individual impact of each ground cover.

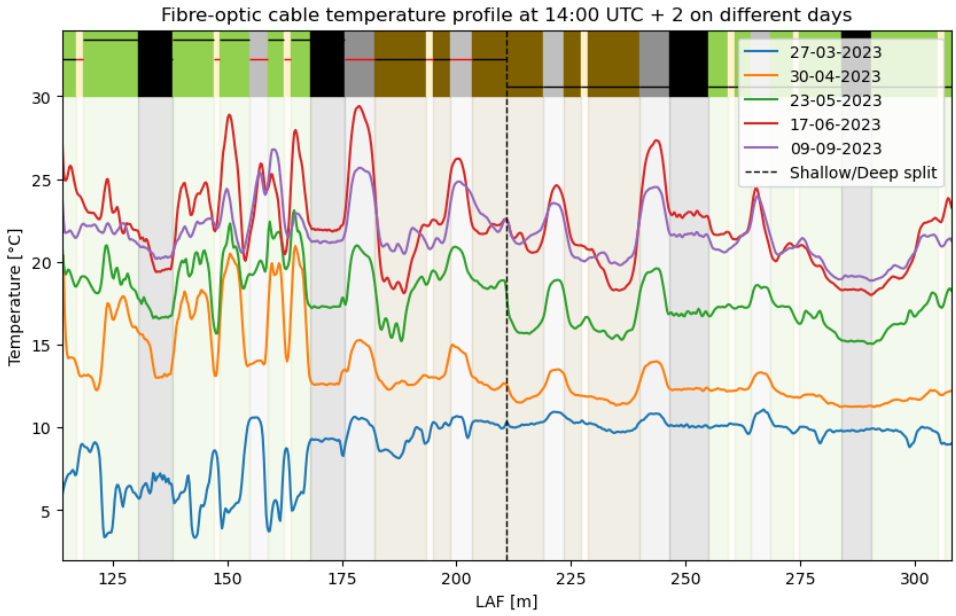

Figure 4.2.: DTS measurements on different dates at 14:00 UTC+2, displaying the temperature profile from the shallow (starting from the left) to the deep sections of the fibre-optic cable. The coloured band indicates the surface above the location of the fibre-optice cable; green = vegetation on local soil substrate, beige = sandy pavement, black = cable loops, light grey = light concrete pavement, dark grey = dark concrete pavement, brown = vegetation on roofing substrate (see Figure 3.2a). The lines on these coloured bands indicate the depth of the cable (10cm, 30cm, or 60cm) as well whether or not the cable is encased by a ribbed pipe (red).

Such a plot can be seen in Figure 4.5. The shallow section of the cable exhibits variable depths and is also encased by a ribbed pipe to protect it from heavy traffic, as illustrated in Figure 3.1. Unfortunately, this configuration does not provide a complete picture of the soil temperature at depths of either 10 centimetres or 30 centimetres. However, as observed in previous results, soil temperature patterns in horizontal direction are propagated vertically, allowing for a qualitative assessment of the soil temperature in areas with missing spatial data.

In the two-dimensional plots, the measurements show that the soil directly beneath the stone pavement is notably warmer than the surrounding soil. Generally, soil beneath vegetated areas appears cooler than the surrounding soil, regardless of whether it is the local sandy soil or the roof substrate soil. In the shallow section of the cable, the soil temperature beneath the sandy pavement is cooler, whereas in the deep section, this cooling effect is less noticeable. An interesting anomaly in the shallow section is observed in the vegetated plot on the right, the second one from the bottom. While vegetation typically results in soil cooling, this plot registers the highest temperature along the cable during that measurement. This anomaly is likely due to the plot being excavated for drainage system installation a few days prior to the measurement, resulting in the removal of vegetation and predominantly bare soil, increasing the heat transmitted into the soil.

To display both the shallow and deep temperature profiles within the Heat Square in one figure, the data can be presented as a cable in a three-dimensional plot like in Figure 4.6. This approach allows for a better spatial understanding of the temperature differences between depths. As noted earlier, it is evident that soil temperature at greater depths exhibits less variation and is cooler at 14:00LT compared to lower depths. The coldest measured temperature is found beneath the Urban Jungle Project at a depth of 60 centimeters. This area is furthest from the dark pavement and closer to the surrounding buildings, suggesting that a combination of sandy pavement and shade results in the lowest soil temperatures. Conversely, the highest measured temperature is located beneath bare soil at a depth of 10 centimeters. Furthermore, the heating of the soil is attenuated in deeper layers beneath the stone pavement sections, with temperatures decreasing by approximately 1.5°C from a depth of 30 centimeters to 60 centimeters.

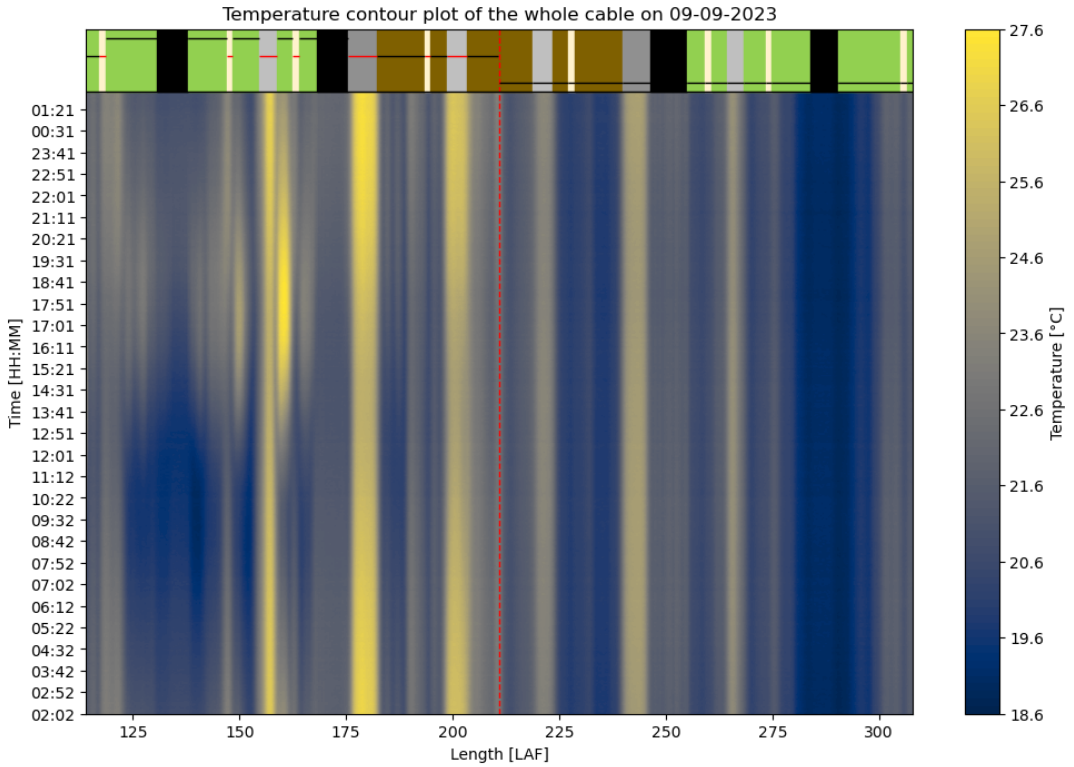

Figure 4.3.: Contour plot of the DTS measurements on the 9th of September, displaying the temperature profile from the shallow (starting from the left) to the deep sections of the fibre-optic cable. The coloured band indicates the surface above the location of the fibre-optic cable; green = vegetation on local soil substrate, beige = sandy pavement, black = cable loops, light grey = light concrete pavement, dark grey = dark concrete pavement, brown = vegetation on roofing substrate (see Figure 3.2a). The lines on these coloured bands indicate the depth of the cable (10cm, 30cm, or 60cm) as well whether or not the cable is encased by a ribbed pipe (red). The temperature is plotted approximately every 125 seconds.

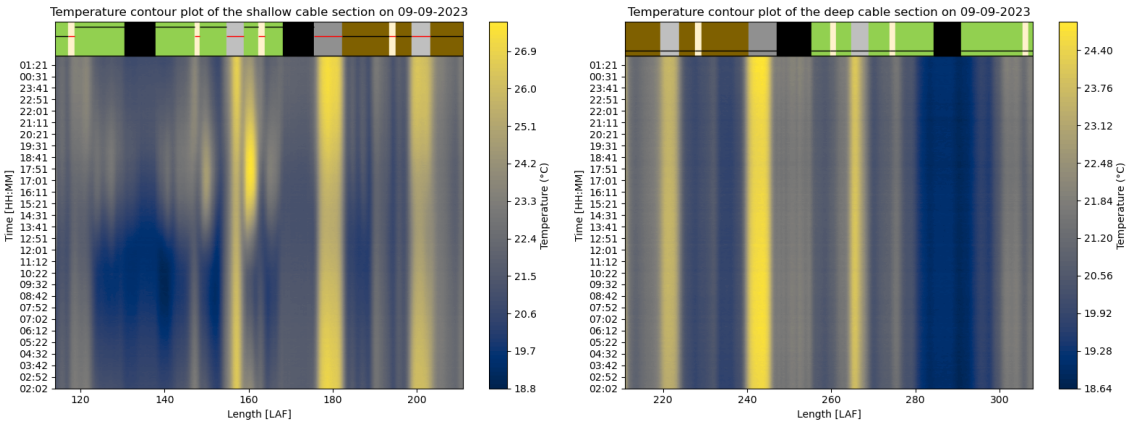

Figure 4.4.: Contour plots of the DTS measurements on the 9th of September, displaying the temperature profile in the shallow (left) and deep (right) sections of the fibre-optic cable. The temperature is plotted approximately every 125 seconds.

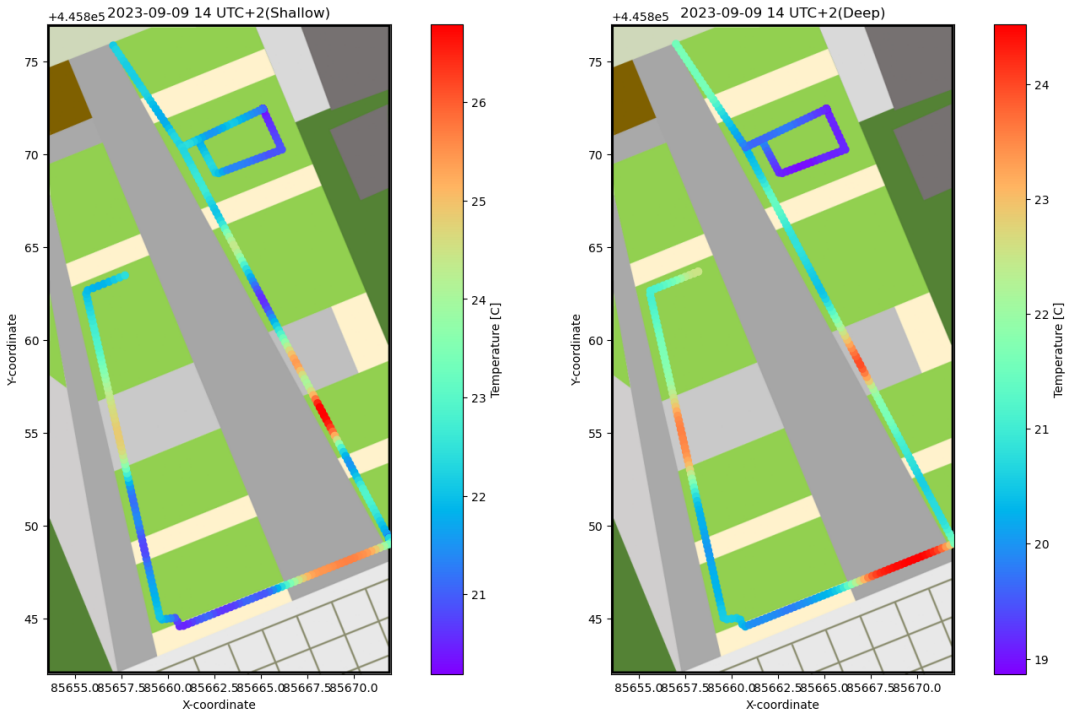

(a) (b)

Figure 4.5.: Temperature plot along the fibre-optic cable in a top down view of the Heat Square. The plots provide a snapshot of the soil temperature at 14 UTC+2 on 09-09-2023 for both the (a) shallow and the (b) deep sections of the cable.

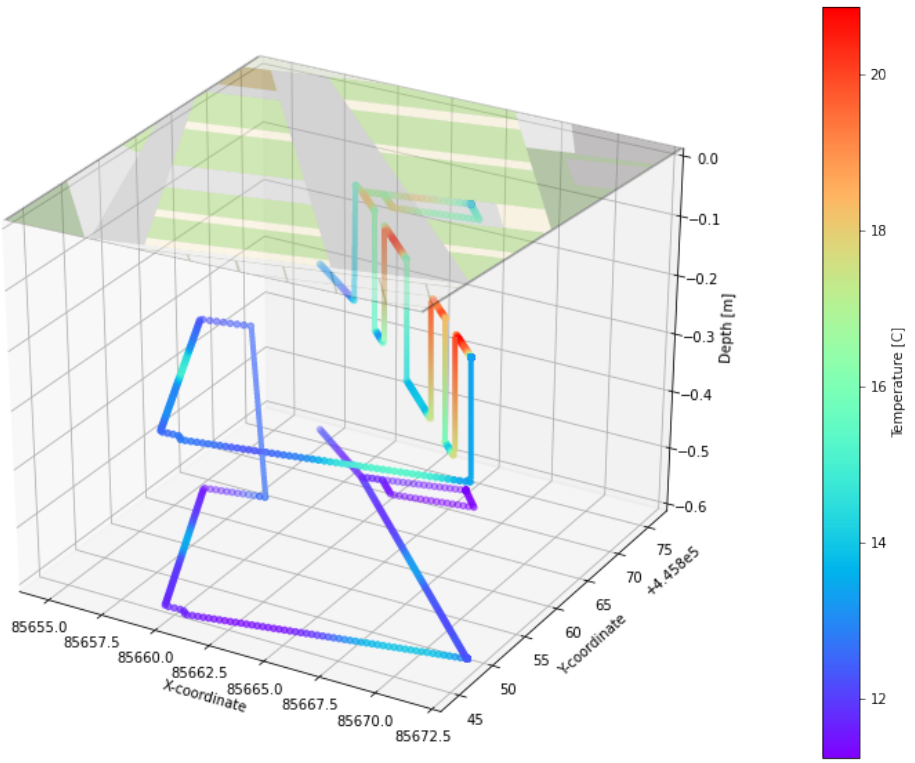

Figure 4.6.: 3D-plot of the DTS measurements on the 9th of September, displaying the temperature profile measured by the DTS system with respect to its location in the soil. Note that the plot is not plotted in scale to facilitate the view of the plot.

4.1.2. Correlation tensiometers

Figure 4.7 demonstrates the soil temperature plotted at the locations of the tensiometers within the Heat Square. Generally, the measured temperature from the DTS system closely aligns with that from the tensiometers. However, there are some discrepancies noted, particularly in plots 2 and 5 (refer to Figure 3.3 for plot locations). Conversely, plots 1, 3, and 7 show a satisfactory match between the DTS and tensiometer measurements. This validation step is essential for future steps, to ensure that the DTS system is a trustworthy metric to compare the results of the ENVI-met simulations.

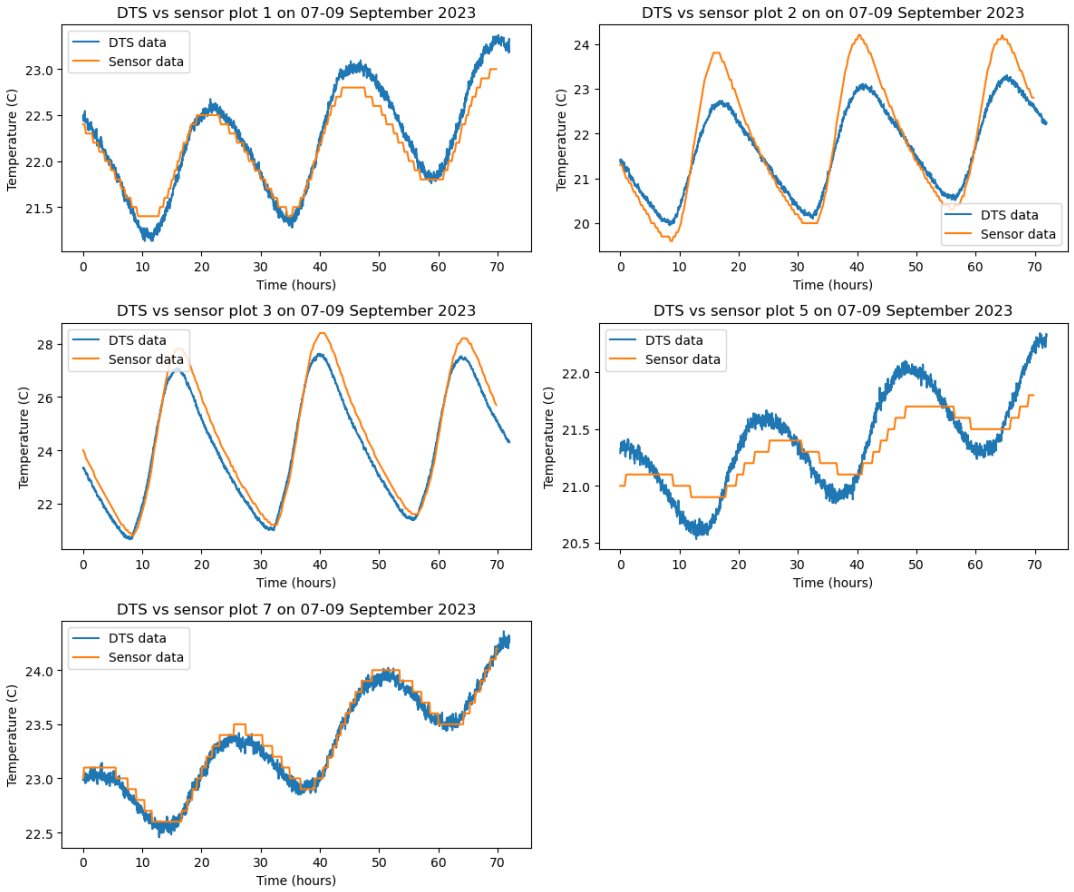

Figure 4.7.: Soil temperature measurements from the DTS system and the tensiometers installed within the Heat Square. The data shows the temperature measured from the study timeframe of 7th of September 2023 up until the 10th of September 2023. The DTS data is provided with an accuracy of up to 8 decimals in °C whereas the tensiometer data measures the temperature with an accuracy of 1 decimal in °C.

In plot 2, while the DTS system captures the diurnal pattern of soil temperature reasonably well, it fails to match the high temperature peaks recorded by the tensiometers. This inconsistency could stem from slight displacements of either the tensiometer or the fibre-optic cable post-installation, likely due to ongoing construction activities in the area. Presumably, the tensiometer is located at a slightly shallower depth than the fibre-optic cable at this location due to the low and high values being more extreme, but not much shallower that there is a lag in the diurnal pattern of the soil temperature. Similarly, in plot 5, both the diurnal pattern and the extreme temperature values do not align between the DTS and tensiometer measurements. Here, it is probable that the tensiometer is situated deeper in the soil than the fibre-optic cable, resulting in attenuated temperature values and a lag in the diurnal pattern. Construction activities might have led to the displacement of either sensor, causing them to end up in different locations.

Figure 4.8 presents the correlation between the different tensiometers and the DTS system in a single plot. This correlation plot provides a visual representation of how closely the temperature

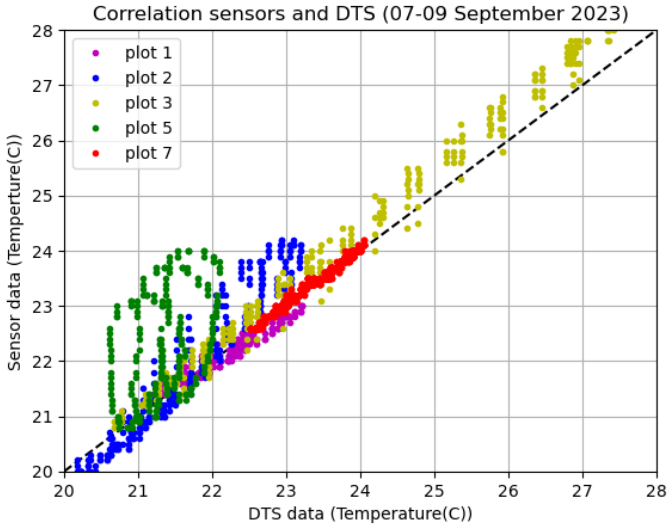

Figure 4.8.: Correlation plot between the DTS system and tensiometers installed within the Heat Square. The temperature measured by the DTS system is plotted on the x-axis and the temperature measured by the tensiometer for the same time and location is plotted on the y-axis.

measurements align. If the plotted data points follow the dashed line, it indicates that the DTS system and the tensiometers measure roughly the same temperature. As previously mentioned, it's evident that the measurements in plot 2 exhibit discrepancies, particularly regarding the high temperature peaks. Consequently, for the higher temperature range, the data points deviate upwards from the expected correlation line. In plot 5, the temperature measurements demonstrate much lower correlation, resulting in more scattered data points across the plot.

4.1.3. Thermal behaviour per cooling measure

The cooling strategies implemented in the new Heat Square include increased vegetation, compacted sand pavement by Koers, light-coloured pavement, dark-colored pavement, vegetation in roof substrate, and planted trees with root system not integrated into the soil. While the direct effect of each cooling strategy is not entirely clear from the DTS measurements alone, preliminary assumptions can be drawn from the measured temperature results:

- It is evident that dark pavement significantly contributes to soil heating, while lighter pavement reduces this effect but still contributes to heating. Compacted sand pavement appears to prevent the soil underneath from heating up as much as surrounding soil, likely due to its relatively high albedo.
- The impact of roofing substrate on thermal behavior compared to local sandy soil is unclear, as both show similar temperatures in the deep section of the cable at a depth of 60 centimeters.
- Vegetated surfaces notably cause cooler soil temperatures, as seen in the loop of cable on the north part of the Heat Square being considerably cooler than the rest of the cable for both shallow and deep cable sections. Moreover, sections with bare soil and minimal vegetation exhibit the highest soil temperatures along the cable, highlighting the cooling impact of vegetation on soil temperature.
- Regarding the cooling effect of trees in the southernmost compacted sand pavement, periodic cooling is observed, aligning with the locations of the trees above the ground. This cooling is likely due to the shadow cast by the trees intercepting incoming shortwave radiation, providing a cooling effect on the soil throughout the day.

4.2. ENVI-met results

The validation process of the ENVI-met model involves comparing soil temperatures at different depths simulated by the model with those measured by the DTS system. After multiple iterations and simulation runs to refine the model, additional parameters beyond soil temperature—such as air temperature and T_{mrt}—are analysed. The aim of this approach is to assess the suitability of the ENVI-met model for accurately simulating sub-surface conditions in an urban environment. Once validated, the model can be utilised to compare various cooling strategies and their impacts on the urban microclimate. This chapter will describe some of the steps taken to refine the model and the troubleshooting involved, which resulted in the final versions of the model.

4.2.1. Model iterations

First iteration

After running the first successful 24-hour simulation, which modelled TGV with a timestep of one hour, it was clear that the model required a certain 'spin-up' time to initialise properly. As shown in Figure 4.9, there is a comparison between the measured temperatures on June 17th by the DTS system and the modeled temperatures on the same date by ENVI-met, following the profile of the DTS system's fiber-optic cable. It is evident that the model exhibited very little variance in soil temperature, which is expected because it takes considerable time for temperature changes to penetrate deeper soil layers. The shallow sections of the cable show some variance, but compared to the DTS measurements, the deeper sections of the modelled temperature display minimal variation. Ignoring the scale of temperature variance, the simulated results also do not exhibit similar 'peaks and valleys' in the graph. This indicates that the difference in soil thermal behavior caused by surface properties is not well represented by the ENVI-met model.

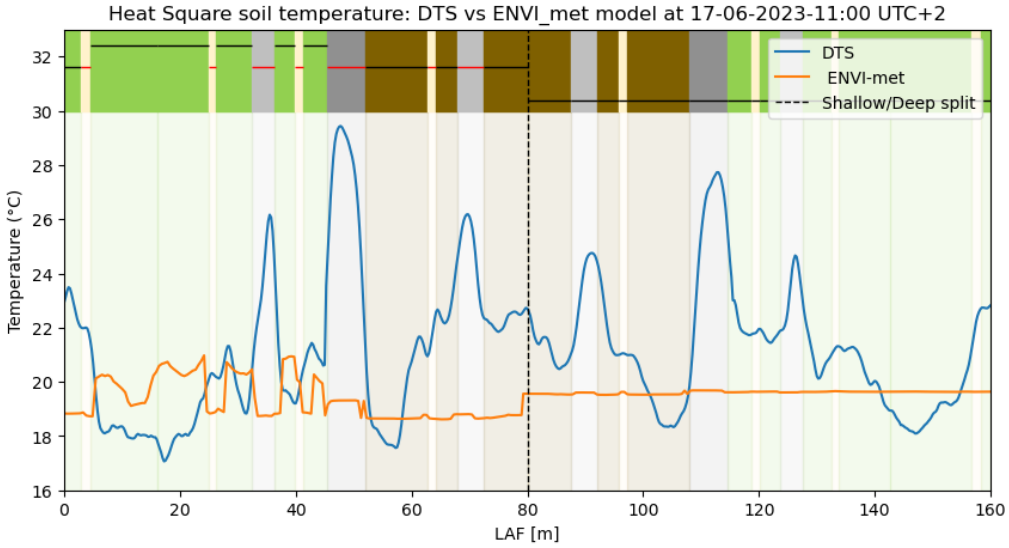

Figure 4.9.: Temperature profile of the fibre-optic cable plotted in LAF versus Temperature on the 17th of June 2023 at 11:00 UTC + 2. The orange line plots the temperature of the simulated 'virtual' fibre-optic cable as a result from the ENVI-met model (first successful simulation).

To examine a broader timeframe rather than just a snapshot of the day, diurnal temperature plots are provided in Figure 4.10. Specific points along the fiber-optic cable within the Heat Square are plotted to determine if the thermal behavior is well represented in the soil's diurnal pattern. The temperature anomalies for all plots are too significant to be considered a good fit for the DTS system. The only simulated point that even remotely resembles the actual DTS measurement is the modeled soil beneath the bright stone cover; the maximum temperature difference is approximately 1.5°C, and the lowest value occurs around the same time at 11:00 LT. However, the highest value of the fiber-optic cable is at 19:00 LT, while the highest temperature of

the ENVI-met model is at 23:00 LT. It is important to note that ENVI-met only outputs simulation results with a time resolution of one hour.

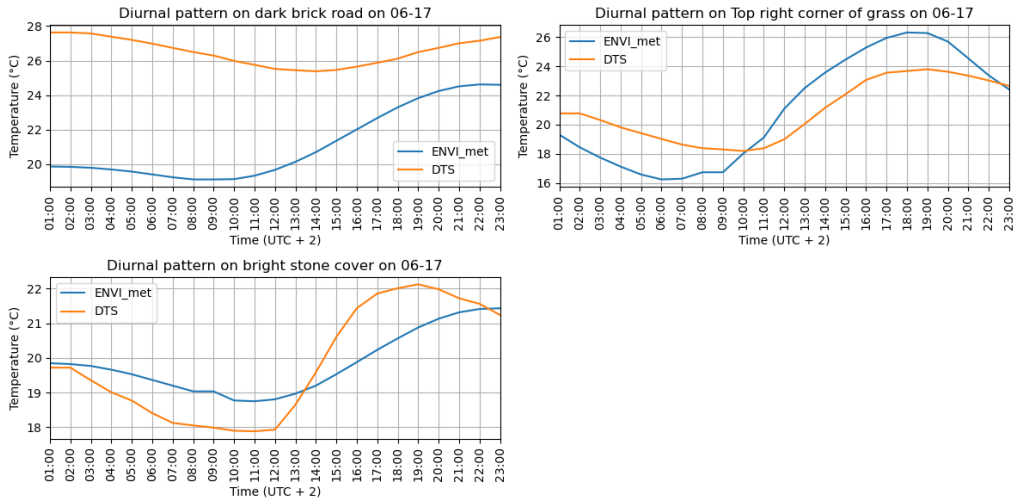

Figure 4.10.: Temperature profile of the fibre-optic cable plotted in time versus Temperature at 30 cm on the 17th of June 2023 at specific points of the fibre-optic cable. The blue line plots the temperature of the simulated 'virtual' fibre-optic cable as a result from the ENVI-met model (first successful simulation).

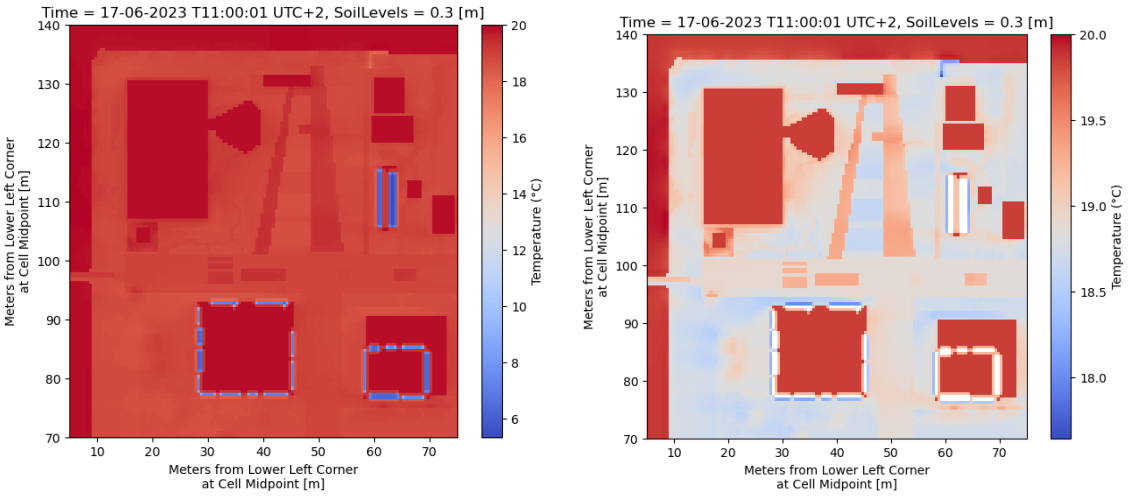

(a) (b)

Figure 4.11.: Soil temperature plot of the Heat Square at a depth 0.3 metres at 11:00 UTC+2 on the 17th of June 2023 (first successful simulation). The image on the left displays shows the unfiltered temperature values while the image on the right shows the same plot after removing extreme values from simulation errors

Figure 4.11a provides a representation of how ENVI-met computed the soil temperature at a depth of 30 centimeters. Notably, the soil temperature below some of the windows of the buildings is extremely low compared to the rest of the soil, with values that are quite unrealistic. By running the model for a longer duration, we aim to eliminate these errors. A plot of the soil temperature at a depth of 30 centimeters is shown in Figure 4.11b, with the anomalies removed. Here, the soil temperature beneath buildings and water bodies appears warmer than the rest of the soil, even though it is known that air temperatures are higher than the computed 20°C. Most likely the warm above-surface conditions needed more time to penetrate into deeper soil layers. In general, the soil beneath paved surfaces is warmer than the soil beneath vegetated areas. At this point in time, there is little to no influence from shaded areas.

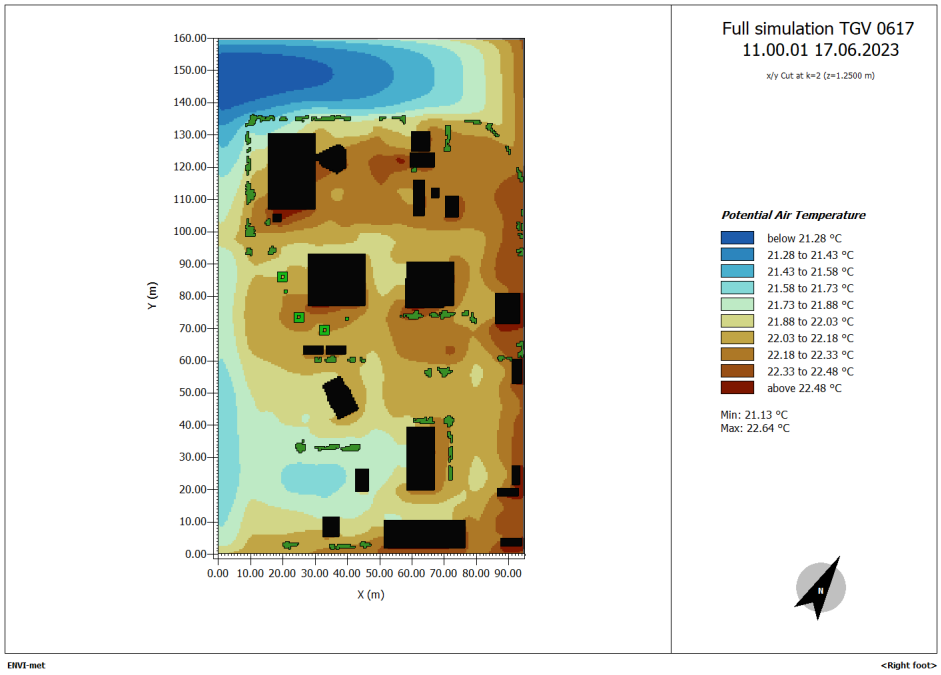

(a)

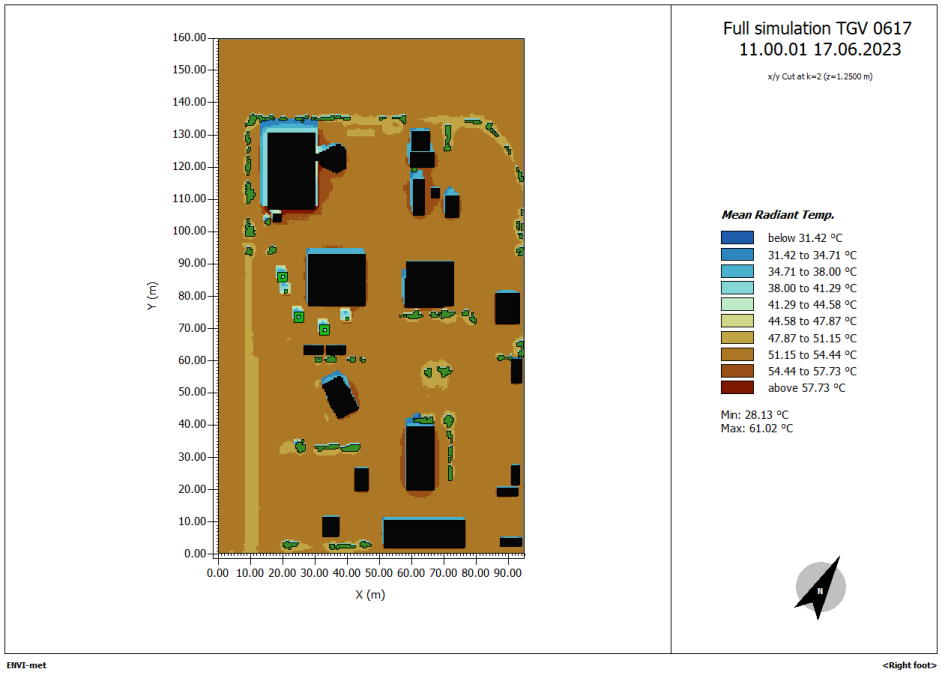

(b)

Figure 4.12.: (a) Air Temperature and (b) Mean Radiant Temperature throughout TGV at 1.25m height computed by ENVI-met after the first successful simulation (17-06-2023 at 11:00 UTC+2

In addition to soil temperature, it is insightful to examine other parameter results, such as air temperature and T_{mrt}. Figure 4.12b shows the air temperature and T_{mrt} at a height of 1.25 meters above the surface. The air temperature across the entire Green Village shows variations ranging from 21.13°C to 22.64°C, with the highest temperatures concentrated around the Heat Square. This area is more densely built-up compared to the rest of TGV, which likely contributes to the higher temperatures observed. The surrounding areas of the Heat Square are less relevant for this specific research, so for future simulations, it would be beneficial to model only the Heat Square and its immediate surroundings. This focused approach will provide more detailed and relevant results for the study.

The air temperature alone does not provide sufficient insights into the observed phenomena from the simulation results. To better understand the thermal conditions, we can examine the T_{mrt}. The T_{mrt} values across the entire model area show a broader range, spanning from 28.13°C to 61.02°C. Despite this wide range, the T_{mrt} throughout most of TGV remains relatively consistent. The average T_{mrt} is between 47.87°C and 51.15°C, with obvious deviations in shaded and wind-sheltered areas, where T_{mrt} values are significantly lower and higher, respectively.

Third iteration

Figure 4.13 depicts the temperature profile of the fibre-optic cable compared to the ENVI-met model's profile on September 9, 2023, at 14:00 LT. This time was selected for its favorable conditions—sufficient spin-up time and peak daytime temperatures. Compared to the initial simulation, there is a noticeable improvement in temperature variation, indicating that the extended simulation time has allowed atmospheric temperature changes to better influence the deeper soil layers of the Heat Square. Although the deeper sections of the fibre-optic cable still exhibit less variation than the shallow sections, suggesting that further extension of simulation time might be beneficial, the overall 'peaks and valleys' in the simulated profile align more closely with the fibre-optic data than before. However, discrepancies remain, particularly in certain sections of the cable.

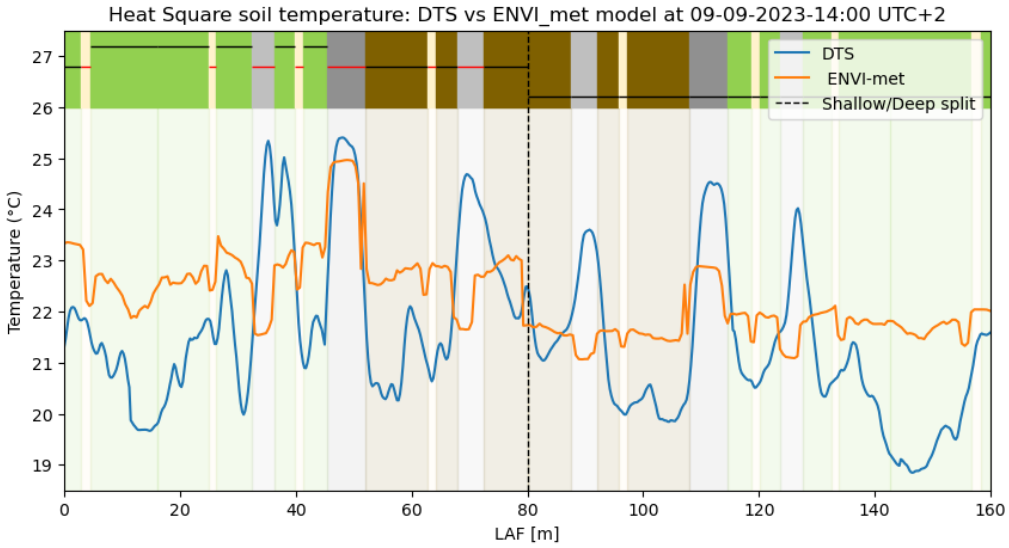

Figure 4.13.: Temperature profile of the fibre-optic cable plotted in LAF versus Temperature on the 9th of September 2023 at 14:00 UTC + 2. The orange line plots the temperature of the simulated 'virtual' fibre-optic cable as a result from the ENVI-met model (third successful simulation).

The comparison of the previously selected points from the first simulation are again depicted in Figure 4.14. Contrary to expectations, this simulation reveals a more significant mismatch in the diurnal temperature patterns compared to the initial simulation. The temperature differences for soil under paved surfaces are approximately 2°C, whereas soil beneath grass grown on local soil exhibits even more pronounced discrepancies. Additionally, the timing of temperature peaks varies significantly across all points, with no clear systematic error affecting their timing. These

inconsistencies highlight the need for substantial model adjustments to enhance its accuracy and performance.

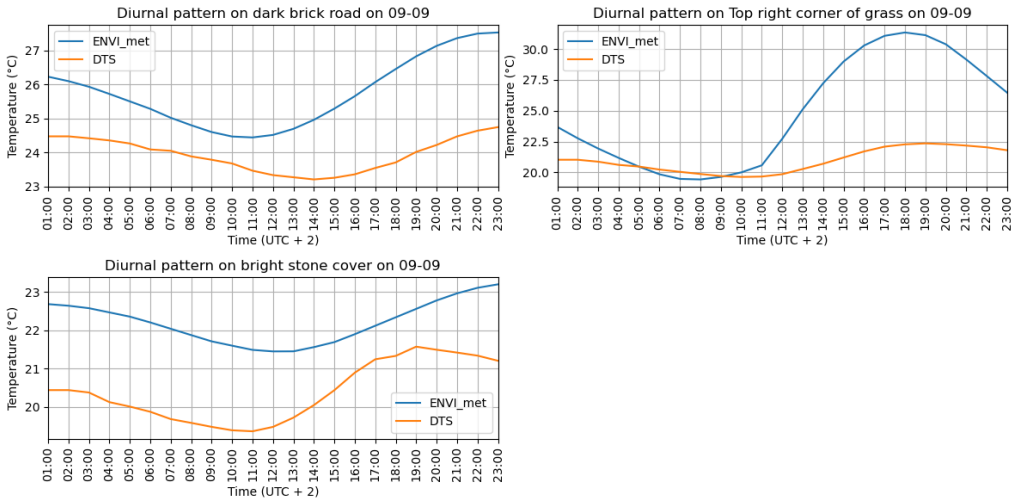

Figure 4.14.: Temperature profile of the fibre-optic cable plotted in time versus Temperature at 30 cm on the 9th of September 2023 at specific points of the fibre-optic cable. The blue line plots the temperature of the simulated 'virtual' fibre-optic cable as a result from the ENVI-met model (third successful simulation).

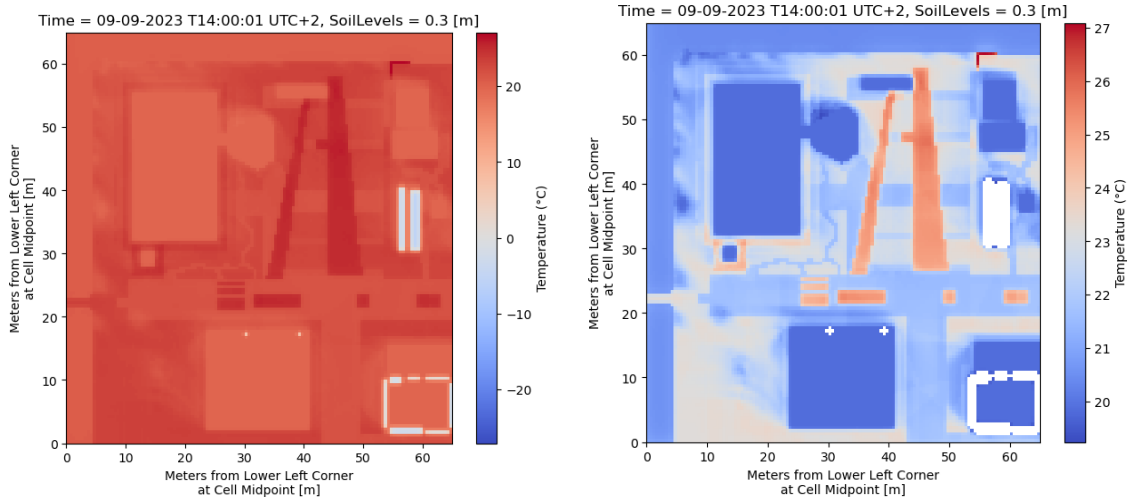

(a) (b)

Figure 4.15.: Soil temperature plot of the Heat Square at a depth 0.3 metres at 11:00 UTC+2 on the 9th of September 2023 (third successful simulation). The image on the left displays shows the unfiltered temperature values while the image on the right shows the same plot after removing extreme values from simulation errors

The results for soil temperature at a depth of 30 centimetres in Figure 4.15, reveal exceptionally low soil temperatures beneath some building windows around the Heat Square. The areas affected by these anomalies are smaller compared to the first simulation. After correcting for these anomalies, the differences between iterations become evident. Specifically, the temperature range has significantly increased from 2.5°C in the first simulation to 7.5°C in the third simulation, indicating that a longer simulation time allowed for better penetration of above-surface conditions into the soil. The air temperatures for the first simulation range from 10°C to 26°C, while the air temperature for the third simulation ranges from 15°C to 29°C. Both temperature ranges were obtained from the weather station installed at TGV. Given that both simulations experienced a similar temperature difference between the highest and lowest value, the difference in soil temperature range between iterations is not due to the different weather forcing.

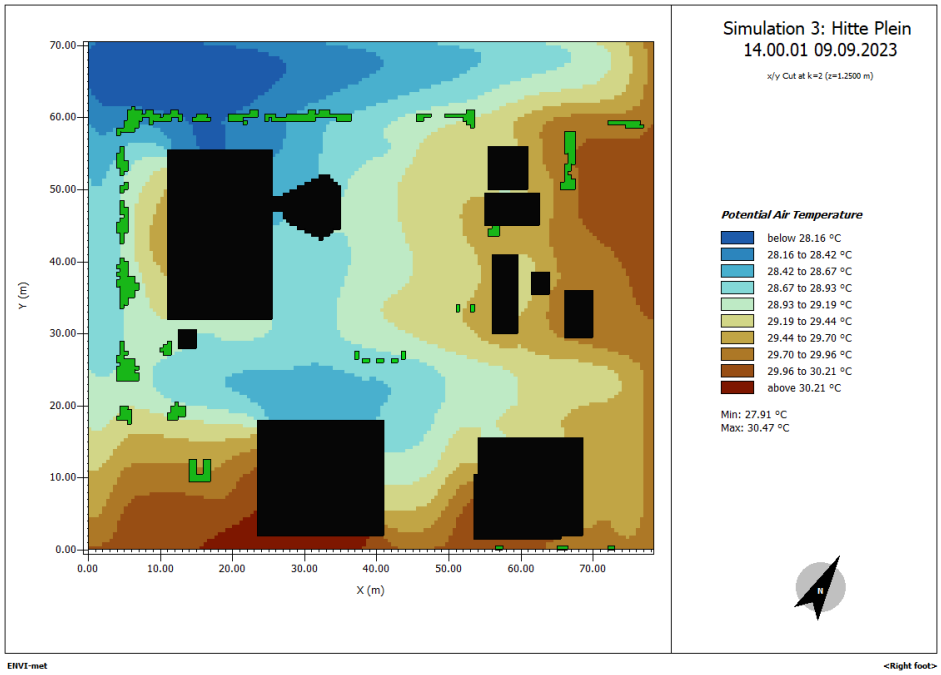

(a)

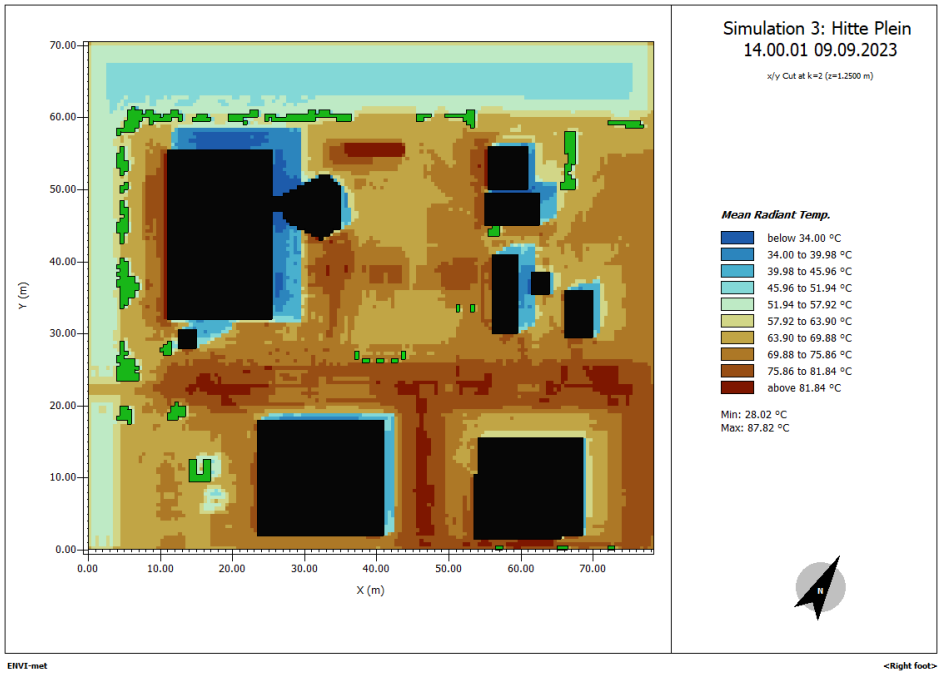

(b)

Figure 4.16.: (a) Air Temperature and (b) Mean Radiant Temperature throughout the Green Village at 1.25m height computed by ENVI-met after the third successful simulation (09-09-2023 at 14:00 UTC+2

The soil temperature results reveal a considerable increase in temperature beneath the dark brick pavements compared to the brighter concrete tiles. Surprisingly, the bright concrete actually leads to lower soil temperatures than the vegetated areas that are not shaded by buildings or other vegetation. Looking at these results, shows that the soil temperature in ENVI-met is heavily influenced by the surface cover above. The distinct outlines of the paths around the Heat Square indicate that temperature variations in the soil are primarily influenced by the conditions in vertical direction.

Focusing on the Heat Square, Figure 4.16b presents the air temperature and T_{mrt} from the third simulation, specifically cropped to highlight the Heat Square. Examining the air temperature, it is clear that the Heat Square itself is cooler compared to the surrounding areas, with the exception of the area above the nearby canal. It remains uncertain whether this cooling effect is due to the shading provided by the co-creation centre or the mitigation measures implemented within the Heat Square. In contrast, the T_{mrt} plot more clearly demonstrates that the Heat Square does contribute to cooling relative to other built-up and paved areas. Within the Heat Square, T_{mrt} values range from 63.9°C to 75.86°C, excluding the horizontal dark pavement in the center. In comparison, T_{mrt} values in other paved and built-up areas range from 69.88°C to 81.84°C. The lowest T_{mrt} values are observed in shaded areas and water bodies. Additionally, vegetated areas on the edges of the Heat Square and TGV also show lower T_{mrt} values, ranging from 57.92°C to 69.88°C.

Fifth iteration

The difference between the soil temperatures measured by the fibre-optic cable and those simulated by ENVI-met, as depicted in Figure 4.17, is quite odd. Several sections of the ENVI-met results show a constant temperature of 20°C, which corresponds to the initialisation temperature of the ENVI-met model. This suggests that these areas are either not being properly simulated or that all heat inputs into these sections are dissipating without being accounted for. These sections correspond to the roofing substrate areas, which in reality consist of 40 centimetres of roofing material situated beneath vegetation and above the local soil. This indicates that there might be an issue with the model's parametrisation of the roofing substrate, leading to unrealistic temperature results.

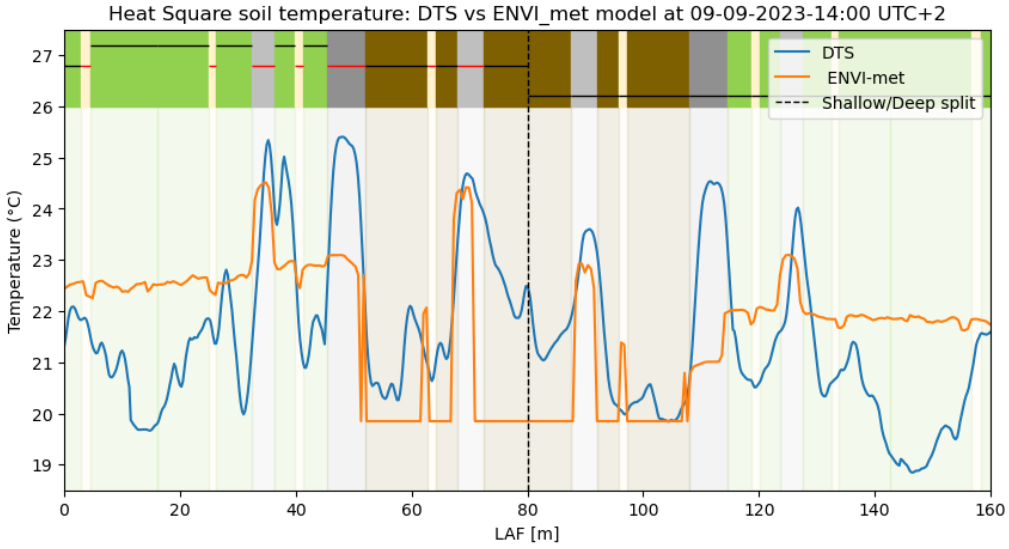

Figure 4.17.: Temperature profile of the fibre-optic cable plotted in LAF versus Temperature on the 9th of September 2023 at 14:00 UTC+2. The orange line plots the temperature of the simulated 'virtual' fibre-optic cable as a result from the ENVI-met model (fifth successful simulation).

Looking besides the errors caused by the parametrisation of the roofing substrate, the timing of some of the temperature peaks are performing better than the previous simulations, which correspond to the light stone pavement at an LAF of 37, 73, 91, and 126 metres. The dark stone

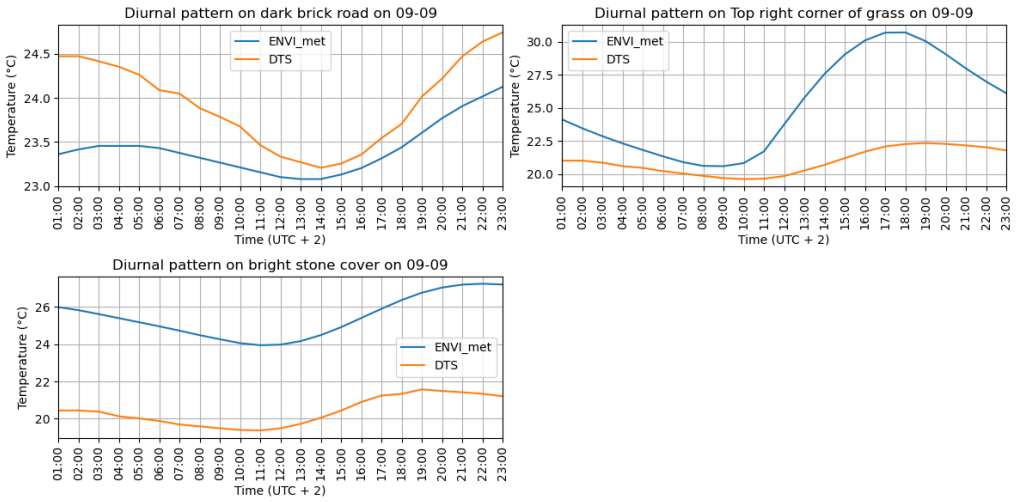

Figure 4.18.: Temperature profile of the fibre-optic cable plotted in time versus Temperature at 30 cm on the 9th of September 2023 at specific points of the fibre-optic cable. The blue line plots the temperature of the simulated 'virtual' fibre-optic cable as a result from the ENVI-met model (fifth successful simulation).

pavement does not result in a much higher soil temperature than the rest of the cable at an LAF of 48 and 112 metres, which is also odd and most likely due to a wrong parametrisation of the surface cover.

Aside from the issues related to the parametrisation of the roofing substrate, it is worth noting that the timing of some temperature peaks in this simulation has improved compared to previous iterations. Specifically, the temperature peaks for the light stone pavement at an LAF of 37, 73, 91, and 126 meters are showing a better approximation of the soil temperature. However, the dark stone pavement does not exhibit significantly higher soil temperatures compared to other sections of the cable at an LAF of 48 and 112 meters.

It is initially expected that the diurnal temperature plots will exhibit minimal correlation due to inherent differences between the DTS system and the ENVI-met model. Nevertheless, it remains useful to assess whether the correlation has improved compared to previous iterations. As shown in Figure 4.18, the correlation between the DTS system and the ENVI-met model is indeed quite low, with temperature differences ranging from 0.2°Cto 7.5°C. Despite these differences, there is an improvement in the timing of temperature extremes. For the first time, the timing of both the highest and lowest temperatures, as well as the onset of the diurnal period, aligns between the DTS system and the ENVI-met model. This consistency marks an improvement over previous simulations. The onset of low temperatures is observed at approximately 14:00 LT for the dark brick road, 10:00 LT for the top right corner of the grass, and 11:00 LT for the bright stone cover. Additionally, ENVI-met computes a greater range of temperature variation for the grass surface cover compared to the paved surfaces, with variations up to 9°C for grass, while paved surfaces show variations between 1°C and 3°C.

Figure 4.19 shows the soil temperature results from the ENVI-met simulation at a depth of 30 centimetres at 14:00 LT. The dark blue spots underneath the roofing substrate plots indicate areas of cooler temperatures. Unlike previous simulations, no plot correction was necessary to remove extreme values. The soil temperatures range from 20°C (the initialisation temperature) to 25°C. Interestingly, the soil beneath the dark pavement is cooler than that beneath the light pavement. This is counterintuitive, as darker pavement would typically be expected to result in higher soil temperatures underneath the surface. This further delineates that the surface cover parametrisation has not been done properly.

Despite the darker pavement resulting in lower soil temperatures underneath, the vegetated areas exhibit the expected lower soil temperatures. This is observed both in the central area of the Heat Square and in the vegetated zones surrounding the co-creation centre and other buildings. The temperature plot also clearly indicates that the soil beneath the vegetation located

to the north of each building is cooler than the surrounding soil. This pattern is evidently caused by the shade produced by the buildings, as the orientation of these cooler areas is the same.

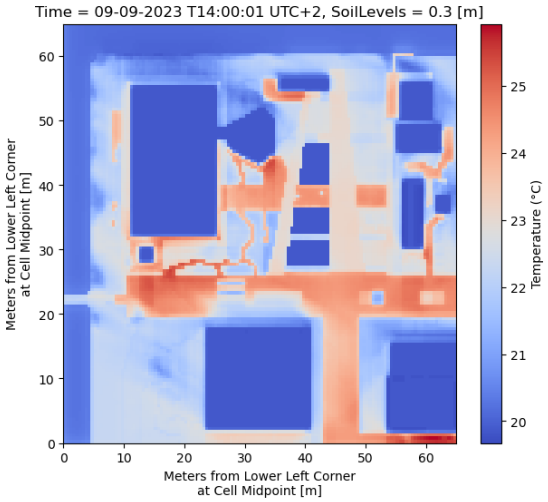

Figure 4.19.: Soil temperature plot of the Heat Square at a depth 0.3 metres at 11:00 UTC+2 on the 9th of September 2023 (fifth successful simulation)

Another notable observation from the simulation results is that the differences in soil temperature between the soil beneath paved and vegetated areas align with expectations. The outline of the paved surfaces is visible in the soil temperature plot, where it is generally expected that the soil beneath paved surfaces is warmer than the soil beneath vegetation. However, in simulation 3, the soil temperature is cooler beneath surfaces made of bright concrete. This finding confirms that the bright concrete surrounding the Heat Square is better parametrised in the fifth iteration compared to the previous ones.

Even though the soil temperature approximation appears to be improving, remarkable errors remain. Some of these errors could be further explained by looking at the the air temperature and T_{mrt} results. Figure 4.20b shows the air temperature and T_{mrt} as in previous simulation results. In Figure 4.20a, the resulting air temperature range has increased by 1.42°C and 1.83°C for the minimum and maximum measured temperatures, respectively. This is noteworthy since the results are for the same time of day and under the same weather conditions. Although these changes are confined to the Heat Square, their impact extends to the surrounding areas. For example, the area south of the co-creation centre experiences an air temperature increase of approximately 2.44°C, which is quite a significant difference for such a small area. It is clear that minor alterations in urban design can have pronounced effects on local thermal conditions.

The T_{mrt} shown in Figure 4.20b displays a more homogeneous spread throughout the Heat Square and its boundaries. The maximum measured T_{mrt} is 6.38°C lower than in the third simulation, and the T_{mrt} above the bright concrete pavement is not as extreme, reaching a maximum of 70.79°C compared to 81.84°C in the third simulation. The effects of the building shade extend further than in the third simulation, though the cause of this is unclear. Lastly, the T_{mrt} above the canal is approximately the same for both the fifth and third simulation results. In general, the soil temperatures from the third iteration were higher than those in the fifth iteration. The lower T_{mrt} results from the fifth simulation could be explained by the cooler soil (and consequently, the surface above it) emitting less heat than the warmer soil in the third simulation, thereby influencing the T_{mrt}.

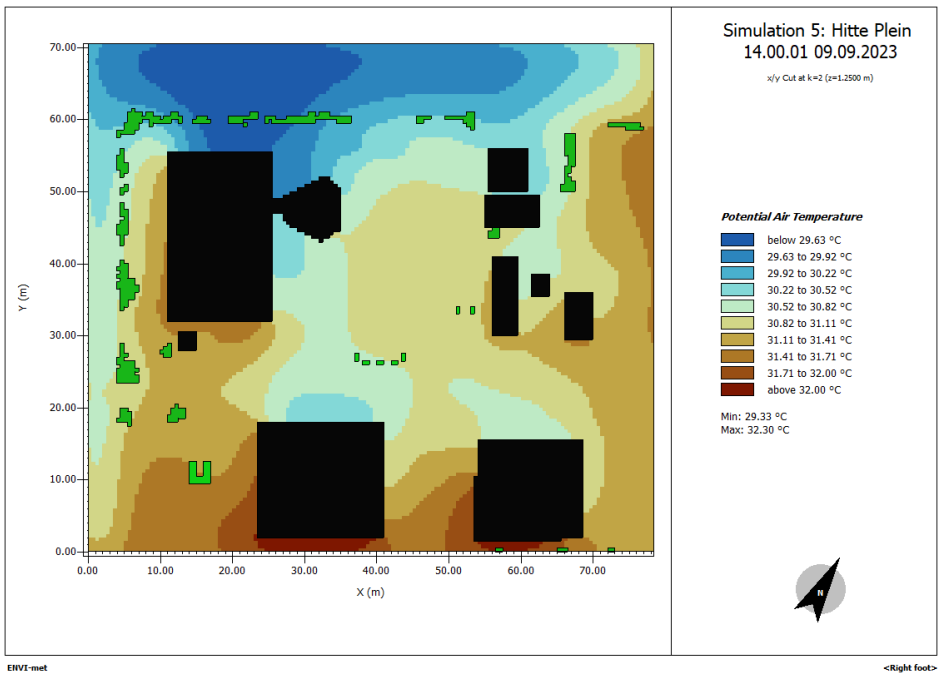

(a)

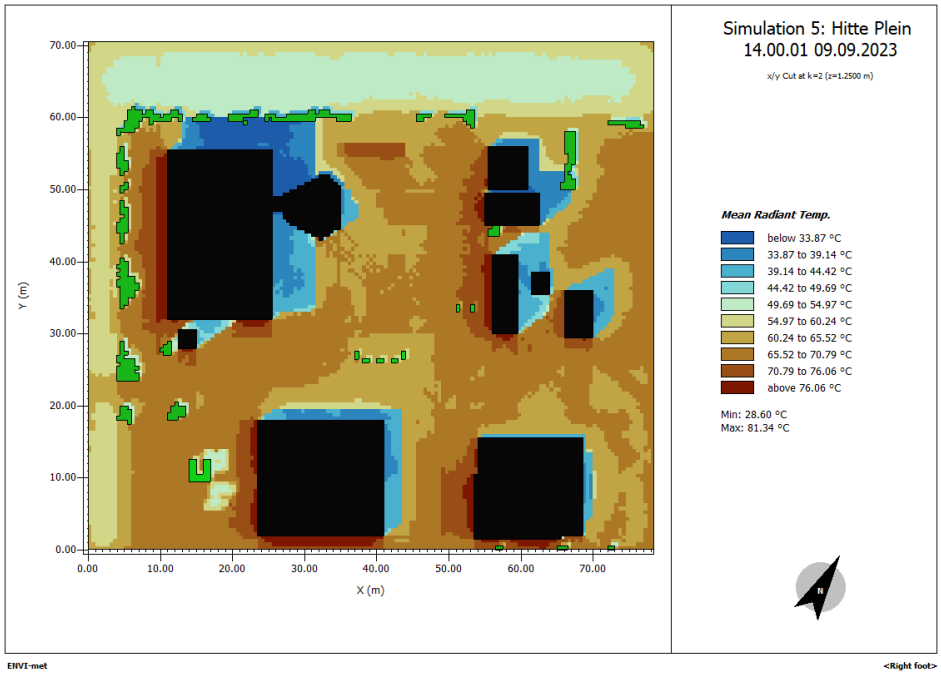

(b)

Figure 4.20.: (a) Air Temperature and (b) Mean Radiant Temperature throughout the Green Village at 1.25m height computed by ENVI-met after the fifth successful simulation (09-09-2023 at 14:00 UTC+2

4.2.2. Benchmark (seventh) iteration

The resulting temperature profile from ENVI-met compared to the measurements of the DTS system is depicted in Figure 4.21. The most noticeable difference between the two is that the ENVI-met results do not capture extreme peaks well; most of the soil temperature results are centered around 21.5°C. It appears that the above-surface conditions have not had sufficient time to penetrate into the deeper subsurface. One potential solution to this issue is to run the simulation with a much longer spin-up time. However, the challenge with this solution is that the currently used spin-up time of three days already requires a significant amount of computation time.

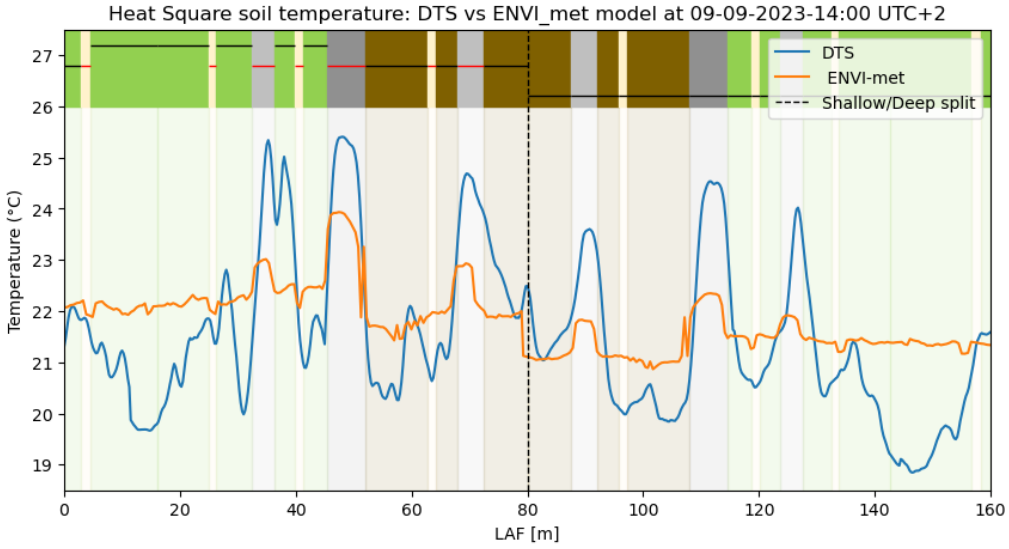

Figure 4.21.: Temperature profile of the fibre-optic cable plotted in LAF versus Temperature on the 9th of September 2023 at 14:00 UTC+2. The orange line plots the temperature of the simulated 'virtual' fibre-optic cable as a result from the ENVI-met model (seventh and final successful simulation).

The onset of extreme values correlates much better than in previous iterations. Specifically, the sections underneath the stone pavements show a good match in terms of timing. This was already the case in the results of the fifth simulation, except for the soil temperature under the dark stone pavement. However, for the sections between an LAF of 0 to 25 metres and 135 to 160 metres, it can be observed that the temperature variation is relatively small in the final simulation results as well as the results of the fifth simulation.

The diurnal temperature plots in Figure 4.22 are somewhat similar to the results from the fifth iteration, except for the plot of the diurnal pattern beneath the dark brick pavement. The timing is offset by approximately two hours regarding the onset of the maximum and minimum values, but the temperature differences range from only 0.1°C to 1°C. In all cases, the temperature resulting from the ENVI-met simulation is higher than that measured by the DTS system. The timing of the maximum and minimum values matches slightly better. Comparing this result with the initial temperature profile plot in Figure 4.21, it makes sense that the results are as they are; the ENVI-met temperatures are centered around 21.5°C at 14:00 LT, whereas the temperature measured by the DTS system is often lower than the ENVI-met temperature, except for the high peaks beneath the stone pavement.

Comparing the previous results of the soil temperature to those from the seventh simulation in Figure 4.23, the area surrounding the Heat Square shows no immediate pattern differences. In general, the main difference is that the soil temperature from the fifth simulation is considerably warmer under paved areas. Vegetated areas surrounding the Heat Square have more or less the same soil temperature at a depth of 30 centimetres. However, within the Heat Square, the soil temperature varies, which is the area of primary interest.

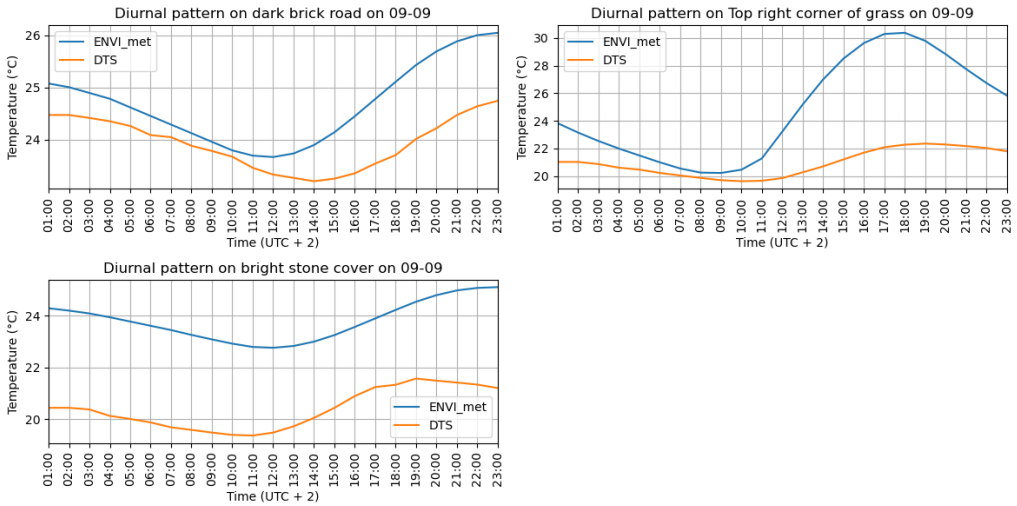

Figure 4.22.: Temperature profile of the fibre-optic cable plotted in time versus Temperature at 30 cm on the 9th of September 2023 at specific points of the fibre-optic cable. The blue line plots the temperature of the simulated 'virtual' fibre-optic cable as a result from the ENVI-met model (seventh successful simulation).

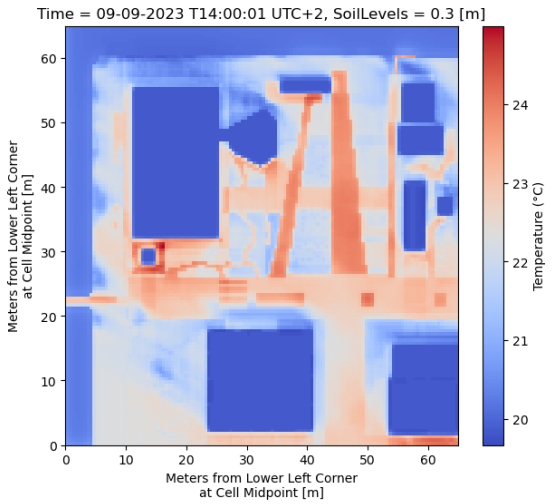

Figure 4.23.: Soil temperature plot of the Heat Square at a depth 0.3 metres at 11:00 UTC+2 on the 9th of September 2023 (seventh successful simulation)

From the seventh simulation, the most notable improvement is the soil temperature beneath the roofing substrate. In previous results, there was no change in temperature in this area. This improvement was achieved by using a simpler schematisation of the soil profile with material properties already included in the software library. The soil temperature underneath the roofing substrate is approximately the same as that beneath the other vegetated plots, except for those vegetated plots with a large amount of bare soil which was caused by construction works. These patterns are also visible in the DTS results.

The light and dark pavements result in the highest soil temperatures beneath the surface, with the soil beneath the dark pavement exhibiting the highest temperatures within the Heat Square. This is contrary to the fifth simulation, where the light pavement resulted in higher soil temperatures than the dark pavement. This new observation is consistent with the soil temperature measured by the DTS system. The overall behaviour remains similar for both the ENVI-met model and the DTS system, which measures the real-case scenario.

Lastly, the air temperature and T_{mrt} of the seventh simulation are shown in Figure 4.24b. Com-

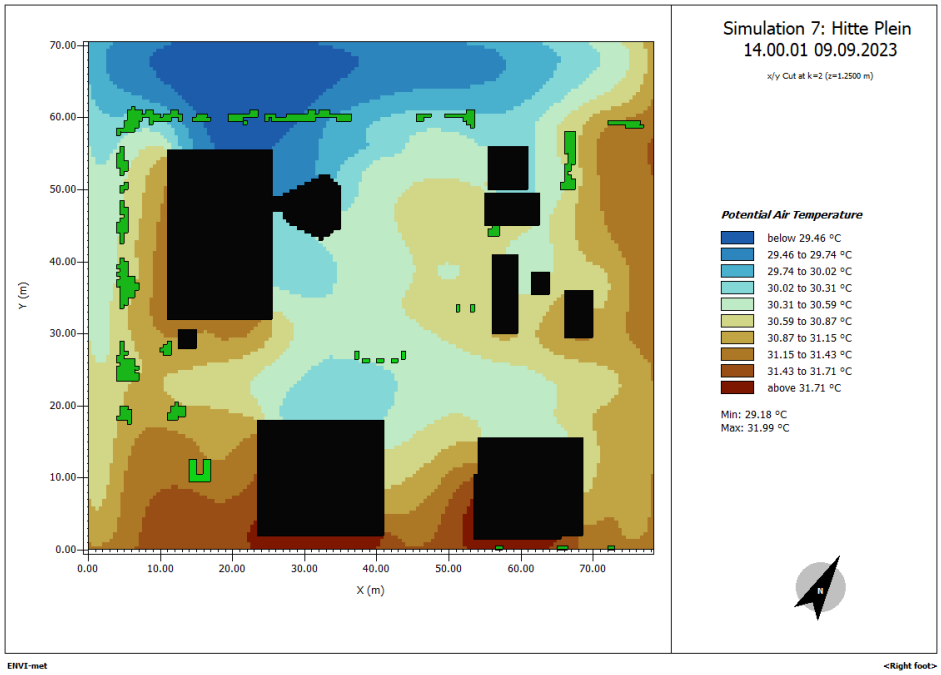

(a)

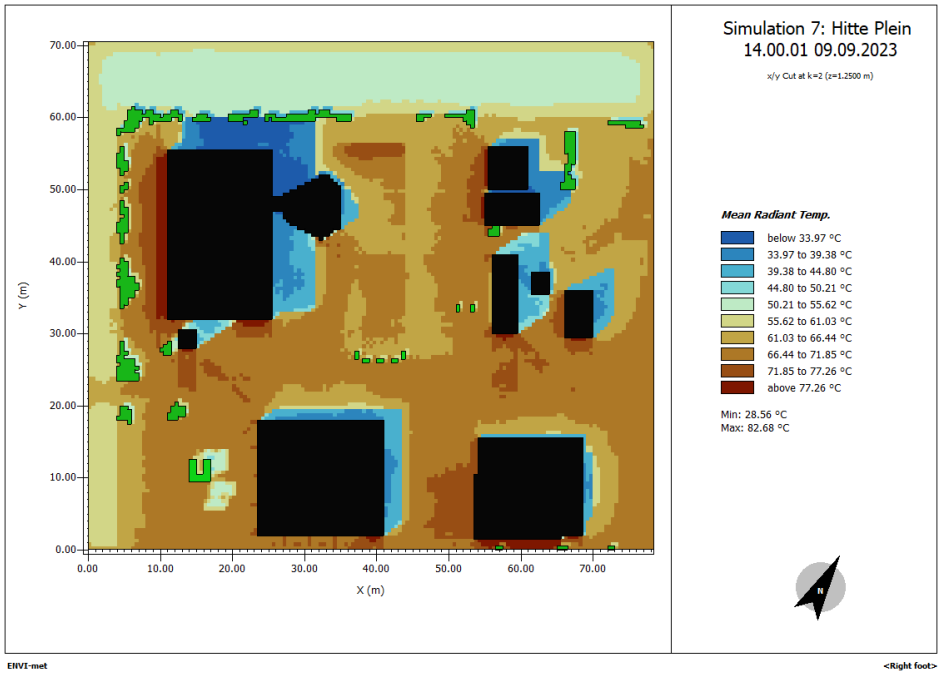

(b)

Figure 4.24.: (a) Air Temperature and (b) Mean Radiant Temperature throughout the Green Village at 1.25m height computed by ENVI-met after the seventh successful simulation (09-09-2023 at 14:00 UTC+2

pared to the results of the fifth simulation, the temperature range does not change significantly; it ranges from a minimum of 29.33°C to 29.18°C and a maximum of 32.30°C to 31.99°C. However, the distribution of the air temperature varies in different areas. In general, the area surrounding the Heat Square has become warmer, particularly above the canal and near the buildings on the side facing away from the Heat Square. On the other hand, the air temperature within the Heat Square is cooler in the seventh simulation, with average temperatures of 30.45°C compared to 30.97°C in the fifth simulation. This difference of 0.52°C is quite significant for the scale modelled in these simulations, considering the temperature variations that could occur in simulations of much larger urban areas.

The T_{mrt} resulting from the seventh simulation is similar to the T_{mrt} resulting from the fifth simulation, just like the air temperature. The ranges went from a minimum of 28.60°C to 28.56°C and a maximum of 81.34°C to 82.68°C. The areas with the highest T_{mrt} are those unshaded sections near buildings that are exposed to direct sunlight, whilst the areas with the lowest values are those that are shaded from buildings and trees, more so than the areas above the water bodies in the model. In general, the average T_{mrt} becomes slightly lower in the seventh simulation compared to the fifth simulation, but only by a small margin. There is no apparent direct correlation between the resulting T_{mrt} and the soil temperature by looking at the images, which is expected given that the timescale of soil temperature variations is longer than that of the T_{mrt}.

4.2.3. Comparison DTS vs. ENVI-met

Considering the large amount of data obtained from both the DTS system and the ENVI-met model, it is beneficial to present some raw data side by side. Table 4.1 and Table 4.2 display the measured and simulated soil temperatures beneath the center of each section. The ENVI-met results represent the soil temperature at the location corresponding to where the fibre-optic cable is placed. Each section is numbered according to the path the fibre-optic takes in Figure 3.1, starting from the northernmost point of the cable in clockwise direction. For an overview of each ground cover and mitigation measure please refer back to Figure 3.2a.

Table 4.1.: Measured soil temperatures at the middle of each section within the Heat Square. The sections are ordered following the path of the fibre-optic cable in clockwise direction, starting from the northernmost point. The measured soil temperatures are from September 9, 2023 at 14:00 UTC+2.

Section	DTS at 10 cm [°C]	DTS at 30 cm [°C]	DTS at 60 cm [°C]
Vegetation 1 (local)	-	22.18	21.53
Sand 1	-	21.86	20.92
Vegetation 2 (local)	22.46	-	20.43
Sand 2	-	22.03	21.03
Vegetation 3 (local)	21.81	-	20.5
Concrete light 1	-	25.25	23.97
Vegetation 4 (local)	26.57	-	20.88
Sand 3	-	21.63	20.69
Vegetation 5 (local)	22.89	-	21.59
Concrete dark	-	25.5	24.19
Urban Jungle Project	-	20.86	19.97
Vegetation 6 (roof)	-	21.76	20.26
Sand 4	-	21.09	20.19
Vegetation 7 (roof)	-	21.17	21.36
Concrete light 2	-	24.71	23.46
Vegetation 8 (roof)	-	22.69	21.31

Table 4.2.: Simulated soil temperatures at the middle of each section within the Heat Square, following the path of the fibre-optic cable. The sections are ordered in clockwise direction, starting from the northernmost point. The measured soil temperatures are from September 9, 2023 at 14:00 UTC+2.

Section	ENVI at 10 cm [°C]	ENVI at 30 cm [°C]	ENVI at 60 cm [°C]
Vegetation 1 (local)	-	22.13	21.37
Sand 1	-	21.88	21.56
Vegetation 2 (local)	22.25	-	21.43
Sand 2	-	22.03	21.23
Vegetation 3 (local)	22.14	-	21.39
Concrete light 1	-	23.0	21.91
Vegetation 4 (local)	22.47	-	21.52
Sand 3	-	22.13	21.27
Vegetation 5 (local)	22.46	-	21.51
Concrete dark	-	23.93	22.35
Urban Jungle Project	-	21.63	21.01
Vegetation 6 (roof)	-	21.97	21.19
Sand 4	-	21.88	21.12
Vegetation 7 (roof)	-	21.73	21.01
Concrete light 2	-	22.88	21.81
Vegetation 8 (roof)	-	21.89	21.07

At first glance, the ENVI-met soil temperature results exhibit similar patterns to the DTS results regarding which ground covers result in the highest and lowest soil temperatures. However, there is insufficient variation in soil temperature, particularly in the deeper layers, which are centered around 21.5°C. In the shallow section, the model does not capture the extreme high and low peaks well, although it shows the proper response per ground cover. More discrepancies arise with other ground covers: the sandy pavement does not reflect as much solar radiation in ENVI-met as the DTS results indicate, and both the local soil substrate and roofing substrate do not respond as expected. In this study, the DTS system's measurements are regarded as the actual soil temperatures since they have been validated by comparison with tensiometers. Nonetheless, it is important to consider that human and environmental factors could displace the fibre-optic cable of the DTS system, potentially leading to inaccurate soil temperature measurements.

4.2.4. Correlation ENVI-met and anemometers

Figure 4.25 shows a comparison plot of the computed air temperature values at the locations of the anemometers versus the actual measured temperatures, to check whether the simulated the air temperature better approximate in-situ measurements. Five anemometers were installed within the Heat Square, but one of them (number 4) lacked sufficient data for this comparison. The hourly temperature is plotted in °C for the day the simulations were conducted, specifically on the 9th of September 2023. Various metrics can be used to compare the results and assess the model fit other than visually assessing the results. The Root Mean Squared Error (RMSE), Mean Absolute Error (MAE), and Coefficient of Determination (R^2) for each of the anemometers were computed and then averaged to provide an insight into the model fit.

The average computed RMSE for the air temperature within the Heat Square is 1.54°C. This means that, on average, the air temperature computed by the model deviates by 1.54°C from the measured values. Considering the range of the daily temperature values, with a minimum of 17.2°C and a maximum of 31.1°C, this RMSE represents an acceptable performance given that the range of variation is much larger than the RMSE. Since this application relies more on a qualitative assessment of the urban microclimate rather than precise temperature predictions, this level of accuracy is reasonable. The average computed MAE for the air temperature within the Heat Square is 1.22°C. Comparing the RMSE to the MAE means that there are not many outliers in the computed data, since both metrics are relatively close. The RMSE is higher due to

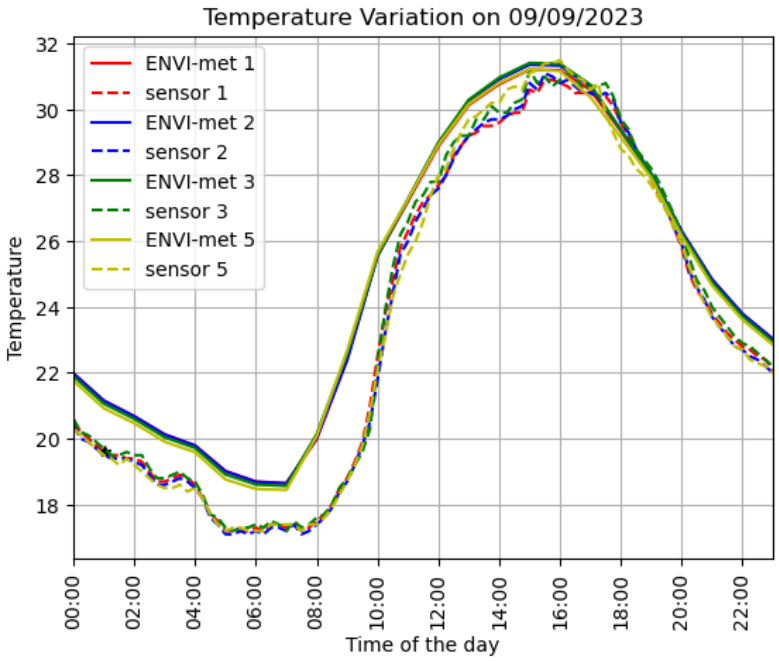

Figure 4.25.: Air temperature measurements from ENVI-met simulation results (seventh and final iteration) versus on-site measurements from several ultrasonic anemometers placed within the Heat Square. The graph shows the simulated and measured hourly values for the 9th of September 2023.

the squaring of the error value before averaging. If there were extreme outliers, the RMSE would be much larger than the MAE.

Visually inspecting the plotted graph, the model captures the temperature most accurately from 12:00 LT onwards, with most deviations occurring earlier in the day when the temperature values are the lowest. The model seems to capture high air temperatures better than low air temperatures. The R^2 provides a statistical comparison of the measured and computed air temperatures. For this case, the computed R^2 is 0.9038, meaning that 90.38% of the variance in air temperature is explained by the model. This suggests the model performs well in capturing the variability of the air temperature throughout the day.

Overall, the air temperatures from the model match the measured air temperatures reasonably well, despite deviations for the lower temperatures. This implies that the significant mismatch in approximating the soil temperature measured by the DTS system is likely not caused by the above surface conditions.

4.2.5. Scenarios

Despite the soil temperatures from the ENVI-met simulations not approximating the soil temperatures measured by the DTS system as desired, it has been confirmed that the air temperatures present a reasonably good match. Therefore, it can be interesting to perform simulations of various scenarios to assess their impact on the urban microclimate and their atmospheric conditions. Since the subsurface conditions are just as important as the atmospheric conditions in the urban microclimate, examining the subsurface of various scenarios can provide valuable insights, even if the simulation does not perfectly depict real-life conditions. The following section of this chapter will present results from various simulation scenarios, using the results from the seventh iteration as a benchmark for comparison.

Concrete Square

The initiative to construct the Heat Square was driven by the previous configuration, which only consisted of bright concrete slabs designed to support heavy traffic. This setup led to increased heat stress for users of the surrounding area, prompting the need for reconstruction to mitigate heat stress. An ENVI-met model was created to simulate the previous situation, where the Heat Square was solely covered with bright concrete pavement as provided in the ENVI-met software (see Figure 2.3a). The surrounding area remained unchanged in the model to isolate the effects of the Heat Square on the urban microclimate of TGV, making sure that any observed changes were due to the modifications in the Heat Square alone.

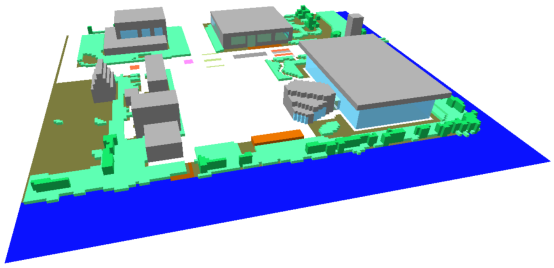

Figure 4.26.: Model schematisation of the Heat Square (concrete square scenario)

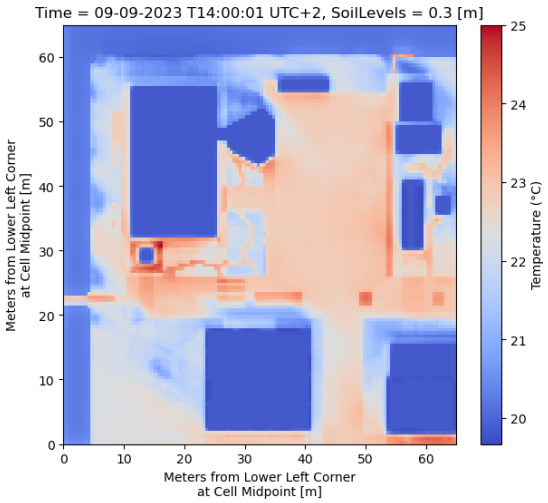

Figure 4.27.: Concrete square scenario: Soil temperature plot of the Heat Square at a depth of 0.3 metres at 14:00 UTC+2 on the 9th of September 2023

The difference in soil temperature between the concrete square scenario and the current Heat Square configuration is clear (Figure 4.27). In the old setup, which consisted of a large slab of concrete, the soil temperature remains relatively constant across the entire square. On average, this soil temperature is higher than in the new configuration (22.8°C). Interestingly, the temperature under the dark pavement in the new layout is much more extreme compared to the concrete square (24°C). This might argue the benefits of the new layout when it comes to maintaining lower soil temperatures. Although the overall soil temperature is generally lower, the highest temperatures are significantly more extreme under the dark pavement.

The air temperature and T_{mrt} plots for the benchmark scenario (Figure 4.24b) and the concrete square scenario (Figure 4.28b) show notable differences. Although the air temperature ranges are similar, the distribution of air temperature within the Heat Square varies significantly. Surprisingly, the benchmark scenario shows higher air temperatures than the concrete square scenario at a height of 1.25 meters above the surface. In the benchmark scenario, air temperatures range from 30.31°C to 30.87°C, while in the concrete square scenario, they range from 29.9°C

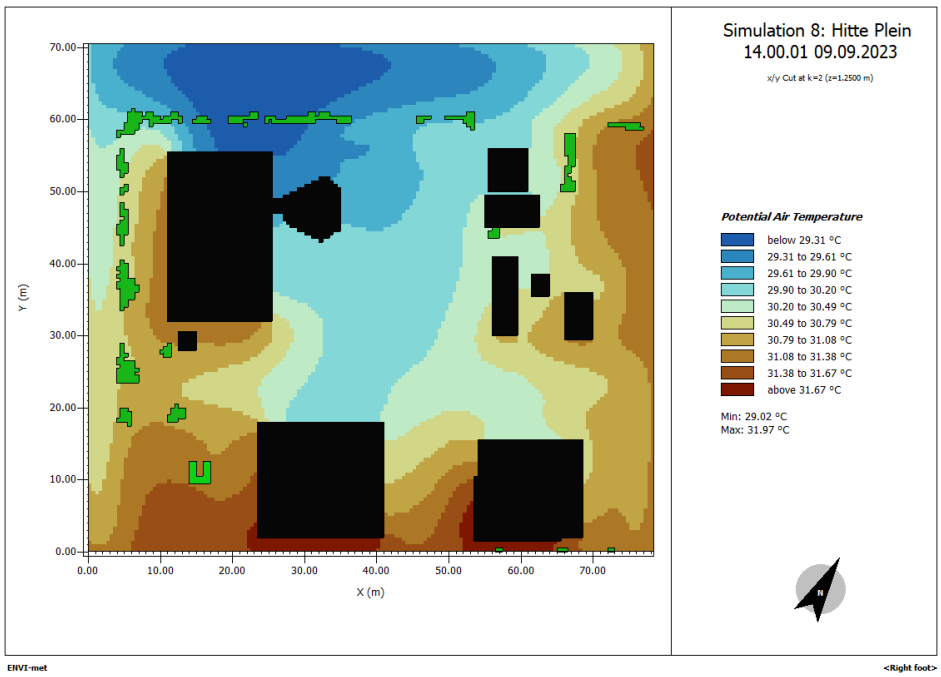

(a)

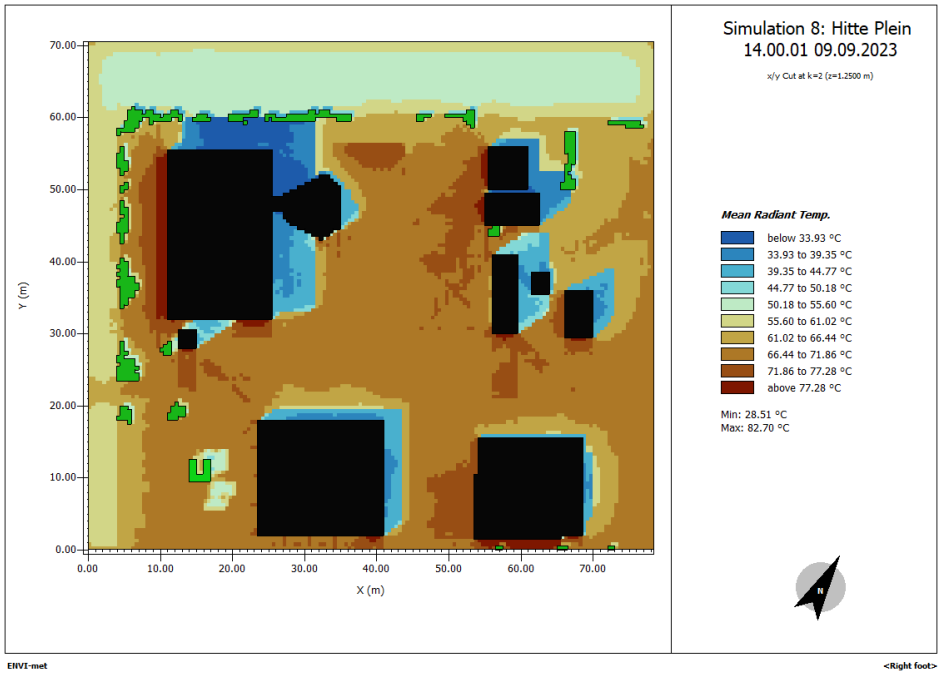

(b)

Figure 4.28.: Concrete square scenario: (a) Air Temperature and (b) Mean Radiant Temperature throughout the Green Village at 1.25m height computed by ENVI-met (09-09-2023 at 14:00 UTC+2)

to 30.49°C. This indicates an approximate temperature difference of 0.4°C. While this difference may not seem high, it is significant given the small size of the area. In larger urban areas, these differences could be more enhanced.

Conversely, the T_{mrt} values are lower by a bigger margin in the benchmark scenario compared to the concrete square scenario. In the benchmark scenario, T_{mrt} range from 55.62°C to 66.44°C, whereas in the concrete square scenario, they range from 61.02°C to 71.86°C. The differences in T_{mrt} can be as much as 5°C. Considering that the T_{mrt} is a thermal comfort index that takes more factors into account than just air temperature, it can be concluded that the benchmark scenario does indeed result in cooling of the Heat Square compared to the concrete square scenario.

Cooling measures

Based on observed intermittent results from previous simulations of the Heat Square, a new model schematisation has been made with a focus on further enhancing heat stress mitigation. The primary changes to the design include replacing dark concrete with light concrete, replacing the roofing substrate with local soil substrate, and adding taller vegetation (such as trees) to increase shading within the Heat Square. The large paved driveways were retained to allow heavy traffic in the Heat Square, while the sand pavements were kept in areas that do not require heavy traffic. This revised model scenario was simulated under the same weather conditions as the benchmark scenario to assess whether the new design improves urban cooling according to ENVI-met.

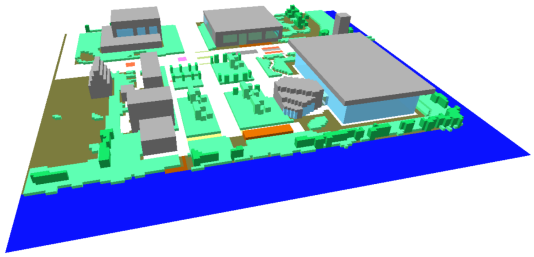

Figure 4.29.: Model schematisation of the Heat Square (Cooling measures scenario)

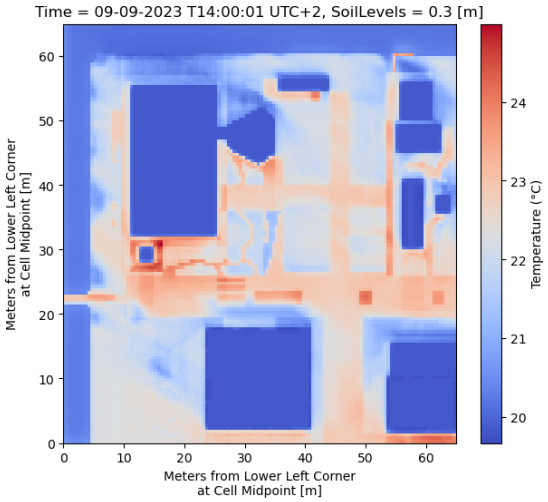

Figure 4.30.: Cooling measures scenario: Soil temperature plot of the Heat Square at a depth of 0.3 metres at 14:00 UTC+2 on the 9th of September 2023

Regarding soil temperature, the impact of removing the dark concrete pavement is immediately evident, as the soil temperature no longer reaches the extreme values associated with the dark

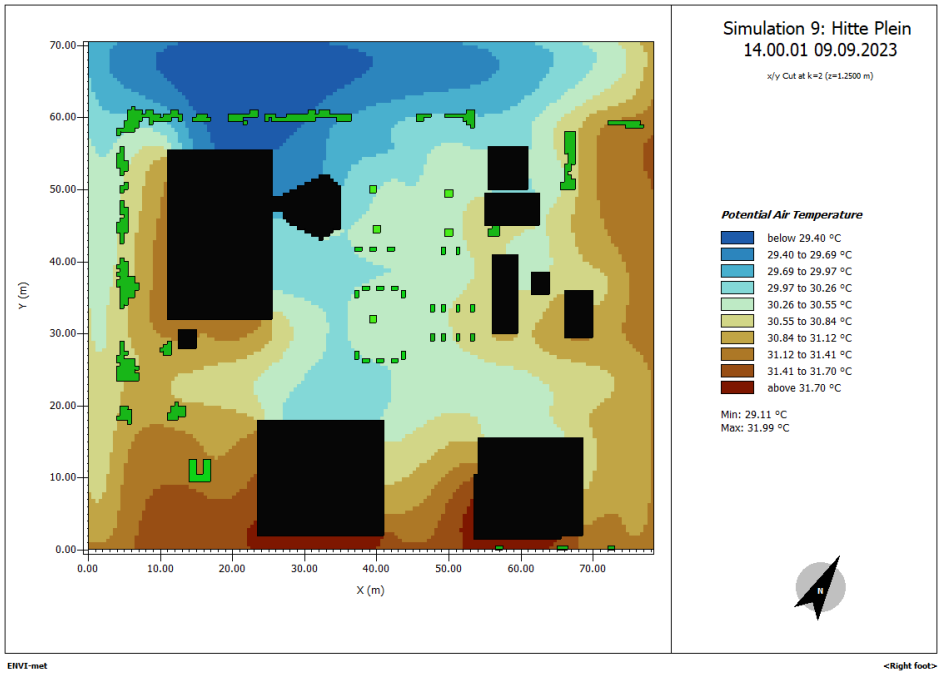

(a)

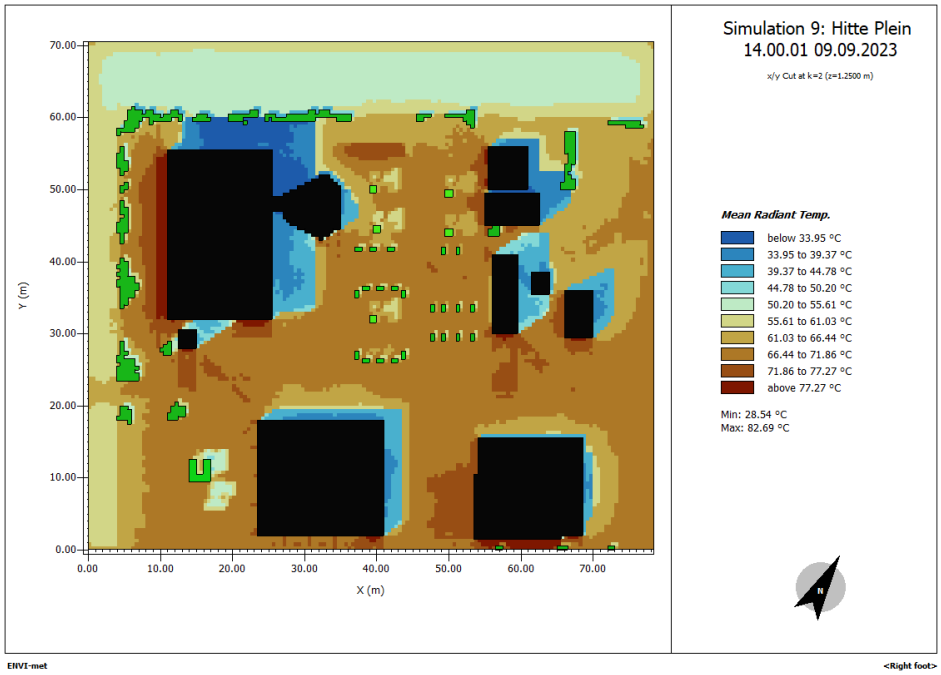

(b)

Figure 4.31.: Cooling measures scenario: (a) Air Temperature and (b) Mean Radiant Temperature throughout the Green Village at 1.25m height computed by ENVI-met (09-09-2023 at 14:00 UTC+2)

concrete. Additionally, the shading provided by the vegetation appears to slightly reduce the soil temperature under the light concrete pavement in some areas, lowering the soil temperature up to 0.6°C at 0.3 metres depth. Overall, this new layout effectively lowers the soil temperature beneath the Heat Square.

The addition of taller vegetation and lighter coloured pavement in the new scenario reduces the local air temperature. As seen in Figure 4.31b, there is a reduction of up to 0.3°C in air temperature at a height of 1.25 meters above the surface. However, the air temperature ranges in the area surrounding the Heat Square remain unchanged with a similar distribution.

The T_{mrt} shows notable differences. Replacing dark concrete pavement with light concrete pavement leads to T_{mrt} increases of up to 5.41°C in some areas. This is unexpected, as the goal of the new scenario was to reduce thermal discomfort. Nonetheless, shaded areas by the tall vegetation show concentrated cooling, with T_{mrt} decreases of up to 11°C. Therefore, in terms of thermal comfort rather than air temperature, tall vegetation performs better than light concrete.

Low-resolution

Earlier in this chapter, we discussed potential reasons why the soil temperature profile computed by ENVI-met does not align with the temperature profile measured by the DTS system. One frequently mentioned reason was the large spin-up time required to initialise the soil temperatures of the Heat Square. Due to the extensive computation time needed, the model was initially limited to simulating 72 hours. For larger model schematisations, it would also be required to decrease the model resolution in order to get results without having too wait far too long for them.

It was hypothesised that by simulating more days (in advance of the 9th of September) and thereby increasing the spin-up time of the model, the soil profile computed by ENVI-met would better match the DTS results. To test this, a new model was schematised with the same dimensions in meters but a larger grid size. The model resolution was halved, increasing the grid sizes in the x, y, and z directions from 0.5 m x 0.5 m x 0.5 m to 1 m x 1 m x 1 m. This change reduced the number of cells by a factor of $2^3 = 8$. Instead of simulating the model for 72 hours, it was simulated for 144 hours under the same weather conditions as the previous simulations. The model took 52 hours and 43 minutes time to compute, compared to 109 hours and 47 minutes for the benchmark scenario, while also simulating twice the time in weather forcing. This means the low-resolution model can produce results over 4 times as fast as the benchmark scenario.

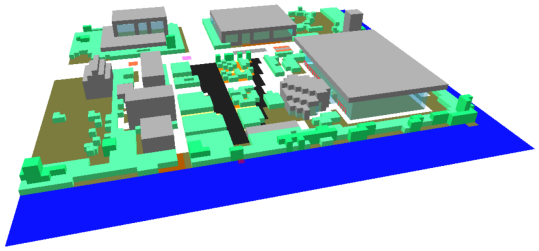

Figure 4.32.: Model schematisation of the Heat Square (Low resolution scenario)

Comparing the soil temperature plot in Figure 4.33 to the soil temperature from the benchmark scenario in Figure 4.23 shows a greater range in soil temperatures. The soil temperature at a depth of 30 centimeters under the dark concrete pavement is warmer in the low-resolution scenario (25.5°C) compared to the benchmark scenario (24°C). Similarly, the light concrete pavement shows higher soil temperatures, while the soil temperature under the vegetated plots remains relatively consistent. Overall, it appears that the high temperatures are more extreme, while the low temperatures did not decrease compared to the benchmark scenario.

This observation is further supported by Figure 4.34, which clearly shows that all high-temperature peaks are more extreme. The average temperature is higher for every point in the temperature

profile, but the low values still do not approximate reality any better than the benchmark scenario. While the high peaks are closer to the real-life scenario, the low peaks remain a challenge.

One possible cause is the weather forcing executed for the simulation from 04-09-2023 to 09-09-2023, which used the average weather forcing from the other simulations conducted between 07-09-2023 and 09-09-2023. In reality, the three days prior to the period from 07-09-2023 to 09-09-2023 were colder. This difference could explain why the average temperature increased overall; the Heat Square was exposed to hot weather for a longer period than in the real-life scenario. Ideally, the average weather forcing should have been applied for the entire period from 04-09-2023 to 09-09-2023.

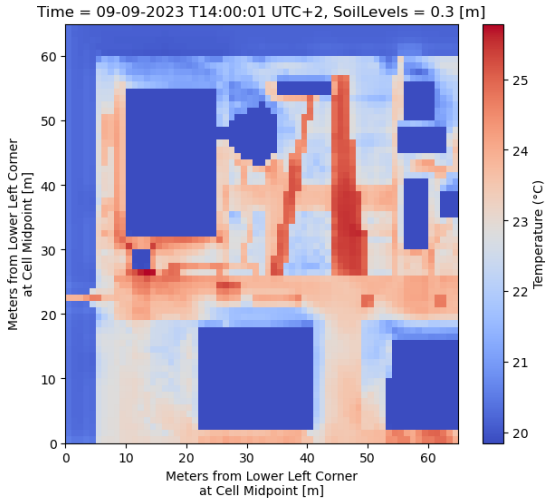

Figure 4.33.: Low resolution scenario: Soil temperature plot of the Heat Square at a depth of 0.3 metres at 14:00 UTC+2 on the 9th of September 2023

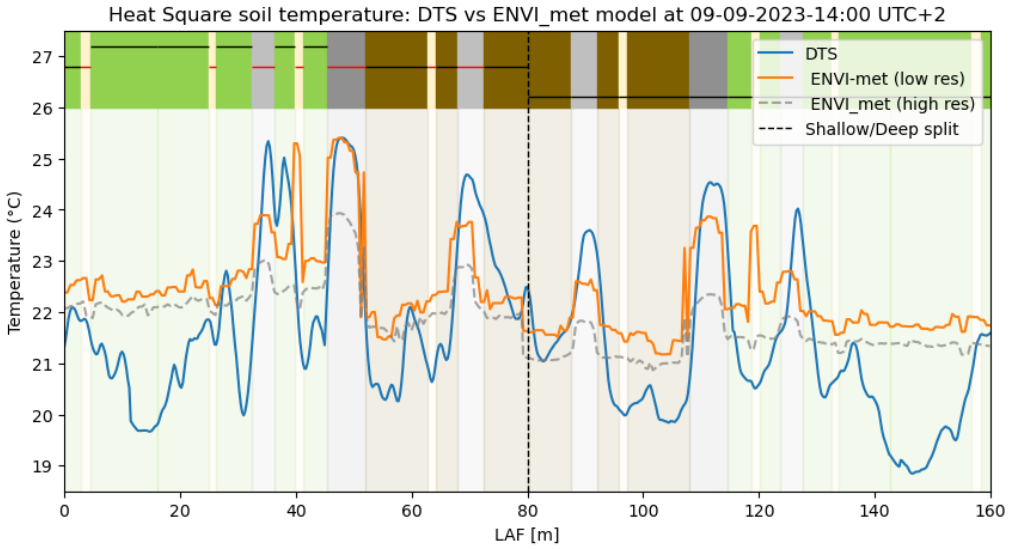

Figure 4.34.: Temperature profile of the fibre-optic cable plotted in LAF versus Temperature on the 9th of September 2023 at 14:00 UTC+2. The orange line plots the temperature of the simulated 'virtual' fibre-optic cable as a result from the ENVI-met model (low-resolution scenario). The dashed line is the temperature profile from the seventh successful simulation of the Heat Square, which is used as a benchmark result to compare to various scenarios.

The air temperature from the low-resolution scenario in Figure 4.35b displays a similar distribution throughout the Heat Square but with an overall lower temperature of approximately 0.25°C. Additionally, the low-resolution model seems to result in a generally higher T_{mrt} throughout the

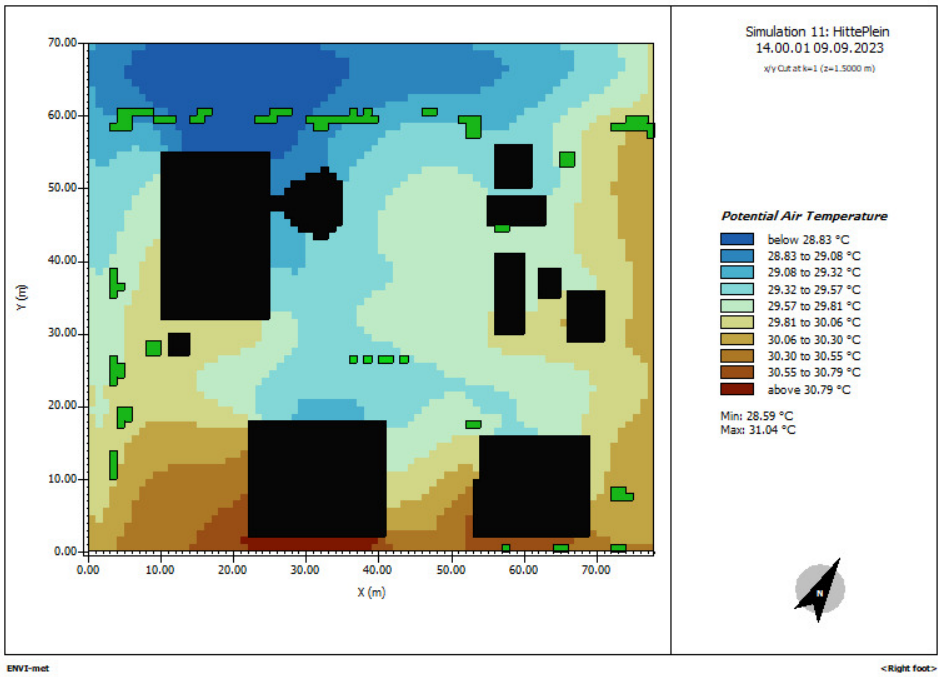

(a)

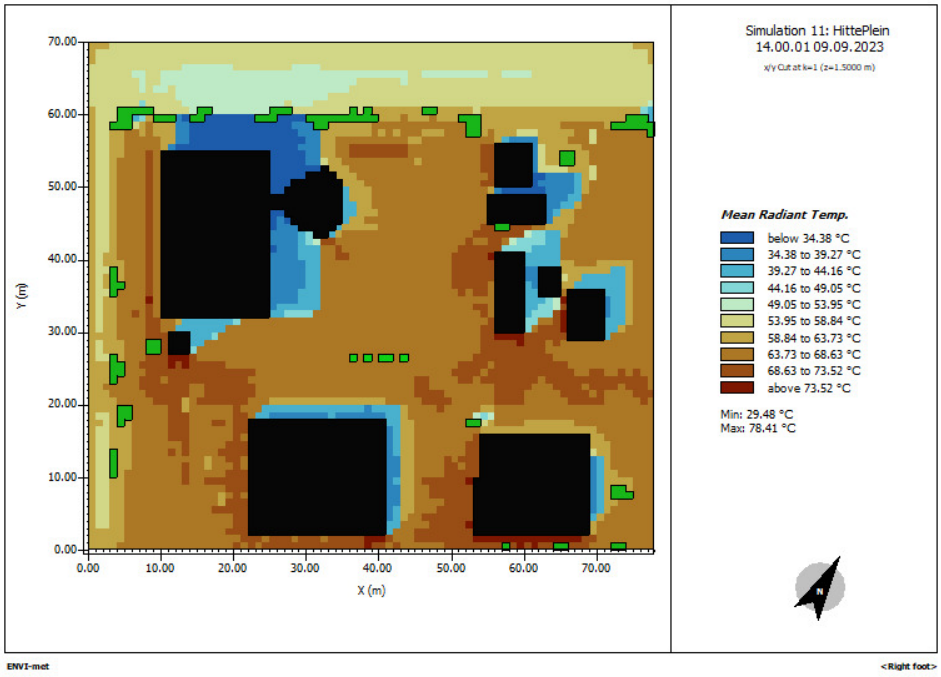

(b)

Figure 4.35.: Low resolution scenario: (a) Air Temperature and (b) Mean Radiant Temperature throughout the Green Village at 1.5m height computed by ENVI-met (09-09-2023 at 14:00 UTC+2)

Heat Square. In the low-resolution scenario, the T_{mrt} does not drop below 63.73°C, whereas in the benchmark scenario, some areas are as low as 55.62°C. These differences could be attributed to the effects of using a low-resolution model, which alters the spatial representation and interaction of elements within the model.

Geographical and Climatological scenarios

As a final test to assess how the current layout of the Heat Square would react to scenarios unrelated to its layout but related to other geographical and climatological scenarios, two alternative simulations were performed. One scenario retained the same weather forcing as before but situated the Heat Square in a dry area, implying the removal of the canal that currently passes by TGV. The other scenario is based on one of the extreme weather projections from the IPCC's Sixth Assessment Report (AR5) (IPCC, 2023). Specifically, the RCP2.6 scenario was utilised, which assumes significant efforts to curb emissions, which is in line with TGV's objectives. According to this scenario, temperatures may increase by 0.3°C to 1.7°C by the end of the 21st century. Thus, the RCP2.6 scenario implemented an overall 1.7°C increase in weather forcing, while maintaining the same distribution in the diurnal cycle.

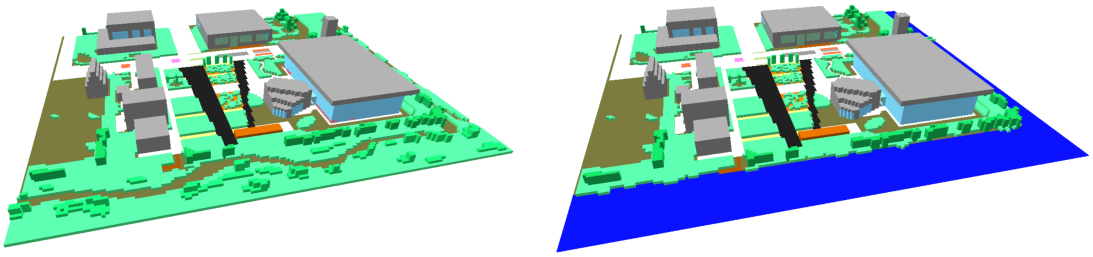

(a) (b)

Figure 4.36.: Model schematisations of the Heat Square (No-water (a) and RCP2.6 (b))

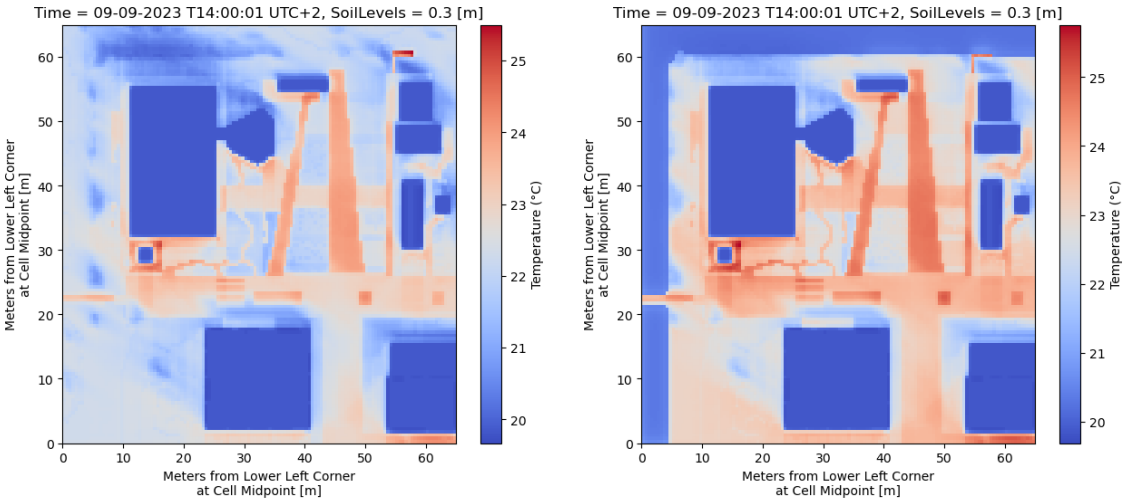

(a) (b)

Figure 4.37.: No-water (a) and RCP2.6 (b) scenario: Soil temperature plot of the Heat Square at a depth of 0.3 metres at 14:00 UTC+2 on the 9th of September 2023

The soil temperature in the no-water scenario experiences a higher range of temperatures. Moreover, the areas where the water body used to be experience a significant increase in soil temperature, as do the areas nearby. However, within the Heat Square, the temperature changes are minimal, showing only slight variations.

In the RCP2.6 scenario, the soil temperature also shows a wider range of values, with the entire model area experiencing higher temperatures at a depth of 30 centimeters. Table 4.3 provides the resulting soil temperatures under different ground covers within the Heat Square. The data indicate that the no-water scenario has a negligible impact on soil temperatures, while the RCP2.6 scenario results in an increase of approximately 0.7°C to 0.8°C. This indicates that the increase in soil temperature is somewhat attenuated by the soil above, leading to a smaller increase than that of the weather forcing.

Table 4.3.: Soil temperatures at 30 cm depth under different ground covers per extreme scenario

Soil cover	Benchmark	No water	RCP2.6
Dark	24°C	24°C	24.7°C
Light	22.9°C	22.9°C	23.7°C
Vegetation	22.2°C	22.2°C	22.9°C
Sand	22.2°C	22.2°C	23°C

The air temperatures above the Heat Square in the benchmark scenario are lower compared to the no-water scenario, as expected, but the difference is marginal. The average air temperature in the benchmark scenario is 30.45°C, while in the no-water scenario it is 30.7°C, a difference of only 0.25°C. The water body does provide some cooling to Heat Square, even at a certain distance from it (Figure 4.38b). The T_{mrt} increases by approximately 0.9°C on average, indicating a relatively small increase in thermal discomfort compared to other scenarios. This suggests that the absence of the water body at a certain distance does not significantly impact thermal comfort. Instead, alterations within the urban environment of the local area would have a more substantial effect on thermal comfort.

In the RCP2.6 scenario, the mean air temperature above the Heat Square is higher, with an average temperature of 32.15°C at a height of 1.25 meters. This increase corresponds to the 1.7°C rise induced in the weather forcing, indicating that the higher temperatures do not result in a disproportionate increase in air temperature within the Heat Square. This makes sense given the relatively small area being modeled (Figure 4.39b). The T_{mrt} exhibits a similar distribution to the benchmark scenario, with the only noticeable difference being the higher values observed in the RCP2.6 scenario. The T_{mrt} increases by approximately 1.1°C, which is less than the rise in air temperature, showing that an increase in air temperature does not directly amount to an equivalent rise in thermal discomfort.

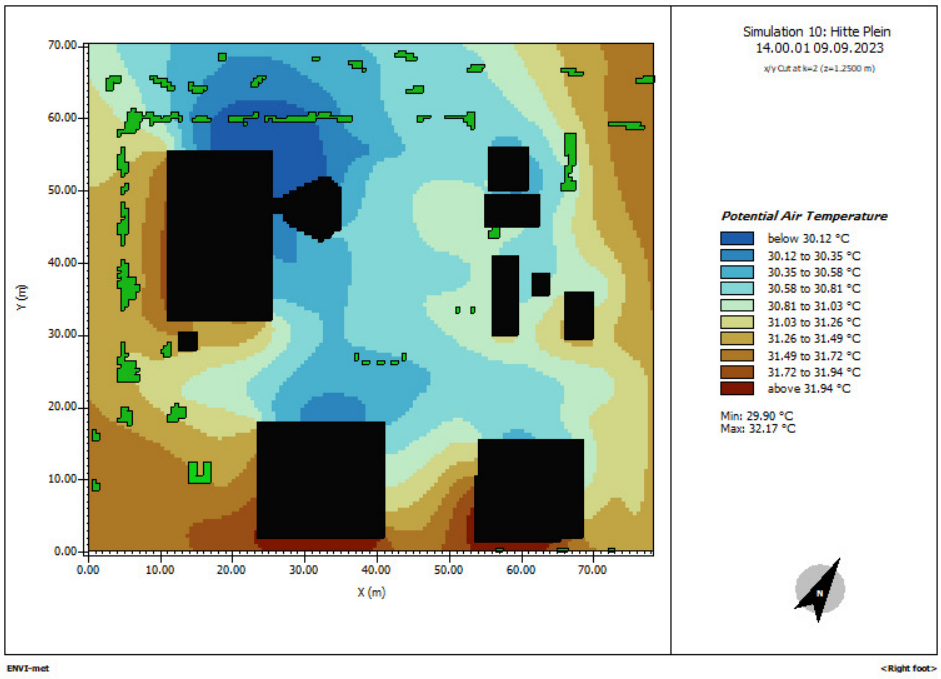

(a)

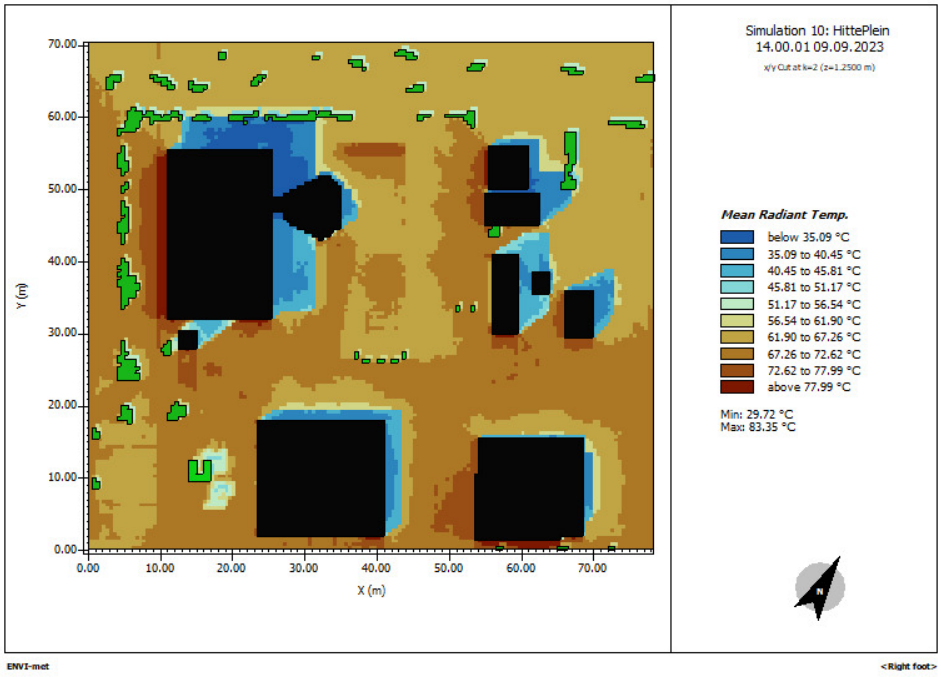

(b)

Figure 4.38.: No water scenario: (a) Air Temperature and (b) Mean Radiant Temperature throughout the Green Village at 1.25m height computed by ENVI-met (09-09-2023 at 14:00 UTC+2)

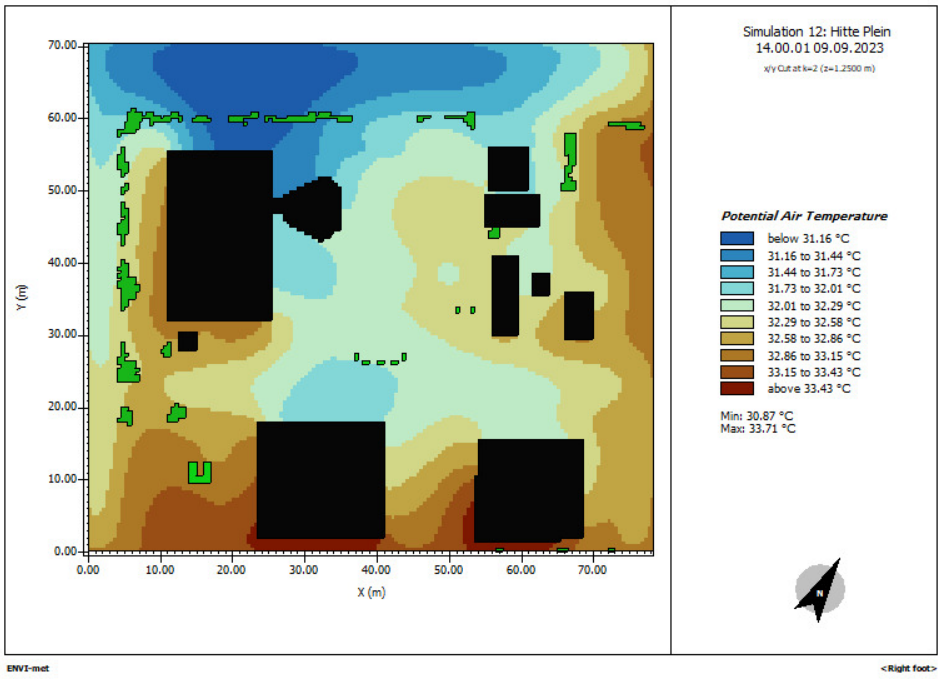

(a)

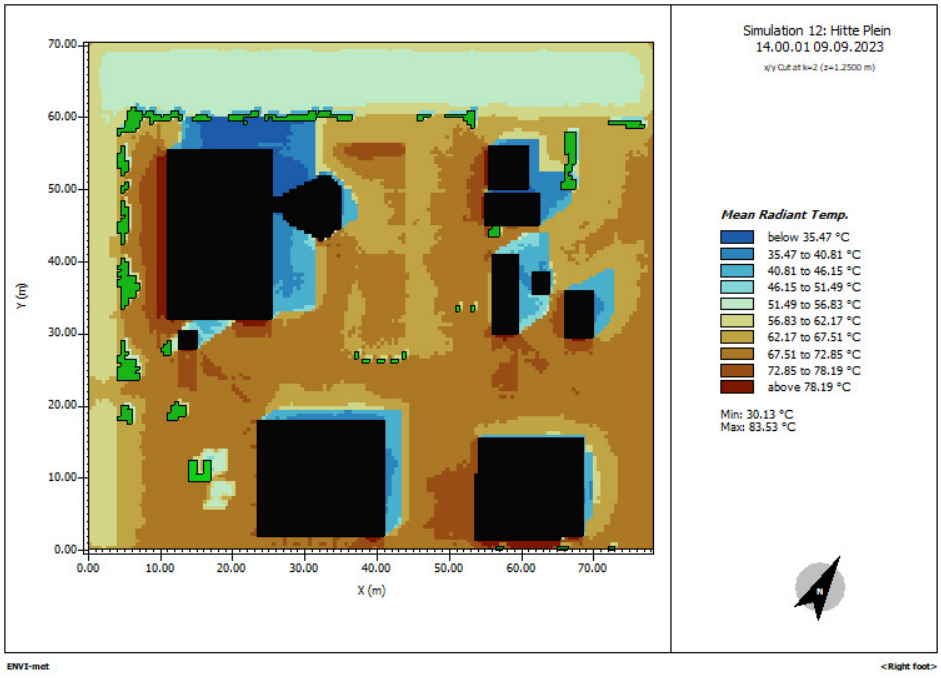

(b)

Figure 4.39.: RCP2.6 scenario: (a) Air Temperature and (b) Mean Radiant Temperature throughout the Green Village at 1.25m height computed by ENVI-met (09-09-2023 at 14:00 UTC+2)

5. Discussion

5.1. The Heat Square

The study stems from the initial design and objectives of the Heat Square, which aim to implement various cooling strategies and climate adaptive innovations, thereby providing an overall cooling effect compared to the previous configuration of the Heat Square. It is important to note that the design of the Heat Square was not specifically tailored to the objectives of this study, seeing as there are multiple stakeholders and objectives to the the construction of the Heat Square. As a result, certain design aspects may conflict with the purposes of this study, which focuses on assessing soil temperature responses to different types of ground cover at various soil depths.

If the design of the Heat Square had been exclusively for the purposes of this study, it might have looked somewhat different. This section of the discussion will examine the design developed by researchers and the Green Village and evaluate it in the context of this study.

5.1.1. Cooling measures

Throughout this report, the various elements implemented within the Heat Square were referred to as 'cooling measures.' However, not all of these elements are intended to provide a direct cooling effect. Some were implemented for comparative purposes or to test other aspects of climate change that are not directly aimed at mitigating the UHI effect. Although many of these elements are omitted from the study, some of these 'cooling measures' are mentioned throughout the report. For the sake of consistency, the general term 'cooling measures' was used. The cooling measures of particular importance to this study include the different paved surfaces (sand, light concrete, dark concrete), the local soil and roofing substrate plots, the Urban Jungle Project, and the variations in mowing frequency.

Paved surfaces

The temperature results from the DTS system in Section 4.1.1 show clear differences between the various pavement types. Diurnal effects are less pronounced in the deeper section of the cable, as illustrated in Figure 4.1, due to the shallow half of the cable being more heavily influenced by short-term changes in surface conditions. Generally, the sand pavement leads to cooling of the soil underneath, with average temperatures on 09-09-2023 being approximately 20°C and 20.7°C at a depth of 60 centimetres. In contrast, the temperatures beneath the light concrete pavement are around 23.6°C and 24°C. The dark pavement results in the highest soil temperature increase, reaching approximately 24.6°C. Comparing the overall temperature profile of the fibre-optic cable on that day, it is clear that the sand pavement contributes to soil cooling, whereas the light and dark concrete pavements result in soil heating. This difference is likely due to the albedo of these surfaces, which is highest for the sand pavement, followed by the light concrete pavement, and lowest for the dark concrete pavement. Higher albedo surfaces reflect more solar radiation, reducing heat absorption and, consequently, soil temperature.

In the ENVI-met model, soil temperature changes are propagated vertically, as detailed in the model structure in Section 2.5. While some lateral heat gradients are visible in the real situation, this is not the case for the ENVI-met model. The soil temperature at a depth of 30 centimeters in Figure 4.23 shows similar phenomena to the measurements of the DTS system; the soil temperature from lowest to highest under each pavement is the sandy pavement, the light concrete pavement, and the dark concrete pavement. These temperatures are approximately 22°C, 23.5°C,

and 24.2°C, respectively. However, the ENVI-met model does not show a significant difference in soil temperature under the sandy pavement as compared to the other pavements as observed in real life. This could be due to the albedo of the sandy pavement being parameterised too low, or the other way around, the albedo values for both concrete pavements being too high. At a depth of 60 centimeters, the soil temperature does not vary much, making comparisons difficult. This is likely because the model's spin-up time is insufficient for significant heat penetration from the atmosphere to the deeper subsurface.

The construction of the sand pavements, compared to the concrete pavements, is quite narrow, making the soil temperature changes less visible in these sections in the DTS results. However, there is a stretch of cable that follows the length of one of the paths, where the Urban Jungle Project is situated, between 180 and 187 LAF for a depth of 30 centimetres. In the DTS results, it is clearly visible that this section cools down considerably. However, we are not able to determine whether this cooling is predominantly due to the sandy pavement, the Urban Jungle Project, or an equal contribution of the two. It would have been interesting for the study to create sandy pavements as wide as some of the concrete pavements to compare the two. As observed, there is some, but not a significant amount of, horizontal heat transport in the soil. The narrow sand pavements, while effective, do not provide enough data to separate the effects of the pavement material from the effects of the Urban Jungle Project in the current setup of the DTS system.

Soil substrate

To properly compare the effects of the different soil substrates on the soil temperature is by examining the temperature measured by the DTS system at the same depth for the different soil substrates. In the current setup of theDTS system, there are no sections of the cable that can be used for a direct one-to-one comparison. In the shallow half of the fibre-optic cable, all sections under vegetation in the local soil substrate are situated at a depth of 10 centimeters, while all sections of the cable under vegetation in the roofing substrate are at a depth of 30 centimeters. For the deep section of the cable, although all of the cable is at the same depth, it is surrounded by the same local soil substrate; the roofing substrate was only placed up to a depth of 40 centimeters. Despite not being able to make a direct one-to-one comparison, we can still examine the soil temperature at a depth of 60 centimeters under the vegetated plots. Because most of the soil above consists of roofing substrate in the plots that use roofing substrate, we can get some information about the heat propagation characteristics of the two soil substrate types.

Looking at Figure 4.1, in general, the soil temperature beneath the vegetation in the local soil substrate is cooler when looking at the deep half of the DTS results. Specifically, comparing the sections between 211 to 218 LAF (approximately 21.2°C) for the roofing substrate and the sections between 275 to 305 LAF (approximately 19°C to 21.8°C) for the local soil substrate. It is, however, important to note that the section mentioned for the vegetation in the local soil substrate is closer to buildings, making it more susceptible to the cooling effects of shade on the soil temperature. This proximity to buildings could result in lower temperatures due to less direct solar radiation and more shading instead of the differences in soil temperature being caused by the different soil substrate.

In ENVI-met, reproducing a soil profile with the same characteristics as the one in the vegetated plots with roofing substrate was challenging. However, different soil types were still input into the model to perform some comparison. The model uses built-in library materials, with the local soil substrate represented by the 'Sandy Loam' soil profile, and the roofing substrate represented by the 'Clay Loam' soil profile, because the roofing substrate material used is Expanded Clay Aggregate. The temperature under the Clay Loam soil profile at a depth of 30 centimeters is cooler than the Sandy Loam soil profile, with averages of 21.5°C and 22°C, respectively (Figure 4.23). This is opposite to the results from the DTS system, where the roofing substrate plots show higher soil temperatures than the local soil substrate plots.

The difference is most likely caused by the specific soil characteristics in ENVI-met for the materials used for the roofing substrate. Key properties such as water content at saturation, field capacity, and wilting point are all higher for the Clay Loam (roofing substrate) than for the

Sandy Loam (local soil substrate). ENVI-met computes the soil temperature based on various variables, including water content. In the real scenario, the roofing substrate consists of relatively large pebbles, which can not hold as much water compared to sand. This characteristic makes it easier for water to evaporate during dry summer days. The pebbles in the roofing substrate likely have lower water content at saturation, field capacity and wilting point than assumed in the ENVI-met model. Therefore, during periods of high temperature and low humidity, the real roofing substrate loses moisture quicker, leading to higher soil temperatures compared to the model's predictions.

Urban Jungle Project

The Urban Jungle Project, located above the fibre-optic cable of the DTS system, significantly influences soil temperatures at various depths. The fibre-optic cable under the Urban Jungle Project is situated at an LAF of 180 to 187 meters for a depth of 30 centimeters and at an LAF of 233 to 240 meters for a depth of 60 centimeters. The DTS system results indicate that soil temperatures under the Urban Jungle Project are considerably cooler than the rest of the cable, both in the deep and shallow sections. The cooling observed under the Urban Jungle Project can be primarily attributed to the shading provided by the tree canopies. The shading effect reduces the amount of direct solar radiation reaching the soil surface, thereby lowering the soil temperature. Additionally, the Urban Jungle Project is situated on top of sandy pavement, which itself contributes to a cooling effect due to the higher albedo of this pavement compared to the rest of the Heat Square. This combined effect of shading from the tree canopies and the reflective properties of sandy pavement creates an enhanced cooling effect on the soil beneath. Other mechanisms, such as tree evapotranspiration, indirectly influence the underlying soil temperature. However, quantifying the specific contribution of this mechanism to overall subsurface cooling is difficult.

In ENVI-met, the Urban Jungle Project was schematized as a row of tall hedges, 2-3 meters in height, placed on top of the sandy pavement section within the Heat Square. While this simplified representation may not perfectly simulate all the cooling effects of the Urban Jungle Project, it does capture the primary mechanism: shading. The hedges provide shading for the underlying soil, which is the predominant cooling mechanism. This results in an approximate 0.3°C decrease in soil temperature at a depth of 0.3 meters compared to the nearby unshaded soil.

Mowing frequency

The urban cooling differences of the mowing frequency in the Heat Square could not be measured by the DTS system. This is due to the mowing frequency plan requiring a longer period for the vegetation to establish according to their specified mowing frequencies. The DTS measurements taken on 09-09-2023 occurred when the vegetation had not yet grown sufficiently to reflect the different mowing treatments. At this time, vegetation on the roofing substrate barely reached a height of 10 centimeters, and the vegetation on the local soil substrate had not grown enough to require mowing (Figure 5.1). Consequently, the ENVI-met model, which was based on the same date as the DTS system's sample temperature measurements, did not account for different vegetation heights caused by the variable mowing frequency. Additionally, due to the limited time available for running simulations, a scenario incorporating different vegetation heights was not simulated. Thus, the study cannot assess the cooling effect of varying mowing frequencies.

5.1.2. DTS set-up and measurement devices

The path of the fibre-optic cable laid out in the subsurface for performing DTS measurements was predetermined prior to the conception of this study. Given the available resources and opportunity to implement a soil temperature monitoring system through DTS, it was installed. However, due to other necessary infrastructure beneath the Heat Square, the placement of the

Figure 5.1.: Vegetation growth on the roofing substrate (top) vs. the local soil substrate (bottom) on 23-08-2023. Two and a half weeks prior to the day of the sample measurements used from the DTS system.

fiber-optic cable was restricted, influencing its final layout. Consequently, the study's scope and objectives were formulated based on the pre-existing fiber-optic cable installation.

This raises the question of whether the formulated scope and objectives are entirely appropriate for the setup, and if alternative research focuses might have been more suitable. Although loops of nearly 8.4 meters in length were included during installation to accommodate potential future research directions, these were not utilised in the current study. One of the main objectives of this study was to investigate the cooling effect of various measures implemented in the Heat Square, which was achieved for the sections traversed by the cable. The cable placement at varying depths in the shallow section was a necessity due to space limitations and the need to protect the cable from heavy traffic.

Ideally, the cable would traverse the center of the vegetated plots to minimise lateral influences from adjacent ground cover types. Currently, the fibre-optic cable mostly runs along the edges of these vegetated plots. Fortunately, the soil temperature phenomena caused by different ground covers at the plot edges do not heavily influence the measurements. It would have been valuable to place multiple rows of cables through one vegetated plot to obtain a comprehensive soil temperature grid. However, such a setup might have hindered other projects within the Heat Square.

In the shallow section of the cable, ribbed pipes were used to protect the fibre-optic cable in areas under paved surfaces, increasing the likelihood of measuring air temperature in the sub-surface instead of soil temperature. The cable is susceptible to measuring the air temperature surrounding it if the soil is not compacted sufficiently. The presence of pipes around the cable, which are less compressible than the soil, increases this risk. Additionally, the possibility exists that the cable has been displaced over time, though there is no efficient way to monitor this. Despite these factors, the potential ambiguity of the results are not visbile, seeing as the results are accurate in comparison to the control measurements by the tensiometers.

5.2. ENVI-met

The initial approach to model the Heat Square and its surroundings was ENVI-met, which seemed the most suitable at the beginning of the study. However, there was limited prior knowledge about the limitations, capabilities, and requirements for using this urban microclimate model. This section of the discussion reviews the results derived from the ENVI-met models, identifies remaining areas of exploration, and considers what could be gained from other research approaches.

5.2.1. ENVI-met vs. other models

ENVI-met was selected as the urban microclimate model for this study because it provides comprehensive outputs, including soil, atmospheric, and radiation parameters. ENVI-met implements a comprehensive soil model into its simulations, providing a clear interface between atmospheric and soil conditions. This made it suitable for combining it with the DTS system, which measures the soil temperatures of the Heat Square. The integration of ENVI-met with the DTS system was crucial to the research objectives, resulting in the research objectives formulated.

Modeling soil and its properties poses significant challenges due to the physical inhomogeneity and susceptibility of soil to various external factors such as erosion, compression, and biotic activity. Soil properties, including organic content, grain size, and strength, vary significantly within the same soil in uncontrolled environments, making precise parameterisation complex and labor-intensive. For this study, global parameters from the ENVI-met software library were used, which increased the potential for errors in approximating soil temperatures.

From the outset, it was clear that approximating soil temperature using ENVI-met would be a challenging task, especially given the novel nature of this approach. However, despite these challenges, the study successfully yielded clear results that offered interesting insights into the soil's response to its urban environment. In hindsight, exploring alternative research directions that integrated both technologies might have led to even more practical and applicable outcomes.

The aim of approximating soil temperature was to subsequently analyse atmospheric conditions and simulate different scenarios based on various thermal comfort indices. ENVI-met provides different outputs on thermal comfort indices other than the T_{mrt}, such as the PET, PMV, and UTCI. Other microclimate models, such as RayMan and SOLWEIG, are also capable of computing these indices ((Matzarakis, 2017)(Lindberg and Grimmond, 2019)). However, these models were not used because they do not allow for the examination of soil temperatures, and can therefore not be validated through DTS system measurements.

While there are alternative methods to validate the RayMan and SOLWEIG models, such as comparing measured in-situ thermal comfort indices to the model outputs, these approaches would not incorporate the DTS system. Additionally, RayMan and SOLWEIG require a more extensive set of input parameters, including radiation measurements, sky view factor maps, and other inputs already needed for ENVI-met((Matzarakis, 2017)(Lindberg and Grimmond, 2019)). Albedo and emissivity of surfaces are also required but can be determined from literature rather than taking direct measurements. These added inputs make it more labor-intensive to set up a model with RayMan and SOLWEIG compared to the already extensive process of formulating an ENVI-met model.

In hindsight, the model could have been used solely for assessing various scenarios and the cooling effect of the Heat Square without validation. In that case, RayMan and SOLWEIG could have been equally valuable models to use instead of ENVI-met. The DTS system could still have been utilised to identify the cooling effect of the measures implemented by analysing the soil temperatures measured. Additionally, an alternative approach could have involved comparing the outputs of ENVI-met, RayMan, and SOLWEIG to in-situ measurements, thereby looking at the strengths and weaknesses to each model. This multi-model comparison would provide a framework for the application of each model, and selection of the right model depending on what the research is trying to achieve.

5.2.2. Parametrisation and modelling

Modelling in ENVI-met is an extensive process but quite straight forward. It requires a selection of building materials, surface covers, wall and soil profiles, and vegetation types and their parametrisation. These parameters define the behaviour of the surfaces to incoming radiation, as well as their heat transmission, and emission, to name a few mechanisms. Several general building and surface materials, soil profiles, and vegetation types are already provided in the software library. However, should there be very specific materials that are not found within this library, the parameters for each material can be input.

The initial approach in creating the Heat Square model required gathering most of the parameters from literature, supported by in-situ measurements of material properties. A key property is the albedo of various surfaces, crucial for determining radiation absorption or reflection, and consequently, the temperature of the material and its surroundings. This property was measured for various surfaces within the Heat Square. Figure 5.1 shows the setup for measuring the albedo of various surfaces within the Heat Square using a NR01 radiometer manufactured by Hukseflux. This was conducted in collaboration with (Middelbeek, 2024) for their research on ground cover impacts on soil temperature.

Table 3.1 presents the albedo measurement results, which were input into some of the materials in the ENVI-met model. Different soil profiles were also created to better match the conditions in the Heat Square. While these adjustments did not lead to the anticipated improvement in the model's performance, the underlying issue became clear upon reviewing the data. The albedo measurements showed similar values, with high values being lower than expected. To ensure the radiometer's accuracy, a high-albedo surface was placed nearby, and the readings quickly reached 0.7, confirming that the radiometer was functioning correctly. It seems likely that the radiometer was not positioned close enough to the surfaces, resulting in measurements that included surrounding areas. Consequently, the measured parameters did not enhance the model's performance, and materials from the software library were used instead.

After determining the materials for the model, their spatial distribution and the geometry of buildings needed to be input into a separate file. This process involved spatial surveying of each surface and building. Google satellite images (Google, 2024) and on-site measurements around the Heat Square and the Green Village were used to log heights and the current situation of the area. The data from this surveying had to be input into a cubic grid with a resolution of 0.5 m x 0.5 m x 0.5 m. This resolution implies that not all geometry dimensions would fit perfectly, as many dimensions are not divisible by 0.5 meters. These discrepancies in geometry could have contributed to differences between the temperatures modelled by ENVI-met and those measured by the DTS system.

Once the model's geometry is finished, simulation can be executed using predefined weather forcing. This requires the manual input of hourly data for air temperature, relative humidity, wind speed and direction, and cloud cover at various altitudes. Additionally, the geolocation and the specific day of the year are required to calculate the radiative forcing. However, the current simulation approached relied on inputting weather data for a single day. Consequently, if the simulation lasts multiple days, the same weather conditions are applied across the entire simulation period. This limitation means that variable weather conditions cannot be adjusted for each day separately. To tackle this, periods were selected where weather conditions remained relatively stable. The dates from 07-09-2023 to 09-09-2023 were chosen for the simulation to minimise variability.

In scenarios where simulations cover days with significant weather changes, a practical approach would be to use averaged weather data for the period. For the simulation with a lower resolution, it is important to note that the weather conditions preceding the simulation period can increase errors in the approximation. Specifically, if the weather before the simulation period differed significantly, using a constant weather forcing may result in an elevated mean temperature. This is what most likely occurred in the simulation of the low-resolution scenario.

5.3. Unforeseen challenges & limitations

Throughout the study, numerous unforeseen challenges and events emerged, complicating the research process. One of the initial challenges was related to the surface conditions of the Heat Square. Upon installation, the DTS system began recording temperature profiles approximately every two minutes. When analysing data from various dates with differing weather conditions, unexpected patterns emerged. Upon reviewing photographs of the Heat Square, it became apparent that the activation of sprinklers on hot days, intended to irrigate the seeded ground, significantly influenced soil temperatures. During extended dry periods, when the vegetation had not yet fully grown, the soil required watering. This irrigation led to cooler soil temperatures on hot days compared to other days with similar weather conditions but without watering. Unfortunately, the irrigation activities were not logged, making it challenging to correlate temperature data with watering events unless they were documented. On a positive note, this underscores the success of the DTS system in detecting unexpected situations. By identifying anomalies in the temperature profile results, the system proves its effectiveness in highlighting irregularities that might otherwise go unnoticed.

Another example of such occurrences involved the Green Village's function as a hub for innovative initiatives, often hosting networking events on the Heat Square. Pop-up canopy tents and food serving tables were set up to provide shade and accommodate guests. The duration of these setups was not logged, introducing variables that potentially affected soil temperature measurements. The presence of people also absorbed heat that would otherwise penetrate the soil, potentially further influencing the data. Additionally, on one occasion, a plot was excavated to install a water storage system near the fibre-optic cable, potentially displacing it (this was detected by the DTS system by looking at anomalies in the results). This displacement could lead to inaccurate temperature measurements in that section. These external factors, which were not documented or controlled, may have significantly influenced the DTS system's results, adding layers of complexity to the study.

Regarding the installation of the measurement devices, significant efforts were made to ensure the precise alignment of the fibre-optic cable along the desired path. This does not mean that results from the DTS system are not susceptible to measurement anomalies from human errors. Prior to laying the cable at each depth, the underlying soil was compacted to prevent further settling and to maintain the intended depth. This procedure was also applied to the shallow sections of the cable, which had varying heights. To protect the cable in these shallow sections from heavy traffic, ribbed pipes were introduced to encase the fibre-optic cable, providing an additional barrier between the soil and the cable. Additionally, the buffing of the cable itself creates an insulating barrier between the cable and the soil. These three aspects of the installation process—compacting the soil, using ribbed pipes, and the buffing of the cable—potentially increased the risk of deviations in soil temperature measurements due to errors from the application of the DTS system.

Verifying the depth of the entire cable would require extensive dismantling of the surface cover, which is impractical. Therefore, we must assume that the cable locations are correct. The measured temperatures were cross-verified against the measurements obtained from tensiometers installed after the construction of the Heat Square was finalised. These tensiometers were manually installed, introducing additional risks of human error. These factors must be considered, as they imply that the soil temperature measurements obtained by the DTS system may not be entirely accurate, and there is a possibility that they do not provide the results we are seeking. In addition, the tensiometers could have been used to verify whether the soil was irrigated or not, as they measure soil moisture levels. However, this verification process was not implemented in the study.

Another aspect of the study that posed a challenge was the setup of the ENVI-met model and its inherent limitations. As previously mentioned, the cubic grid space and the parametrisation of materials within this grid space were restricted to predetermined sizes and parameters. In reality, not everything fits perfectly into a cubic grid, and materials have imperfections resulting in inhomogeneous properties. Additionally, the model had difficulty simulating weather conditions with wind speeds higher than 5 m/s. This issue arose because the small grid size caused model particles to skip grid cells, leading to floating-point errors. Consequently, the selection of

days for simulation was limited to those with low wind speeds, further narrowing the range of suitable days for accurate simulation.

Modeling the vegetation in the Heat Square proved challenging due to its variability. ENVI-met offers two options for representing plants: simple and complex plants. Simple plants are characterized by predefined attributes, such as 'grass 25 cm tall' or 'hedge 1m dense', and occupy entire grid cells within the model. This can oversimplify reality, where plant distributions are often irregular. Similarly, complex plants in ENVI-met are limited in precision; they are defined by the number of grid spaces they occupy, with input parameters including leaf emissivity, shortwave transmittance, Leaf Area Index (LAI), and yearly leaf cover distribution. Despite these inputs, accurately reproducing existing plants remains a challenge.

To accurately simulate the urban microclimate of the Heat Square for a given day, the model must be initialised with precise weather conditions at the start of the day. This could be achieved by inputting the initial conditions for the entire Heat Square, including air and soil temperatures, moisture, radiation, and wind parameters. However, ENVI-met is unable to input start parameters in sufficient detail to achieve a perfect match with observed results, and comprehensive measurements of these parameters is not feasible due to the high labour and costs associated with installing sensors throughout the area. The alternative approach involves spinning up the model by applying weather forcing from several days prior to the desired simulation day. Ideally, the perfect spin-up time for the model would span the entire period from the construction of the Heat Square to the simulation date. However, this would require an impractically large amount of computational power and storage space to store intermittent model results.

5.4. Positioning research within academic literature

In this chapter, we position this study within the available academic literature to demonstrate its relevance, originality, and contribution to the field. This section aims to compare the results and methodology with existing studies, identifying how the work done aligns with or diverges from other research. By placing this study within the context of existing literature, we underscore the insights and advancements this research contributes to the understanding of urban microclimates and the application of technologies like DTS and ENVI-met for urban heat monitoring.

5.4.1. Comparison of findings

Multiple studies have utilised ENVI-met for microclimate analysis in small urban environments. For instance, Aleksandrowicz et al. (2023) aimed to compare T_{mrt} results from ENVI-met with monitored values, based on concerns raised in previous studies about the model's ability to accurately simulate solar irradiance effects. The study found that using default albedo values from the ENVI-met material library led to relatively high T_{mrt} values, ranging from 48°C to 68°C in unshaded areas, which is relatively close to this study's benchmark model results (55°C to 77°C). The study suggests that inputting self-measured albedo values significantly reduces this overestimation, lowering T_{mrt} by approximately 8°C on average (Aleksandrowicz et al., 2023). This implies that the T_{mrt} values found in this study are likely higher than they should be, probably due to the default albedo values in the library not accurately reflecting the Heat Square's conditions. Similar findings were reported by Sinsel et al. (2022) and Szucs et al. (2014), who also noted ENVI-met's tendency to overestimate T_{mrt} values.

Regarding the different heat mitigation measures implemented, Taleghani (2018a) examined various strategies across multiple urban settings. The study concluded that vegetation and high-albedo surfaces were the most effective solutions for improving outdoor thermal comfort (Taleghani, 2018a). However, when comparing these two approaches, vegetation outperformed high-albedo surfaces due to the re-radiation of heat towards pedestrians by the latter, a finding that aligns with the results of this study. The recommendation was made to use high-albedo surfaces only in areas where re-radiated solar radiation does not impact pedestrian zones Taleghani (2018a).

A study conducted in Sydney analysed the impact of various heat mitigation strategies on peak ambient temperature (Mohajer et al., 2022). The research observed a reduction in peak ambient temperatures ranging from 0.47°C to 1.35°C, achieved by increasing surface albedo and expanding ground and roof greenery (Mohajer et al., 2022). In comparison, this study found a 0.4°C decrease in air temperature in the benchmark scenario relative to the concrete square scenario, which is somewhat lower. However, this difference can be attributed to the larger urban area covered in Mohajer et al. (2022)'s study. Despite this, the magnitude of temperature reduction in both studies is comparable, indicating consistent trends across different studies. It is worth noting that several studies, including the one from Taleghani (2018a) and Mohajer et al. (2022), do not consider the cooling effects of water features—a factor that this study has briefly explored.

When comparing soil temperature patterns from this study to others, there is limited literature available, as few studies utilise DTS for urban microclimate analysis. Bottcher and Zosseder (2022) conducted soil temperature measurements across an urban environment to examine both anthropogenic and natural causes of urban groundwater heating. While the study acknowledged the impact of anthropogenic influences, such as heat output from underground structures, it emphasised the significant role of surface boundary conditions above the groundwater or soil (Bottcher and Zosseder, 2022). This aligns with the findings of this study, which also concluded that surface properties above the soil are the primary factors affecting soil temperature, aside from weather conditions. Similarly, Zhang et al. (2022) used DTS to monitor soil temperature in an urban environment, although their focus was on vertical measurements by inserting a fiber-optic cable into boreholes. They found that soil temperatures vary most near the surface, stabilising at depths between 10 and 20 meters (Zhang et al., 2022). Their study was specifically concerned with the thermal responses of the subsurface for the management of shallow geothermal use (Zhang et al., 2022).

5.4.2. Contribution to knowledge

This study succeeds the work of Mao (2022), which examined the thermal behavior of the Heat Square before its redevelopment. One of the objectives of this redevelopment was to establish a comparison between the previous and current configurations of the Heat Square, as well as to evaluate various heat mitigation strategies. This research evaluates both the atmospheric and sub-surface responses of the Heat Square using DTS and ENVI-met, to perform a comparative analysis of different scenarios and heat mitigation strategies. Given the close collaboration between the Green Village, research institutions, and municipalities, these results can be instruments for developing strategies for mitigating the UHI effect and informing policy development for future urban planning initiatives.

The use of DTS for urban microclimate analysis and soil temperature monitoring is uncommon in the literature, particularly when examining horizontal temperature profiles beneath various surfaces. This study demonstrates that a setup like the one implemented in the Heat Square can provide valuable and insightful data on heat distribution in the soil at a small scale. While most studies rely on point measurements at different locations, focusing on a concentrated area reveals the significant variability in soil temperatures, not only across different urban environments but also within a small space. Although the installation of DTS may present challenges, such as needing to adjust the depth for other infrastructure or encasing the cables in ribbed pipes for protection, the system's results proved to be accurate and reliable.

Bottcher and Zosseder (2022) and Zhang et al. (2022) emphasise the importance of monitoring soil temperature in urban environments, highlighting its relevance not only for maintaining soil and vegetation health but also for geothermal energy applications and safeguarding groundwater quality. The DTS system used in this study demonstrates the potential of this tool for high-detail soil temperature monitoring. Despite the relatively small scale of the setup in this study, the fiber-optic cable can extend up to 2 kilometers (Schilperoort, 2022), making it applicable for monitoring larger areas and adaptable to a wide range of urban contexts.

Other studies utilising ENVI-met often overlook the soil model results, focusing primarily on inputting soil parameters to initialise simulations (Feng et al., 2024). In contrast, this study emphasizes analysing the outcomes generated by the soil model. Although the soil temperatures

recorded by the DTS system were not precisely matched by the ENVI-met model, both methods demonstrated similar climate response patterns within the Heat Square. The qualitative alignment of these results suggests that discrepancies may arise from either the model's parameterisation or the structure of the soil model itself. As a result, this study highlights potential areas for improvement, whether through improved schematisation of urban environments or refining the soil model's formulation. Overall, it can be said that soil temperature is often overlooked in urban microclimate modeling, despite being a crucial factor in understanding the UHI effect.

6. Conclusions and Recommendations

6.1. Conclusions to the research questions

In this study, we have combined two distinct tools to assess the urban microclimate in a controlled environment: Distributed Temperature Sensing (DTS) and the Computational Fluid Dynamics (CFD) model ENVI-met. DTS was used as a validation instrument for the ENVI-met model to determine its reliability in examining sub-surface conditions of the urban microclimate. The implementation of the ENVI-met model was then extended to its more common application of simulating atmospheric conditions in urban environments under various urban, geographical, and meteorological scenarios. The primary objective of this study was divided into several research questions, which we will address based on the study's findings.

1. What is the soil temperature measured by the DTS system at different depths under different types of ground cover?

The observation date of September 9, 2023, was selected for analyzing the DTS system data due to favorable weather conditions: consistent temperatures in the days leading up to it, warm regional temperatures highlighting UHI effects, and minimal wind, which reduced the risk of ENVI-met model errors. The data from this date, recorded at 14:00 LT, show distinct soil temperature patterns, presented in Table 4.1.

The highest soil temperatures were observed under the fourth vegetation plot, where recent excavation and poor maintenance left the soil bare. This, combined with the proximity of the cable to the surface, resulted in temperature anomalies. Excluding this plot, the warmest temperatures were found under the concrete pavements, with dark concrete being slightly hotter than light concrete. In contrast, the lowest temperatures were recorded under the Urban Jungle Project, though it remains unclear whether this cooling effect was due to the shading of the trees or the underlying sandy pavement, as similar low temperatures were observed under sandy pavements elsewhere. Overall, the soil temperature varied from coolest to hottest under the following ground covers: Urban Jungle Project, sandy pavement, vegetation on roofing substrate, vegetation on local soil substrate, light concrete pavement, and dark concrete pavement.

2. What is the soil temperature measured by the CFD model ENVI-met at different depths under different types of ground cover?

For the CFD results, simulations were conducted using weather data from September 7 to September 9, 2023, due to the consistent weather conditions during this period. The seventh iteration of the model, which took 109 hours and 47 minutes to simulate just three days of this relatively small urban environment, was used to produce benchmark results against DTS data and compare different scenarios. The ENVI-met model's calculated soil temperature profile along the fibre-optic cable on September 9, 2023, at 14:00 LT is shown in Figure 4.21, with temperatures under different ground covers detailed in Table 4.2.

The model successfully shows varying soil temperature responses based on the surface cover above. Sandy pavements reflect a significant portion of the incoming radiation, leading to cooler soil underneath. In contrast, concrete pavements warm the soil considerably more than the other ground covers. ENVI-met does not account for any lateral spread of soil heat; warming or cooling is propagated solely in the vertical direction. This observation is clear when looking at the areas surrounding the Heat Square, which remained unaffected by the varying schematisations of the Heat Square in each iteration.

3. How do the results from the CFD model ENVI-met compare to the measured soil temperatures by the DTS system, and how can it be further improved upon for other applications and contexts?

ENVI-met bases soil temperatures on ground covers and the soil pack above, whereas the DTS system shows varying temperature peaks, indicating influences beyond the soil profile above the fibre-optic cable. Lateral effects are not considered in ENVI-met. The model accurately captures the response of different concrete pavements and the Urban Jungle Project, showing the highest soil temperatures under concrete and the lowest under the Urban Jungle Project. However, discrepancies arise with other ground covers.

The differences between ENVI-met and DTS results could stem from several factors. Firstly, the model's spin-up time was likely not enough to properly initialise the model. A longer spin-up time would improve the model's approximation of the Heat Square's climatic conditions during the observation period. Secondly, the thermal properties of various surfaces, ground covers, and soils could be more precisely measured. Adjusting ENVI-met's material properties based on these measurements would result in a more realistic soi temperature response.

Accurately modeling a real urban environment remains challenging due to the inherent heterogeneity in material properties, climate, external factors, and geometry. Simulations are predictive tools rather than exact replicas of an urban environment's response to climatic conditions. Nonetheless, ENVI-met is valuable for creating urban environment models and making qualitative predictions without costly sensor installations and monitoring. Its capabilities can greatly aid decision-making for adapting to evolving urban climates.

4. What does the ENVI-met model tell us about the response of the Heat Square to different urban, geographical and meteorological scenarios?

In Section 4.2.5, soil temperature, air temperature, and Mean Radiant Temperature (T_{mrt}) are analysed across different simulated scenarios. The Heat Square on September 9, 2023, at 14:00 LT showed cooler air temperatures and T_{mrt} compared to surrounding areas, except for the canal and shaded regions. Air temperature ranged from 30.31°C to 30.87°C at a height of 1.25 meters, while T_{mrt} ranged from 61.03°C to 71.85°C.

- Comparing the benchmark design to the concrete square, the benchmark layout showed significantly lower thermal discomfort and soil temperatures, despite the concrete square design having potentially lower air temperatures. This suggests that the benchmark design is effective in increasing thermal comfort.
- Interestingly, dark concrete sometimes resulted in lower T_{mrt} values than higher albedo surfaces like sandy pavement, indicating that reflected radiation can increase thermal discomfort more than heat emission from hotter surfaces. For instance, in the 'cooling measures' scenario, replacing dark concrete with light concrete reduced subsurface and air temperatures, but increased the T_{mrt}.
- To test the impact of a longer spin-up time, a low-resolution scenario was simulated for twice the duration. Results indicated better approximation of high temperature peaks, confirming the initial hypothesis. However, low temperature peaks remained difficult to simulate, likely due to incorrect model parametrisation. The low-resolution model ran nearly four times faster than the benchmark, emphasising the importance of balancing resolution with run time.
- Finally, two 'extreme' weather scenarios—removal of the surrounding water body and an RCP2.6 temperature increase—were simulated. Both scenarios resulted in higher air temperatures within the Heat Square compared to the benchmark. However, the absence of the water body had a negligible effect on air temperature and T_{mrt}, suggesting limited impact without significant wind. The RCP2.6 scenario showed an air temperature increase equivalent to the weather forcing, with a smaller T_{mrt} increase, indicating that rising air temperatures do not directly translate to proportional increases in thermal discomfort.

6.2. Recommendations

To provide an outlook for this study, it is important to review how its findings can inform future research. Firstly, areas for improvement are explored, addressing the technical and methodological issues that could enhance the accuracy and reliability of the results. Following this, future research directions are proposed, focusing not only on the specific context of the Heat Square but also on broader applications within urban microclimates.

6.2.1. Improving the current study

DTS setup and the Heat Square

To improve the results of the DTS system, the depth of the fibre-optic cable in the shallow sections should be adjusted to align with the study's target depths. Excavating the entire cable is not feasible as it would require dismantling a large portion of the Heat Square. However, some cable loops, as illustrated in Figure 3.1, can be relocated to desired areas. Ideally, these loops can be buried near the existing cables at a depth of 30 centimeters, instead of 10 centimetres in the shallow sections of the cable. This adjustment will enable a proper comparison between the roofing substrate and the local soil substrate at a depth of 30 centimetres. This aids in creating a vertical soil profile for the vegetated plots in local soil substrate by adding more temperature measurements on a vertical direction. Additionally, other cable loops can be used to create a comprehensive gridded soil temperature plot for one of the vegetated plots, allowing for the analysis of the shading effect of the Heat Square on uniformly spread vegetation. Careful excavation is required to avoid unnecessary damage to the existing vegetation. For the deep cable section beneath the roofing substrate, significant excavation to a depth of 60 centimeters and subsequent re-filling would pose a high risk of undesirable displacement of the cable, so this is not feasible.

To improve the assessment of different pavement materials, it is recommended to widen one of the sandy pavements to match the width of the concrete pavements. This adjustment would mean reducing the area of some vegetated plots. Such a modification is valuable for this study as it allows for the comparison of pavements of similar length. If this adjustment is deemed undesirable, an alternative approach could involve temporarily relocating the units from the Urban Jungle Project to facilitate comparing the soil temperature under the concrete pavements, vegetation, and sandy pavement where the Urban Jungle Project is currently standing on. Moving the Urban Jungle Project units nearby pavements which inherently absorb more radiation than the sandy pavement can also help reduce heat stress further.

Furthermore, without altering the Heat Square or the DTS cable layout, it is worthwhile to investigate the impact of mowing frequency on soil temperature. The height of vegetation can significantly influence soil temperature response. Therefore, it is recommended to conduct DTS measurements again after the vegetation in the Heat Square has adapted to their respective mowing frequencies. This approach will provide insights into the relationship between vegetation management practices and soil temperature variations.

ENVI-met

There are several ways to improve the current model built to simulate the Heat Square. One predominantly lies in properly inputting the surface characteristics and thermal properties of surfaces and soils within the Heat Square. Previously the albedo measurements were not performed properly. It is recommended to therefore take samples of each relevant material and soil, and measure their physical and thermal properties in a lab, such as done in Stache et al. (2022) that measured thermal properties of various ground covers. Inputting these measured values will help bring the model of the Heat Square closer to real life scenario. In addition to that, the watering of the vegetation should be logged to input in the model whether the soil has been irrigated or not, which is possible in ENVI-met. Other activities, such as construction work or events, should also be logged to account for their impact when performing DTS measurements

or modeling the Heat Square for a specific day. This logging can be done by visually inspecting the area or cross-referencing with tensiometer data from the desired days.

Currently, only three days were simulated for the modeling of the Heat Square, except for the low-resolution version, which covered six days. It was determined that this low-resolution model outputs results four times faster without a significant deterioration in quality compared to the benchmark model, making the results still usable. Therefore, a longer simulation period should be conducted with this model to better approximate real-life scenarios. This can be achieved by inputting comprehensive weather forcing for all days prior to the desired observation date, a feature that is possible in ENVI-met but was not utilised in this study. Generally, using varying weather forcing equal to the actual weather conditions rather than averaging the weather conditions for simulations will improve the accuracy and reliability of the model's results. A lower-resolution model will also make it possible to simulate weather with higher wind forcing, which posed a problem to the high-resolution model due to the small grid size.

Cooling measures

Insights can be gathered on the best practices for urban heat mitigation within the context of the Heat Square. Analysing the most effective cooling measures based on DTS and ENVI-met results reveals a nuanced picture. Vegetation clearly offers the best overall cooling effect when properly maintained. DTS data show that plots with sparse vegetation due to inadequate maintenance had the highest soil temperatures, with bare soil absorbing most of the incoming radiation and heating up significantly. In contrast, sandy pavement, which reflects much of the radiation, absorbs less heat. However, ENVI-met results indicate that this reflected radiation can increase the T_{mrt} and thus thermal discomfort.

Comparing light and dark concrete pavements shows that, despite dark concrete absorbing more radiation, the reflective properties of light concrete can have a greater negative impact on thermal comfort than the heat emitted by dark concrete. Therefore, while different pavement types influence subsurface cooling and thermal comfort differently, it is important to prioritise these factors based on specific case requirements. The light concrete pavement resulted in lower soil temperatures but at the same time showed increased thermal discomfort. In addition, the hypothesis that dark pavement creates a slight breeze due to heat gradients generated was not supported by DTS or ENVI-met data.

The local sandy soil is preferable to the roofing substrate, as vegetation not only grows faster but also retains moisture longer, resulting in lower soil temperatures underneath. Roofing substrate should be a last resort. Comparing high vegetation with canopies that provide shading to low vegetation shows that high vegetation offers localized cooling where it casts shade but does not significantly outperform low vegetation overall. High vegetation is more resilient to poor maintenance, making it preferable. Similarly, water bodies provide localised cooling and it is not widespread, in conditions with little to no wind.

6.2.2. Future research directions

This study opens up several directions for future research, which will be detailed in this section. Firstly, it has been noted that ENVI-met is not the only tool for calculating thermal comfort indices in urban environments such as PET, PMV, and UTCI. It would be beneficial to compare ENVI-met's results with those from other widely used models like SOLWEIG and RayMan. This comparison would help determine which model is most suitable for specific scenarios, considering the available data and resources. Assessing these models based on their applicability and outcomes could establish a framework for future urban environment studies, enabling researchers to easily select an appropriate modeling approach.

Currently, this study focused on output variables such as soil temperature, air temperature, and T_{mrt}. Future research could explore additional output parameters like turbulence parameters,

radiative fluxes to visualise surface heat balances, and air and soil moisture parameters. Expanding the range of output parameters will provide a more comprehensive understanding of urban microclimate dynamics.

Regarding the DTS system measurements, replacing some of the concrete tiles with white tiles above sections where the fiber-optic cable runs could be an effective way to reduce soil heating, as suggested by Middelbeek (2024). Additionally, the DTS measurements in this study did not include vegetation measurements at different heights, which were influenced by their mowing frequency. Investigating the relationship between the height and mowing frequency of vegetation and its response to varying weather conditions in an urban environment would be valuable. Although this was one of the cooling strategies intended for testing within the Heat Square, the long vegetation growth period did not allow to do so. There are loops of cable available for excavation to measure temperatures above the surface, such as the vertical temperature profile from the soil to a certain depth or through a tree. Incorporating more strategies like varied vegetation measurements and white tiles in the study can improve the understanding and effectiveness of cooling strategies in urban environments.

The implementation of DTS can also be extended to other urban environments where monitoring soil temperature is crucial for groundwater temperature and thermal energy assessments. DTS could effectively monitor the warming effects of infrastructure such as tunnels, buildings, sewer systems and machinery by surrounding these structures with fibre-optic cable, thereby mapping spatial and temporal variations in soil temperature (SUHI effect).

An additional direction for DTS research could involve creating a vertical profile to measure soil temperature at specified depths and extend the measurement to a certain height above the surface, thereby combining both soil and air temperature data. To achieve this, a vertical coil for DTS, as described in Vis (2022), can be employed to overcome the DTS system's limited resolution of 25.4 centimeters. The coil can be inserted into the ground, with another coil positioned directly above the subsurface installation. Developing such a temperature profile could provide valuable insights into the complex dynamics between the soil, atmosphere, and their interface, namely the surface.

Bibliography

J. Acero and J. Arizzabalaga. Evaluating the performance of envi-met model in diurnal cycles for different meteorological conditions. *Theor Appl Climatol*, 131, 2018. doi: 10.1007/s00704-016-1971-y.

J. Acero and K. Herranz-Pascual. A comparison of thermal comfort conditions in four urban spaces by means of measurements and modelling techniques. *Building and Environment*, 93: 245–257, 2015. doi: https://doi.org/10.1016/j.buildenv.2015.06.028.

H. Akbari, H.D Mathews, and D. Seto. The long-term effect of increasing the albedo of urban areas. *Environ. Res. Lett.*, 7, April 2012. doi: 10.1088/1748-9326/7/2/024004.

O. Aleksandrowicz, T. Saroglou, and D. Pearlmutter. Evaluation of summer mean radiant temperature simulation in envi-met in a hot mediterranean climate. *Building and Environment*, 245, 2023. doi: https://doi.org/10.1016/j.buildenv.2023.110881.

F. Ali-Toudert and H. Mayer. Numerical study on the effects of aspect ratio and orientation of an urban street canyon on outdoor thermal comfort in hot and dry climate. *Meteorological Institute, University of Freiburg*, 2004.

F. Ali-Toudert and H. Mayer. Numerical study on the effects of aspect ratio and orientation of an urban street canyon on outdoor thermal comfort in hot and dry climate. *Build Environ*, 41, 2006. doi: 10.1016/j.buildenv.2005.01.013.

ASHRAE. Ashrae fundamentals handbook 2011. *American Society of Heating, Refrigerating, and Air-Conditioning Engineers*, 2011.

M. Atefe and S. Reinhardt. Investigating and analysing the summer season soil temperature conditions on the extensive green roofs in oslo, norway. *University of South-Eastern Norway*, 2020.

S. Boehm, C. Schumer, J. Jaeger, K. Lebling, M. Sima, R. Waite, N. Singh, and A. Lee. State of climate action 2022. *Systems change lab*, October 2022. doi: https://doi.org/10.46830/wrirpt.22.00028.

S. Bonafoni, G. Baldinelli, A. Rotili, and P. Verducci. Albedo and surface temperature relation in urban areas: Analysis with different sensors. *2017 Joint Urban Remote Sensing Event (JURSE)*, pages 1–4, 2017. doi: 10.1109/JURSE.2017.7924612.

F. Bottcher and K. Zosseder. Thermal influences on groundwater in urban environments – a multivariate statistical analysis of the subsurface heat island effect in munich. *Science of The Total Environment*, 810, 2022. doi: https://doi.org/10.1016/j.scitotenv.2021.152193.

I.S. Bowen. The ratio of heat losses by conduction and by evaporation from any water surface. *Physical Review*, 27(6):779–787, 1926. doi: https://doi.org/10.1103/PhysRev.27.779.

M. Bruse. Envi-met 3.0: Updated model overview. *ENVI-met*, March 2004.

M. Bruse and H. Fleer. Simulating surface plant air interactions inside urban environments with a three dimensional numerical model. *Environmental Modelling & Software*, 13:373–384, 1998. doi: https://doi.org/10.1016/S1364-8152(98)00042-5.

S. Chapman, J. Watson, A. Salazar, M. Thatcher, and C. McAlpine. The impact of urbanization and climate change on urban temperatures: a systematic review. *Landscape Ecology*, 32:1921–1935, August 2017. doi: https://doi.org/10.1007/s10980-017-0561-4.

R.B. Clapp and G. Hornberger. Empirical equations for some soil hydraulic properties. *Water Resource Res.*, 14:601–604, 1978.

P. Crank, A. Middel, M. Wagner, D. Hoots, M. Smith, and A. Brazel. Validation of seasonal mean radiant temperature simulations in hot arid urban climates. *Science of the Total Environment*, 749, 2020. doi: https://doi.org/10.1016/j.scitotenv.2020.141392.

J.W. Deardorff. Efficient prediction of ground surface temperature and moisture with inclusion of a layer of vegetation. *Geophys. Res.*, 83:1889–1903, 1978.

N. Debbage and J.M. Shepherd. The urban heat island effect and city contiguity. *Computers, Environment and Urban Systems*, 54:181–194, November 2015. doi: https://doi.org/10.1016/j.compenvurbsys.2015.08.002.

A. Dimoudi and M. Nikolopoulou. Vegetation in the urban environment: microclimatic analysis and benefits. *Energy and Buildings*, 35:69–76, January 2003. doi: https://doi.org/10.1016/S0378-7788(02)00081-6.

J. Dong, S.C. Steele-Dune, T.E. Ochsner, and N. van de Giesen. Determining soil moisture and soil properties in vegetated areas by assimilating soil temperatures. *Water Resources research*, 52(6):4280–4300, May 2016. doi: https://doi.org/10.1002/2015WR018425.

K. Duus and G. Schmitz. Experimental investigation of sustainable and energy efficient management of a geothermal field as a heat source and heat sink for a large office building. *Energy and Buildings*, 235, March 2021. doi: https://doi.org/10.1016/j.enbuild.2021.110726.

K.L. Ebi, T. Hasegawa, K. Hayes, A. Monaghan, S. Paz, and P. Berry. Health risks of warming of 1.5 c, 2 c, and higher, above pre-industrial temperatures. *Environmental Research Letters*, 13(6), June 2018. doi: 10.1088/1748-9326/aac4bd.

J.L Edmonson, I. Stott, Z.G. Davis, K.J. Gaston, and J.R. Leake. Soil surface temperatures reveal moderation of the urban heat island effect by trees and shrubs. *Scientific Reports*, 6(33708), 2016. doi: https://doi.org/10.1038/srep33708.

ENVI-met. Envi-met model architecture, 2023a. URL https://envi-met.info/doku.php?id=intro:modelconcept#module_overview.

ENVI-met. Envi-met support area, 2023b. URL https://www.envi-met.com/training-support/.

ENVI-met. Thermal comfort indices provided by bio-met. *ENVI-met Applications Homepage*, 2024. URL https://envi-met.info/doku.php?id=apps:biomet.

L. Feng, L. Shuai, Y. Zhou, X. Zhang, and J. Sun. Improving the green space arrangement in residential areas from the perspective of tree leaf temperature utilizing scenario simulation in envi-met. *Science of The Total Environment*, 918, 2024. doi: https://doi.org/10.1016/j.scitotenv.2024.170650.

C.V. Gal and N. Kantor. Modeling mean radiant temperature in outdoor spaces, a comparative numerical simulation and validation study. *Urban Climate*, 32, June 2020. doi: https://doi.org/10.1016/j.uclim.2019.100571.

J. Geletic, M. Lehnert, J. Resler, and P. Krc. Application of the utci in high-resolution urban climate modeling techniques. *Applications of the Universal Thermal Climate Index UTCI in Biometeorology*, pages 177–191, July 2021.

Google, 2024. URL https://www.google.com/maps. accessed on 18.07.2024.

A.H. Hartog. An introduction to distributed optical fibre sensors. *CRC Press*, 2017. doi: https://doi.org/10.1201/9781315119014.

J.A. Hiemstra, H. Saaroni, and J.H. Amorim. The urban heat island: Thermal comfort and the role of urban greening. *The Urban Forest*, 7:7–19, February 2017.

B. Holmer, S. Thorsson, and I. Eliasson. Cooling rates, sky view factors and the development of intra-urban air temperature differences. *Geogr.Ann.*, 89A:1–12, 2007.

H. Howard. *Fluid Mechanics(Fifth Edition)*. Elsevier, 2012.

IPCC. Ar6 synthesis report: Climate change 2023. *Contribution of Working Groups I, II and III to the Sixth Assessment Report of the Intergovernmental Panel on Climate Change*, 2023. doi: 10.59327/IPCC/AR6-9789291691647.

B. Janicker, D. Milosevic, and S. Manavvi. Review of user-friendly models to improve the urban micro-climate. *Atmosphere 12*, 1291, 2021. doi: https://doi.org/10.3390/atmos12101291.

V Jankovic and D.M. Schultz. Atmosfear: Communicating the effects of climate change on extreme weather. *Weather, Climate and Society*, 9(1):27–37, January 2017. doi: https://doi.org/10.1175/WCAS-D-16-0030.1.

KNMI, 2024. URL https://www.knmi.nl/klimaat-viewer/kaarten/temperatuur/gemiddelde-temperatuur. accessed on 18.07.2024.

K. Koch, T. Ysebaert, S. Denys, and R. Samson. Urban heat stress mitigation potential of green walls: A review. *Urban Forestry & Urban Greening*, 55, November 2020. doi: https://doi.org/10.1016/j.ufug.2020.126843.

R. Lafortezza, G Carrus, G. Sanesi, and C. Davies. Benefits and well-being perceived by people visiting green spaces in periods of heat stress. *Urban Forestry & Urban Greening*, 8(2):97–108, 2009. doi: https://doi.org/10.1016/j.ufug.2009.02.003.

H. Lee and H. Mayer. Maximum extent of human heat stress reduction on building areas due to urban greening. *Urban Forestry & Urban Greening*, 32:154–167, May 2018. doi: https://doi.org/10.1016/j.ufug.2018.04.010.

D.S. Lemmen and F.J. Warren. Climate change impacts and adaptation:a canadian perspective. *Government of Canada*, 2004.

J.M. Lewis. The story behind the bowen ratio. *Bulletin of the American Meteorological Society*, 76(12): 2433–2443, 1995. doi: https://doi.org/10.1175/1520-0477(1995)076⟨2433:TSBTBR⟩2.0.CO;2.

F. Lindberg and CSB Grimmond. Solweig v2019a. *Department of Earth Sciences, University of Gothenburg, Sweden, University of Reading, UK*, 2019.

Z. Liu, W. Cheng, C.Y. Jim, T.E. Morakinyo, Y. Shi, and E. Ng. Heat mitigation benefits of urban green and blue infrastructures: A systematic review of modeling techniques, validation and scenario simulation in envi-met v4. *Building and Environment*, 200, 2021. doi: https://doi.org/10.1016/j.buildenv.2021.107939.

R. Mahtta, M. Fragkias, B. Guneralp, A. Mahendra, M. Reba, E. Wentz, and K. Seto. Urban land expansion: the role of population and economic growth for 300+ cities. *Urban Sustainability*, 2 (5), 2022. doi: https://doi.org/10.1038/s42949-022-00048-y.

S. Mansouri and E. Zarghami. Investigating the effect of the physical layout of the architecture of high-rise buildings, residential complexes, and urban heat islands. *Energy and Built Environment*, July 2023. doi: https://doi.org/10.1016/j.enbenv.2023.07.004.

Y. Mao. Changing patterns of thermal behaviour of concrete pavements in diurnal periods. *Delft University of Technology*, September 2022.

A. Mathew, S. Khandelwal, and N. Kaul. Analysis of diurnal surface temperature variations for the assessment of surface urban heat island effect over indian cities. *Energy and Buildings*, 159: 271–295, January 2018. doi: https://doi.org/10.1016/j.enbuild.2017.10.062.

T.K.R. Matthews, R.L. Wilby, and C. Murphy. Communicating the deadly consequences of global warming for human heat stress. *Earth, Atmospheric and Planetary Sciences*, March 2017. doi: https://doi.org/10.1073/pnas.1617526114.

A. Matzarakis. Rayman pro: A tool for applied climatology. *RayMan manual version 0.1*, 2017.

L. Middelbeek. Assessing the cooling potential of (modified) ground coverage on the drinking water temperature. *Faculty of Civil Engineering and Geosciences. Delft University of Technology*, 2024.

P. Mirzaei. Recent challenges in modeling of urban heat island. *Sustainable Cities and Society*, 19: 200–206, December 2015. doi: https://doi.org/10.1016/j.scs.2015.04.001.

H. Mohajer, L. Ding, and M. Santamouris. Developing heat mitigation strategies in the urban environment of sydney, australia. *Buildings*, 12, 2022. doi: https://doi.org/10.3390/buildings12070903.

J. Monteith. Evaporation and environment. *Symposia of the Society for Experimental Biology*, 19: 205–234, 1965.

P Osmond and E. Sharifi. Guide to urban cooling strategies. *Australian Government, department of Industry, Innovation and Science*, August 2017.

T. Pohankova and V. Pechanec. Estimating bowen index in urban environment based on landsat 8/9 imagery. *Department of geoinformatics, Palacky University Olomouc, Czechia*, 2024. doi: https://doi.org/10.5194/hess-2024-85.

Population Reference Bureau. 2013 world population datasheet, 2013. URL http://www.prb.org/pdf13/2013-population-data-sheet_eng.pdf.

A. Previati, J. Epting, and G. Crosta. The subsurface urban heat island in milan (italy) - a modeling approach covering present and future thermal effects on groundwater regimes. *Science of Total Environment*, 810, March 2022. doi: https://doi.org/10.1016/j.scitotenv.2021.152119.

C.V. Raman. A new radiation. *Indian Journal of Physics*, 2:387–398, 1928.

B. Schilperoort. Technical note: Using distributed temperature sensing for bowen ratio evaporation measurements. *Hydrol. Eart Syst. Sci.*, 22:819–830, 2018. doi: https://doi.org/10.5194/hess-22-819-2018.

B. Schilperoort. Heat exchange in a conifer canopy: A deep look using fiber optic sensors. *Delft University of Technology*, 2022. doi: https://doi.org/10.4233/uuid:6d18abba-a418-4870-ab19c195364b654b.

B. Schilperoort, C. Rodriguez, B. Wiel, and M. Coenders-Gerrits. A distributed temperature sensing based soil temperature profiler. *EGUspehere*, 2023. doi: https://doi.org/10.5194/egusphere-2023-2292,2023.

R Sharma, L. Pradhan, M. Kumari, and P. Bhattacharya. Assessing urban heat islands and thermal comfort in noida city using geospatial technology. *Urban Climate*, 35, January 2021. doi: https://doi.org/10.1016/j.uclim.2020.100751.

B. Shi, C. Tang, L. Gao, Liu C., and B. Wang. Observation and analysis of the urban heat island effect on soil in nanjing, china. *Environmental Earth Sciences*, 67:215–229, 2012. doi: https://doi.org/10.1007/s12665-011-1501-2.

T. Sinsel. Advancements and applications of the microclimate model envi-met. *Faculty of Geography and Geosciences at the Johannes Gutenberg University of Mainz*, 2021.

T. Sinsel, H. Simon, W. Ouyang, C. dos Santos, P. Shinzato, and M. Bruse. Implementation and evaluation of mean radiant temperature schemes in the microclimate model envi-met. *Urban Climate*, 45, 2022.

A. Solcerova, K. van Emmerik, T. Hilgersom, F. van de Ven, and N. van de Giesen. Uchimizu: A cool(ing) tradition to locally decrease air temperature. *Water*, June 2018.

E. Stache. Manifest: a new nature based urban building standard. *Delft university of technology*, 2021. doi: https://www.euro2021.eu/wiki/639385/manifest.

E. Stache, B. Schilperoort, M. Ottele, and H Jonkers. Comparative analysis in thermal behaviour of common urban building materials and vegetation and consequences for urban heat island effect. *Building and Environment*, 213, April 2022. doi: https://doi.org/10.1016/j.buildenv.2021.108489.

A. Szucs, T. Gál, and H. Andrade. Comparison of measured and simulated mean radiant temperature: case study in lisbon (portugal). *Finisterra*, 49, 2014. doi: https://doi.org/10.18055/Finis6469.

M. Taleghani. Outdoor thermal comfort by different heat mitigation strategies- a review. *Renewable and Sustainable Energy Reviews*, 81, 2018a. doi: https://doi.org/10.1016/j.rser.2017.06.010.

M. Taleghani. The impact of increasing urban surface albedo on outdoor summer thermal comfort within a university campus. *Urban Climate*, 24:175–184, June 2018b. doi: https://doi.org/10.1016/j.uclim.2018.03.001.

the Green Village. How do you make an open and paved urban space climate-proof?, March 2023. URL https://www.thegreenvillage.org/en/hoe-maak-je-open-verharde-ruimte-in-de-stad-klimaatbestendig/.

The Green Village, 2024. URL https://www.thegreenvillage.org/hitteplein/. accessed on 18.07.2024.

S. Thorsson, J. Rocklov, J. Konarska, F. Lindberg, B. Holmer, B. Dousset, and D. Rayner. Mean radiant temperature – a predictor of heat related mortality. *Department of Earth Sciences, University of Gothenburg, Gothenburg, Sweden*, 2023. doi: https://doi.org/10.1016/j.uclim.2014.01.004.

M. Tjernstrom. Some tests with a surface energy balance scheme including a bulk parameterization for vegetation in a mesoscale model. *Boundary Layer Met*, 48:33–68, 1989.

Y. Toparlar, B. Blocken, B. Maiheu, and G.J.F. van Heijst. A review of the cfd analysis of urban microclimate. *Renewable and Sustainable Energy Reviews*, 80:1613–1640, December 2017. doi: https://doi.org/10.1016/j.rser.2017.05.248.

S. Tsoka, A. Tsikaloudaki, and T. Theodosiou. Analyzing the envi-met microclimate model's performance and assessing cool materials and urban vegetation applications-a review. *Sustainable Cities and Society*, 43:245–257, 2018. doi: https://doi.org/10.1016/j.scs.2018.08.009.

United Nations. World urbanization prospects: The 2011 revision highlights, 2012. URL http://www.slideshare.net/undesa/wup2011-highlights.

University of Reading. The surface energy balance, 2023. URL https://www.met.reading.ac.uk/~swrhgnrj/teaching/MT23E/mt23e_notes.pdf.

G. Vis. Spatial temperature measurements and turbulence analysis using dts in the liaise field campaign. *Delft University of Technology*, December 2022.

J. Wang and R.L Bras. Ground heat flux estimated from surface soil temperature. *Journal of Hydrology*, 216, 1999. doi: https://doi.org/10.1016/S0022-1694(99)00008-6.

L. Yang, F. Qian, and K. Song, X. Zheng. Research on urban heat-island effect. *Procedia Engineering*, 169:11–18, 2016. doi: https://doi.org/10.1016/j.proeng.2016.10.002.

YOKOGAWA. Dtsx3000 distributed temperature sensor. *OpreX Field Instruments*, 2023.

T. Zhang. City-wide monitoring and contributing factors to shallow subsurface temperature variability in nanjing, china. *Renewble Energy*, 199:1105–1115, November 2022. doi: https://doi.org/10.1016/j.renene.2022.09.044.

T. Zhang, C. Liu, P. Bayer, L. Zhang, X. Gong, and K. Gu. City-wide monitoring and contributing factors to shallow subsurface temperature variability in nanjing, china. *Renewable Energy*, 199:1105–1115, 2022. doi: https://doi.org/10.1016/j.renene.2022.09.044.

A. Heat Square projects

Table A.1.: Independent projects implemented throughout the Heat Square as of July 2024 (The Green Village, 2024).

Project	Description
Bluebloqs	Rainwater captured from impervious surfaces undergoes purification via a biofiltration system before being utilized for irrigation purposes
Boomveer	Trees with elevated root systems suitable for planting in spaces with limited capacity for extensive underground root systems
DSI/FHVI pit	Compact underground water storage capable of accumulating extreme volumes of water in an infiltration pit
Flowsand	Sponge-like sand that rapidly absorbs water and releases it gradually into the subsurface
Het Briesje	Combination of mowing frequency and ground cover composition to generate a breeze
Urban Cooling System	Semiporous paving that retains water and reduces evaporation
Urban Rainshell	Rainwater storage and purification system consisting of a bed of eco shells
ZOAK bestrating	Ceramic paver that is durable, colorfast, and absorbs rainwater quickly

B. DTS system installation and configuration

This chapter is dedicated to visually illustrating the installation process and configuration of the DTS system.

Figure B.1.: Excavation done prior to the construction of the Heat Square for installation of the fibre-optic cable and other required infrastructure.

Figure B.2.: Fibre-optic cable coil prior to digging the cable into the ground.

(a) Trenches dug at the required depth for the fibre-optic cable.

(b) Stakes which mark the turns of the cable path, used for maintaining tension and locating the cable at different depth.

(a) LAF of cable is marked at every turn and change of pipe encasing.

(b) Fibre-optic cable transitioning from deep to shallow section.

(a) SiliXa Ultima-M computer in control room connected to the fibre-optic cable. The calibration basins are located underneath the computer.

(b) Measurement of sensor location underneath roof substrate.

(a) Sensor hubs to which anemometers and tensiometers are connected.

(b) Distribution of sensor hubs throughout the Heat Square (22-08-2023).

Figure B.7.: Radiometer setup for measuring albedos of various surfaces.

Figure B.8.: Measurement setup for measuring the vertical temperature profile above the surface, connected to the DTS system.

Figure B.9.: Heat Square after construction and some vegetation growth

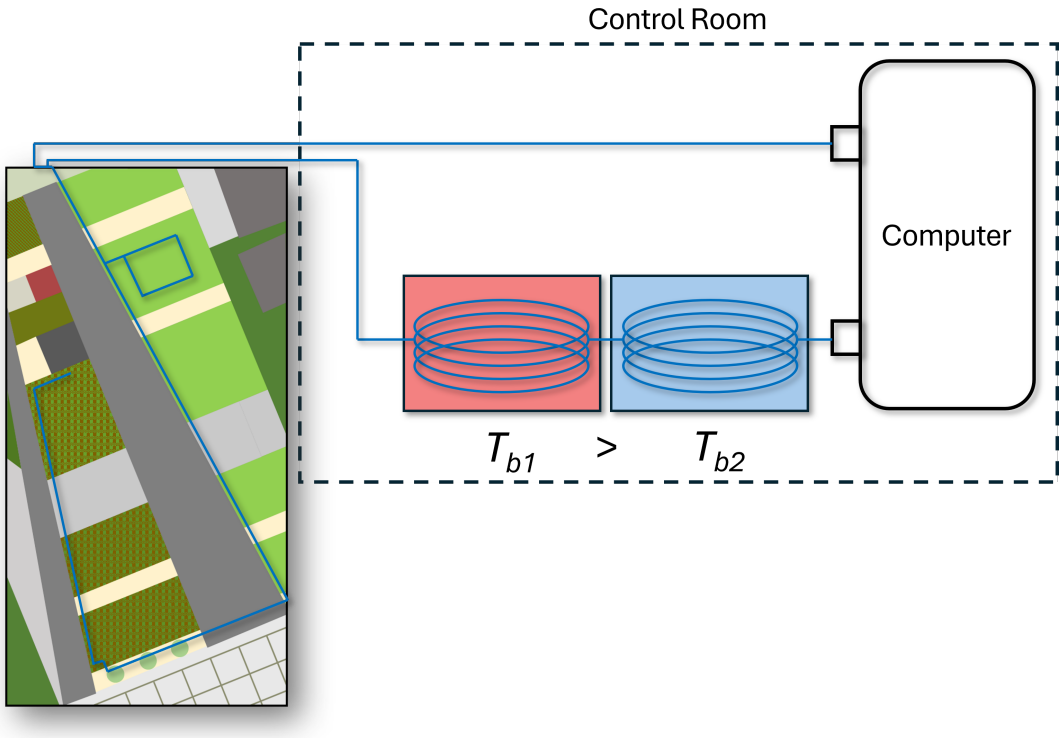

Figure B.10.: Overview of the final DTS set-up used for the Heat Square measurements. The fibre-optic cable is spliced and then connected at both ends to the Silixa Ultima-M computer. Within the control room, one end of the cable traverses through two calibration basins $b1$ and $b2$, where T_{b1} is regulated by a heating element and an aquarium pump. The cable traverses underneath the Heat Square after leaving the control room, crossing the shallow path followed by the deep path, which are the same at different depths.

C. LAF to physical coordinate transformation

To plot the DTS soil temperature measurements within the Heat Square, a transformation from LAF to physical coordinates is necessary. The DTS system records data in temperature versus LAF. The challenge is to determine which LAF value corresponds to which physical location within the Heat Square.

During the installation of the DTS system's fibre-optic cable, key locations were logged and measured by land surveyors. The following image shows the coordinates of each key location in the Dutch 'Rijksdriehoekstelsel' coordinate system.

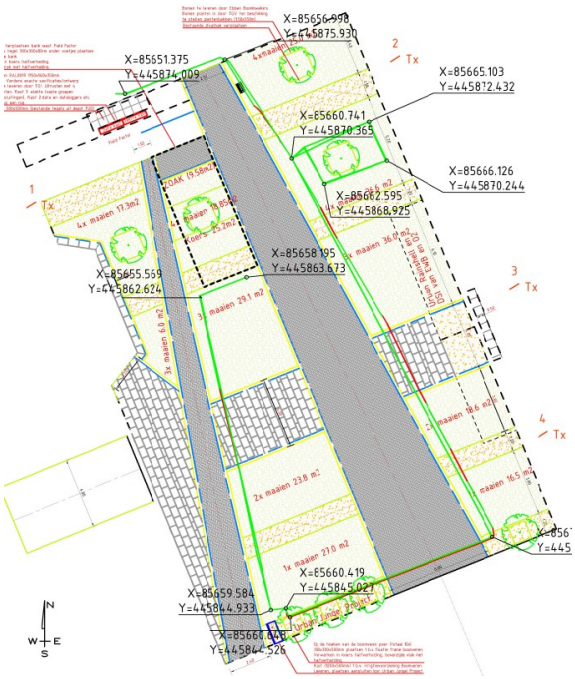

Figure C.1.: Coordinates of DTS cable performed by land surveyors

By identifying the corresponding coordinates and LAF values for each section of the cable, the DTS system's data can be transformed. Currently, only the corner points of the cable are known, so the coordinates of every point between these corners must be determined at a resolution of 0.25 metres. This can be achieved by assuming the cable follows a straight line between each surveyed point with known coordinates. The distance d_i between every point can be computed as illustrated in Figure C.2.

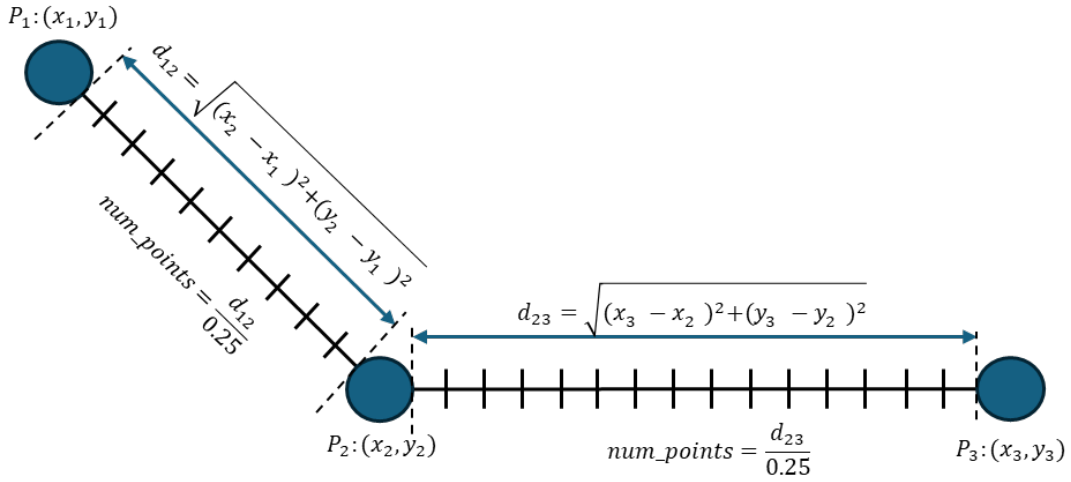

Figure C.2.: Distance between two points d_i with known coordinates x_i, y_i

Using this principle, the coordinates at equally spaced intervals 'num_points' of 0.25 metres are computed and exported using the following Python script:

```python
import csv
import matplotlib.pyplot as plt

# Define the coordinates of points A and B
point_A = (85665.103, 445872.432)
point_B = (85666.126, 445870.244)

# Define the number of equally spaced points we want to find between A and B
num_points = 47

# Calculate the x and y differences between points A and B
delta_x = (point_B[0] - point_A[0]) / (num_points + 1)
delta_y = (point_B[1] - point_A[1]) / (num_points + 1)

# Initialize a list to hold the coordinates of the equally spaced points
points = []

# Loop through the number of equally spaced points we want to find
for i in range(num_points):
    # Calculate the x and y coordinates of the current point
    x = point_A[0] + delta_x * (i + 1)
    y = point_A[1] + delta_y * (i + 1)

    # Add the current point to the list of points
    points.append((x, y))

# Export the list of equally spaced points to a CSV file
with open('equally_spaced_points.csv', 'w', newline='') as file:
    writer = csv.writer(file)
    writer.writerow(['X-coordinate', 'Y-coordinate'])
    for point in points:
        writer.writerow(point)
```

Figure C.3.: Python script for determining coordinates between each corner of the Heat Square

The exported 'equally_spaced_points.csv' file is then combined with another .csv file that includes the coordinates of all LAF points at a resolution of 0.25 metres. Before transforming the DTS data from Temperature vs. LAF to Temperature vs. coordinate (x, y), the DTS data must be resampled to match the 0.25-metre LAF resolution, as the original measurements are exported at a resolution of 0.254 metres. The corresponding vertical coordinate z(soil depth) is incorporated after the transformation of the data in Python.

D. DTS Results

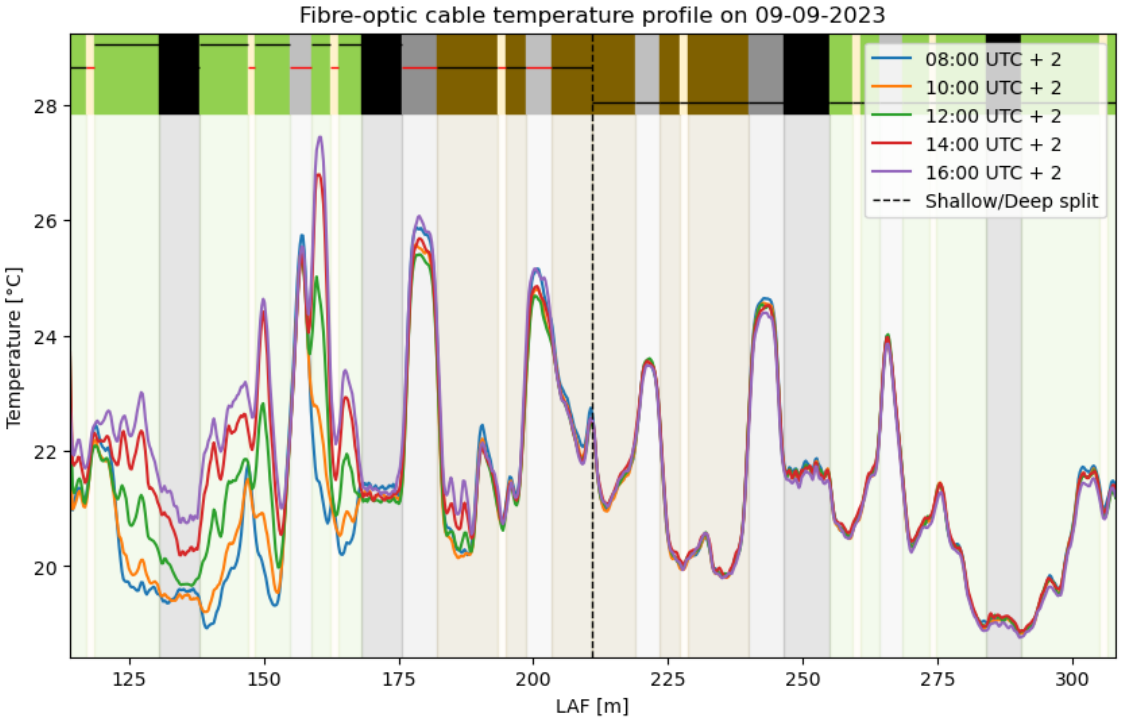

Figure D.1.: DTS temperature profile on September 9, 2023 for different times of the day.

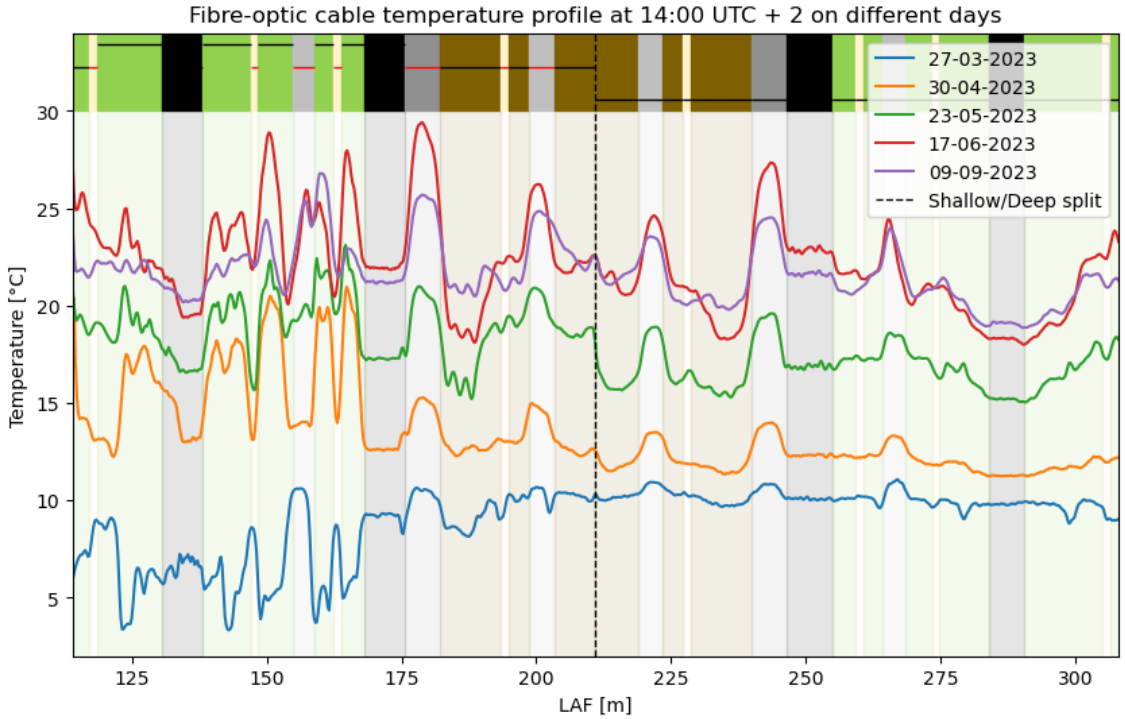

Figure D.2.: DTS temperature profile at 14:00 UTC +2 for different days.

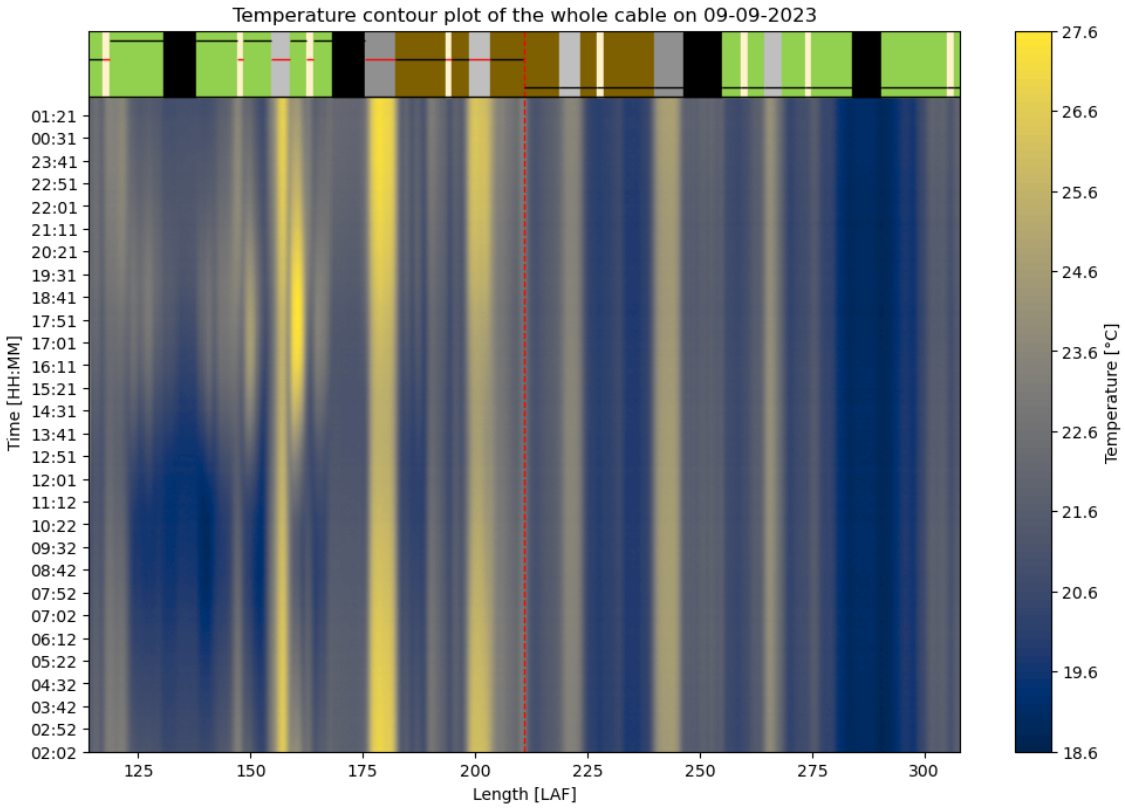

Figure D.3.: Contour plot of DTS results on September 9, 2023.

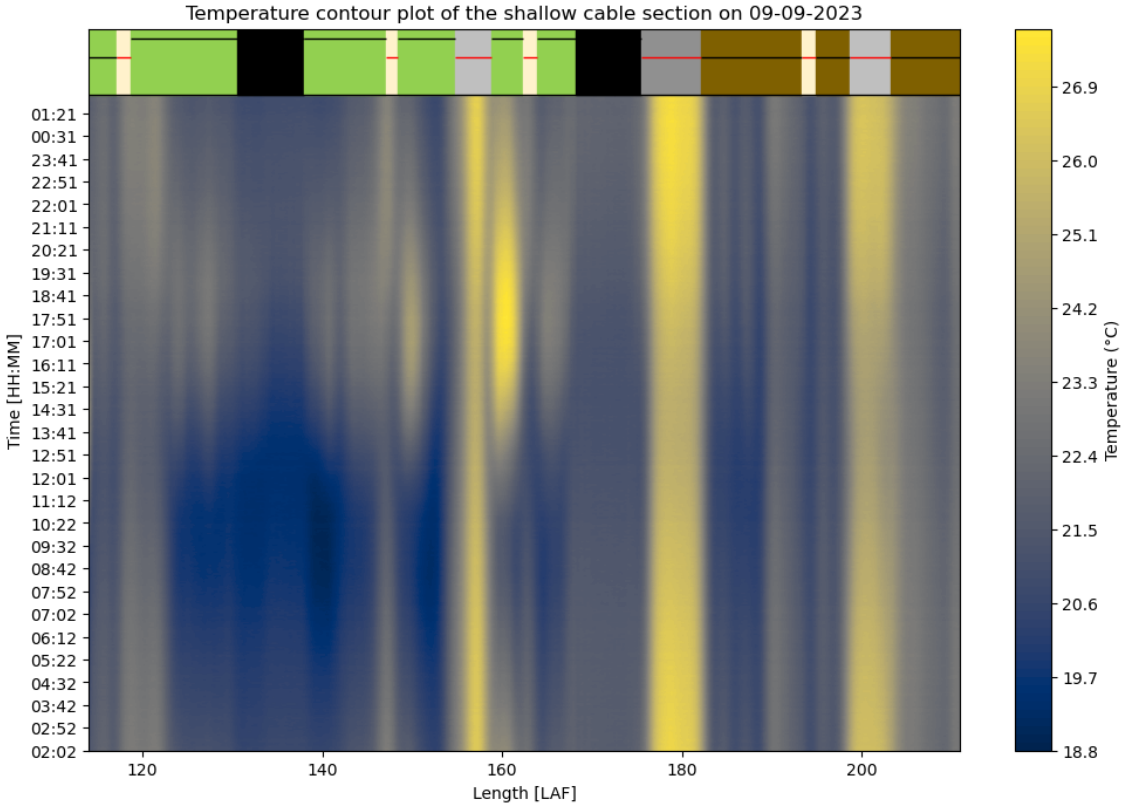

Figure D.4.: Contour plot of the shallow section of DTS results on September 9, 2023.

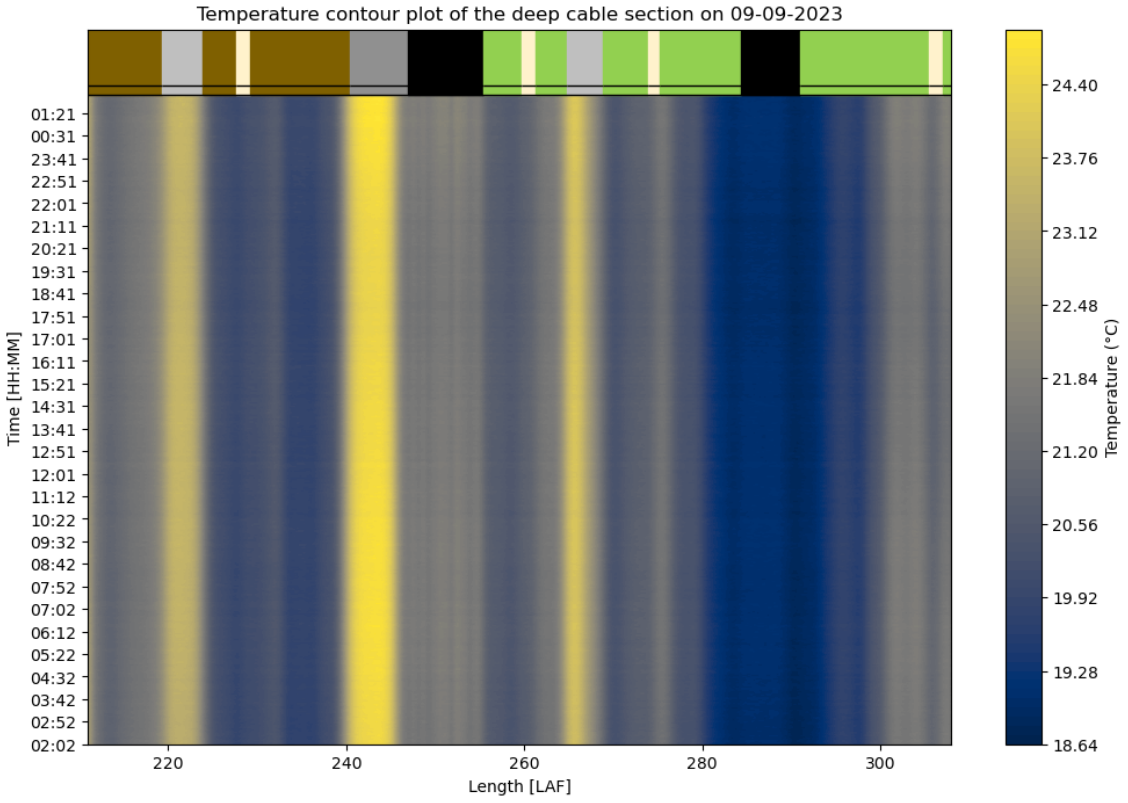

Figure D.5.: Contour plot of the deep section of DTS results on September 9, 2023.

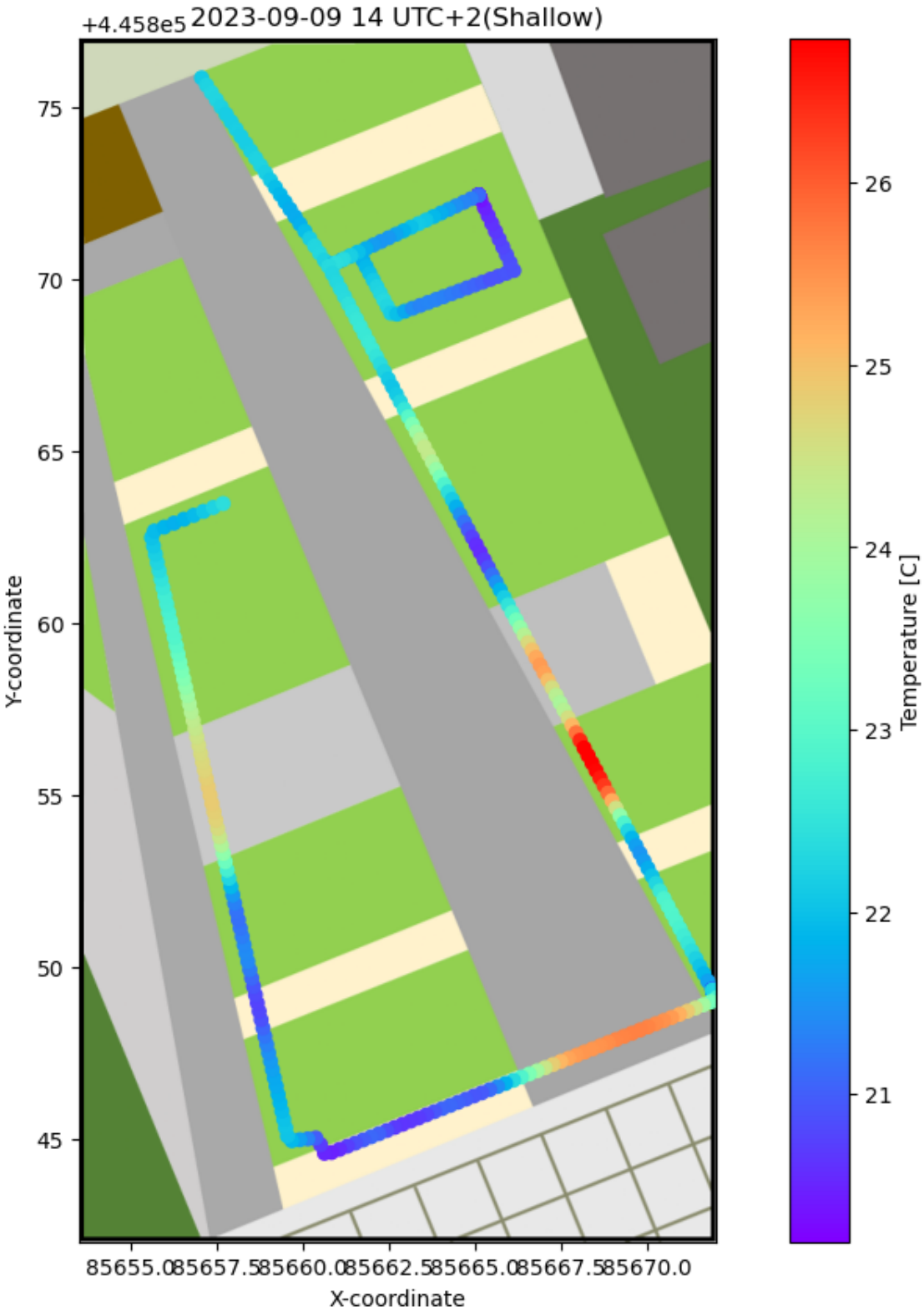

Figure D.6.: DTS plot of the shallow section on September 9, 2023, 14:00 UTC +2.

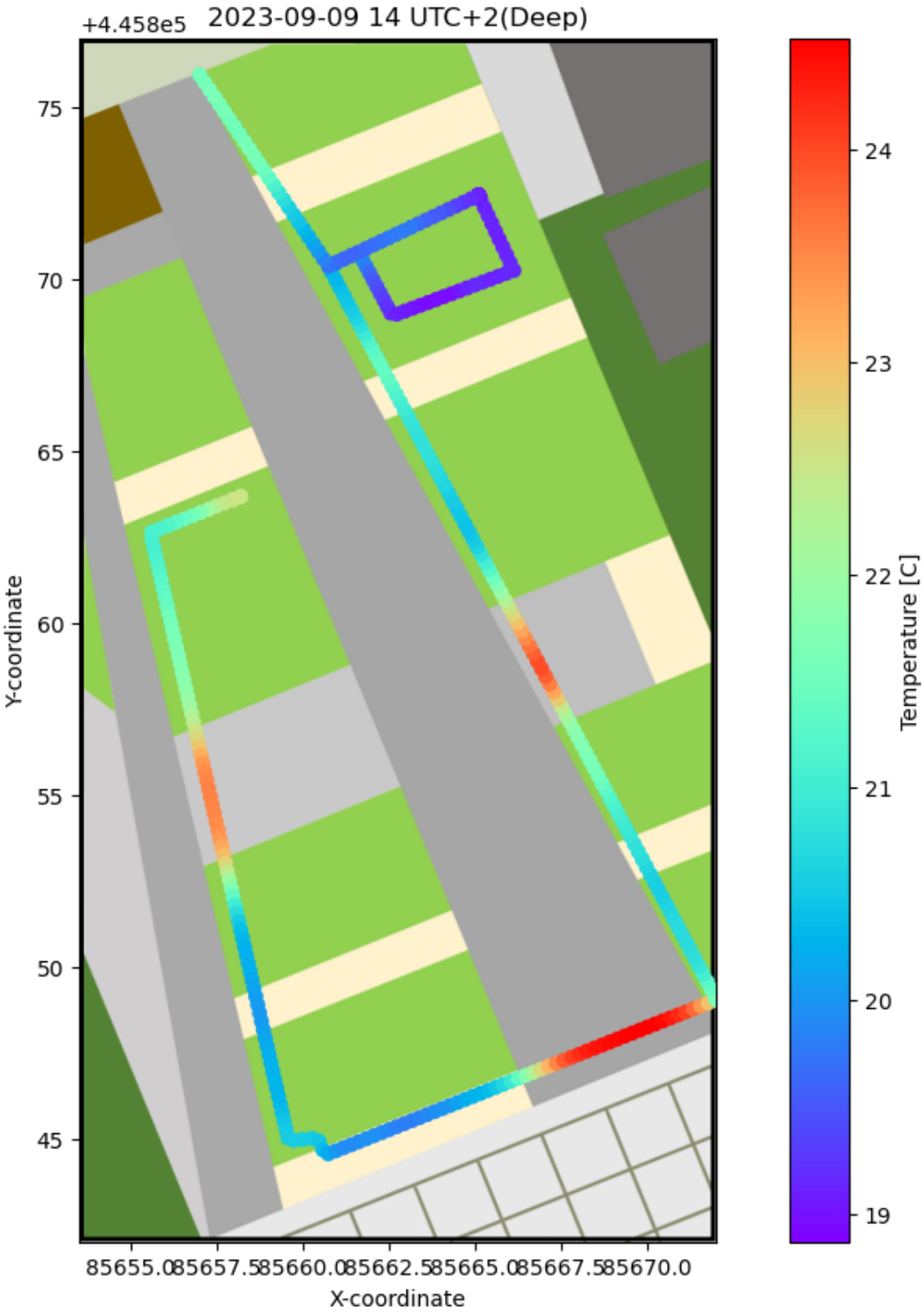

Figure D.7.: DTS plot of the deep section on September 9, 2023, 14:00 UTC +2.

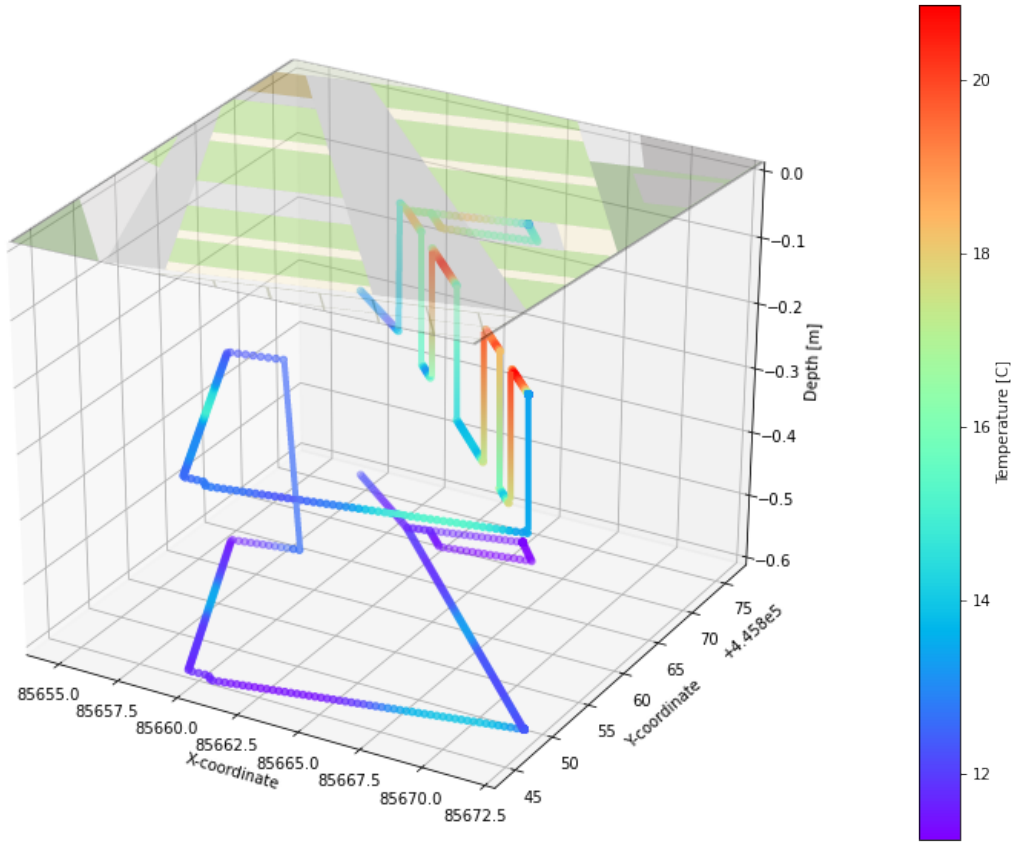

Figure D.8.: DTS 3D plot on September 9, 2023, 14:00 UTC +2.

E. ENVI-met model parameters

This section outlines the parameters utilised in the benchmark (seventh) iteration of the Heat Square model. As a reminder, the final model configuration is as follows:

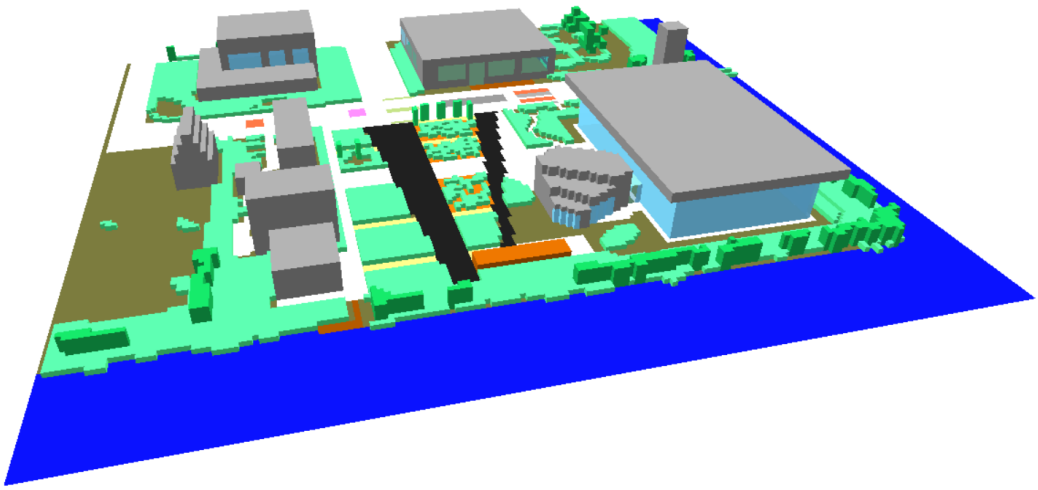

Figure E.1.: Benchmark model schematisation of the Heat Square

The materials used in the model grid were sourced from the ENVI-met database manager module, which allows for the specification or selection of material properties from the software's library. Table E.3 details the materials chosen for the schematisation of the Heat Square, along with their respective properties.

The material properties can be stored in a projectdatabase.edb file. By keeping this file in the project folder, specific materials and their spatial distributions can be assigned to grid cells. The final grid model settings are presented in Table E.1, the file corresponding to the spatial distribution of the grid is save in a .INX file.

Table E.1.: Summary of ENVI-met grid model settings within Spaces module

Parameter	Value
Grid dimensions	157 x 141 x 32 grids
Core domain size	78.5m x 70.5m
Grid size	dx=0.5m dy=0.5m dz=0.5m
Highest building in domain	10m
Height of 3D model top	21.90m
Start telescoping after height	12m
Telescoping factor	20%
Model rotation out of grid north	330

In the ENVI-Guide module, the .INX file can be subjected to pre-specified weather forcing. For the simulation of the benchmark model, the following settings were applied:

Table E.2.: Simulation settings for ENVI-met weather forcing

Parameter	Value
Start Date (YYYY MM DD)	2023 09 07
Start Time (HH MM)	00 00
Total Simulation time (h)	72
Specific humidity in 2500 m (g/kg)	8
Constant windspeed at inflow border (m/s)	1.5
Constant wind direction at inflow (\textdegree())	12m
Microscale roughness length of the surface (m)	0.01

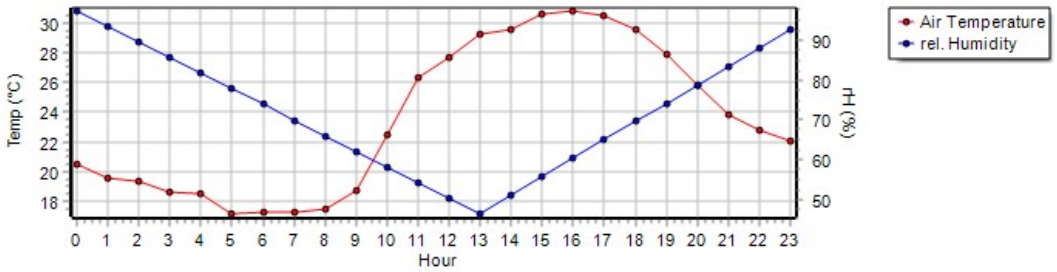

Figure E.2.: Air Temperature and Humidity settings for ENVI-met model simulation.

The output from this module is a .SIMX file, which is then input into the ENVI-core module to initiate the simulation. All resulting model output files are stored within the project folder and can be accessed using the LEONARDO module. Due to the significant computational power required for each simulation, running them on a standalone computer was impractical. Consequently, a virtual server was set up using the Muster Console to handle the computations remotely. The output files were saved onto the remote drive of the Renderfarm at the Faculty of Architecture, within the Delft University of Technology.

Table E.3.: Summary of ENVI-met material properties used: surface (top) and vegetation (bottom) properties

							Material properties								
Name	**Applied Section**	**Database ID**	**Roughness Length**	**Albedo**	**Emissivity**	**Surface Irrigation**	**Water content at saturation**	**Water content field capacity**	**Water content at wilting point**	**Matrix Potential**	**Hydraulic Conductivity**	**Volumetric heat Capacity**	**C & H Constant**	**Heat Conductivity**	**Color**
Sandy Loam	Local soil	000000	0.015	0.2	0.9	False	0.435	0.195	0.114	-0.218	34.1	1.32	4.9	0	'Camo green'
Clay Loam	Roof substrate	0200LO	0.015	0.2	0.9	False	0.451	0.24	0.155	-0.478	7	1.212	5.39	0	'Bronze'
Sandy Soil	Sand pavement	0200SD	0.05	0.4	0.9	False	0.395	0.135	0.07	-0.121	176	1.463	4.05	0	'Pale yellow'
Concrete Pavement Light	Light pavement	0200PL	0.01	0.5	0.9	False	-	-	-	-	-	2.083	-	1.63	'Light grey'
Asphalt Road	Dark pavement	0200ST	0.01	0.12	0.9	False	-	-	-	-	-	2.214	-	1.16	'Black'
Concrete Pavement Grey	Dark concrete	0200PG	0.01	0.3	0.9	False	-	-	-	-	-	2.083	-	1.63	'Dark grey'
Wood planks	Wooden path	0200WD	0.01	0.35	0.9	False	-	-	-	-	-	0.454	-	0.9	'Brown'
Brick road (red stones)	Brick	0200KK	0.01	0.3	0.9	False	-	-	-	-	-	2	-	1	'Red'

			Vegetation properties					
Name	**Applied Section**	**Database ID**	**CO2 fixation type**	**Leaf type**	**Albedo**	**Emissivity**	**Transmittance**	**Plant height**	**Root Zone Depth**
Grass 25 cm aver. dense	Grass	0200XX	C3	Grass	0.2	0.97	0.3	0.25	0.2
Grass 50 cm aver. dense	Grass	0200XY	C3	Grass	0.2	0.97	0.3	0.5	0.5
Hedge dense, 2m	Tall vegetation	0200H2	C3	Decidious	0.2	0.97	0.3	2	1
Hedge light, 2m	Tall vegetation	0201H2	C3	Decidious	0.2	0.97	0.3	2	1
Tree 5 m, dense	Trees	01OSDS	C3	Decidious	0.2	0.97	0.3	5	1

F. ENVI-met model schematisations

This chapter covers the different models simulated in ENVI-met, with each color representing different materials whose properties have been predefined in the database manager within the ENVI-met environment (see Appendix E).

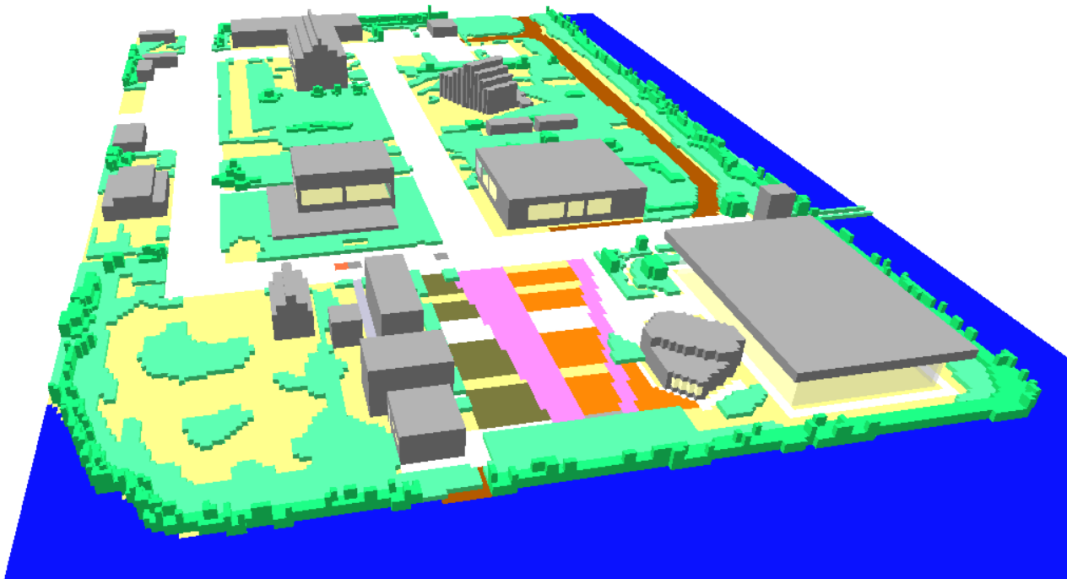

Figure F.1.: Model schematisation of the Green Village (first iteration)

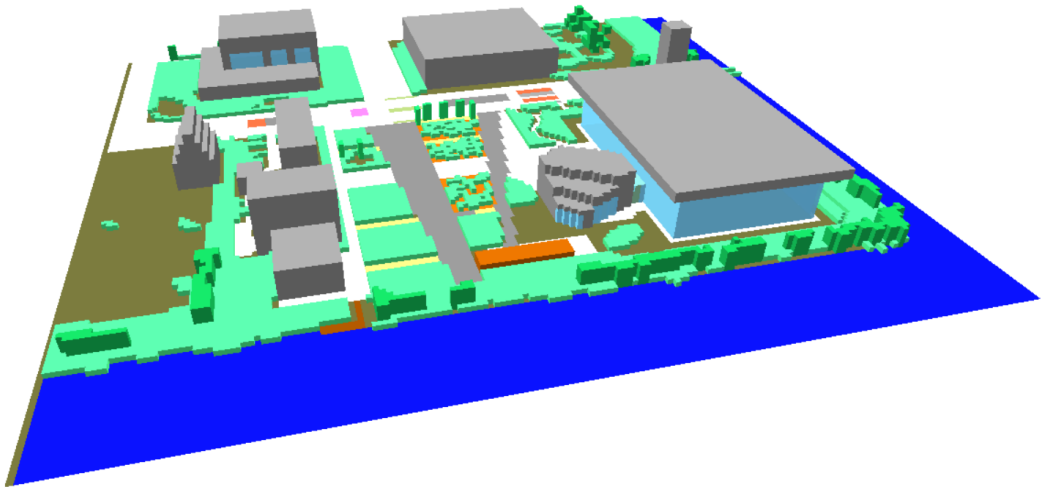

Figure F.2.: Model schematisation of the Heat Square (third iteration), the version containing the full scale of the Green village can be seen in Figure 3.5.

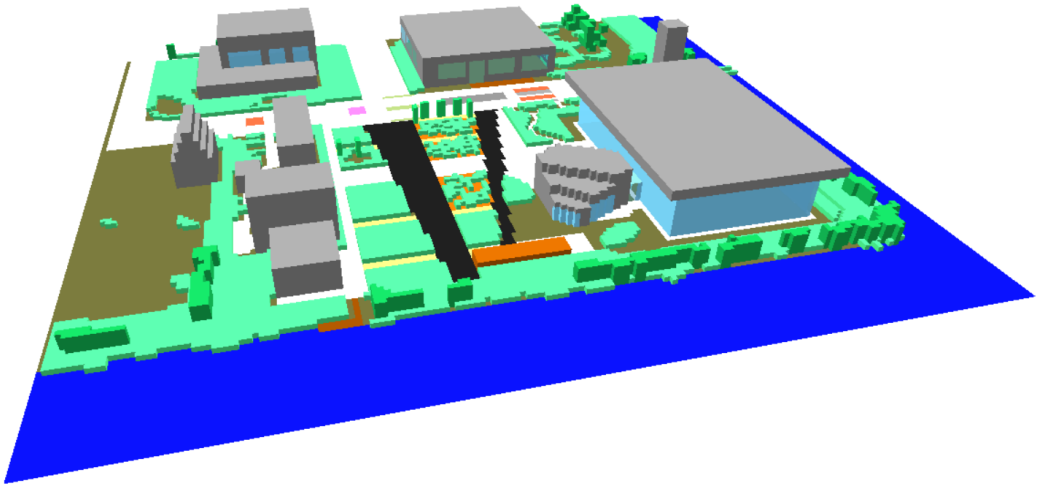

Figure F.3.: Model schematisation of the Heat Square (fifth iteration)

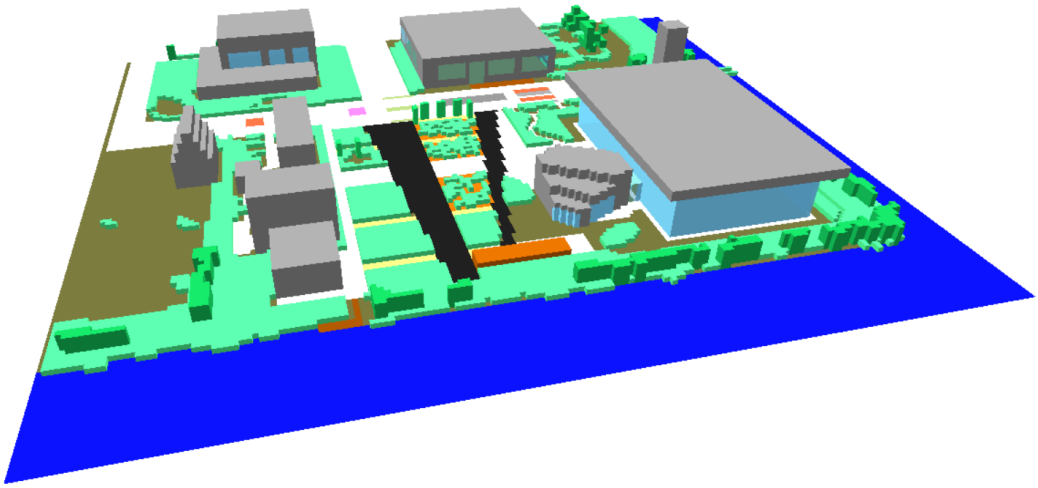

Figure F.4.: Benchmark model schematisation of the Heat Square (seventh iteration)

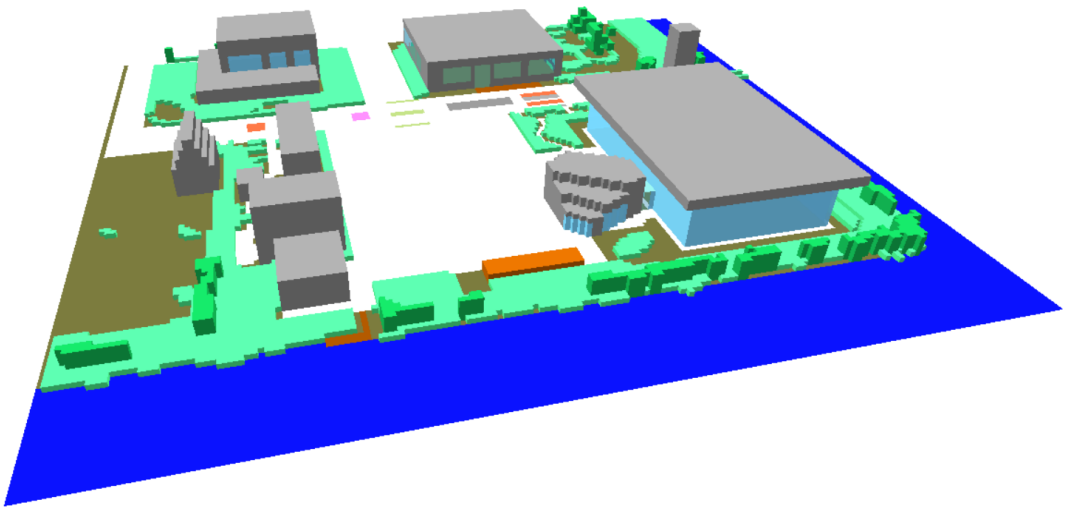

Figure F.5.: Model schematisation of the Heat Square (concrete square scenario)

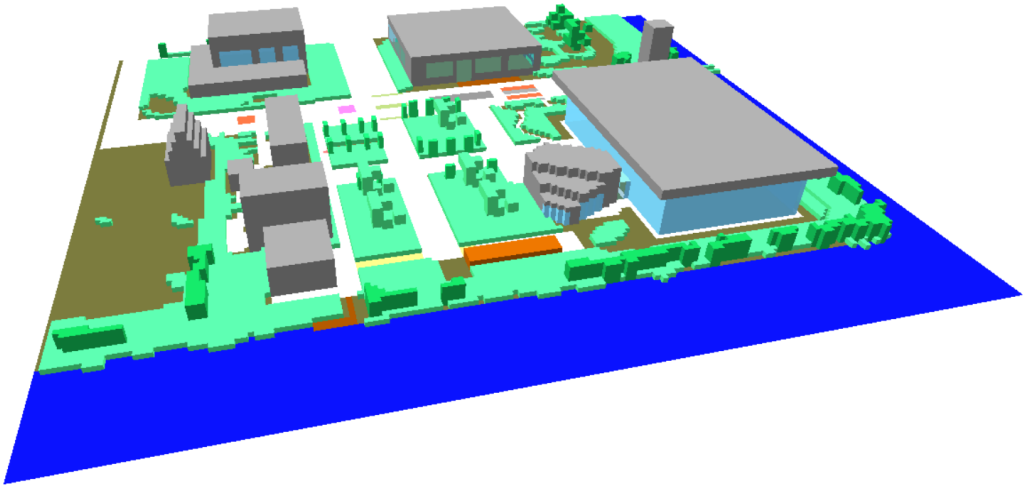

Figure F.6.: Model schematisation of the Heat Square (Cooling scenario)

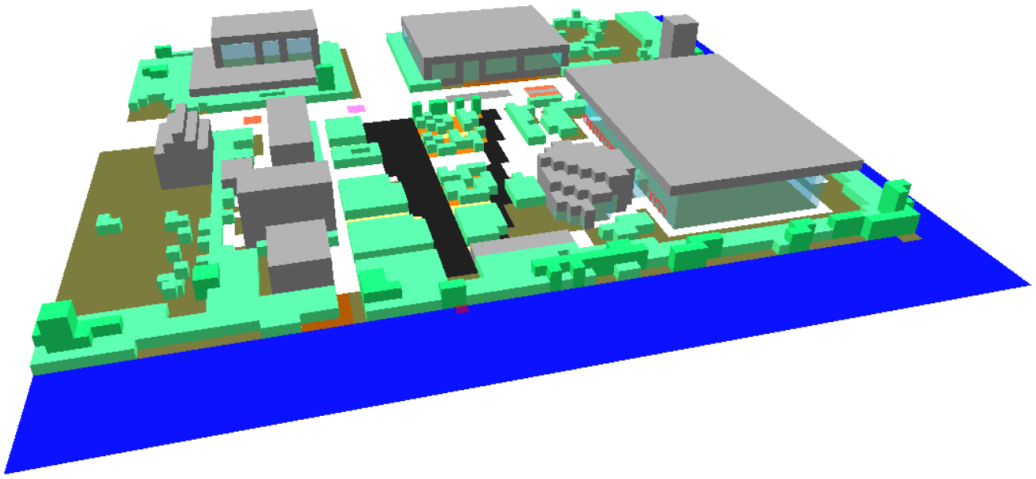

Figure F.7.: Model schematisation of the Heat Square (Low-resolution version)

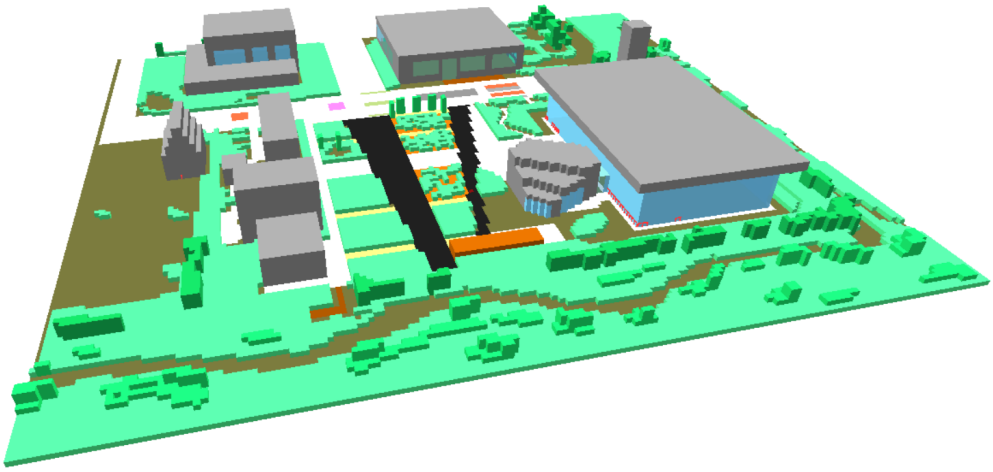

Figure F.8.: Model schematisation of the Heat Square (No water scenario)

Colophon

This document was typeset using LaTeX, using the KOMA-Script class `scrbook`. The main font is Palatino.